ISSUE RESOLUTION STATUS REPORT

KEY TECHNICAL ISSUE: UNSATURATED AND SATURATED FLOW UNDER ISOTHERMAL CONDITIONS

Division of Waste Management
Office of Nuclear Material
Safety & Safeguards
U.S. Nuclear Regulatory Commission

Revision 1
September 1998

Volume II
(Attachments)

ATTACHMENT A

DRAFT FIGURES ILLUSTRATING ELEMENTS OF THE NRC STAFF'S TOTAL SYSTEM PERFORMANCE ASSESSMENT

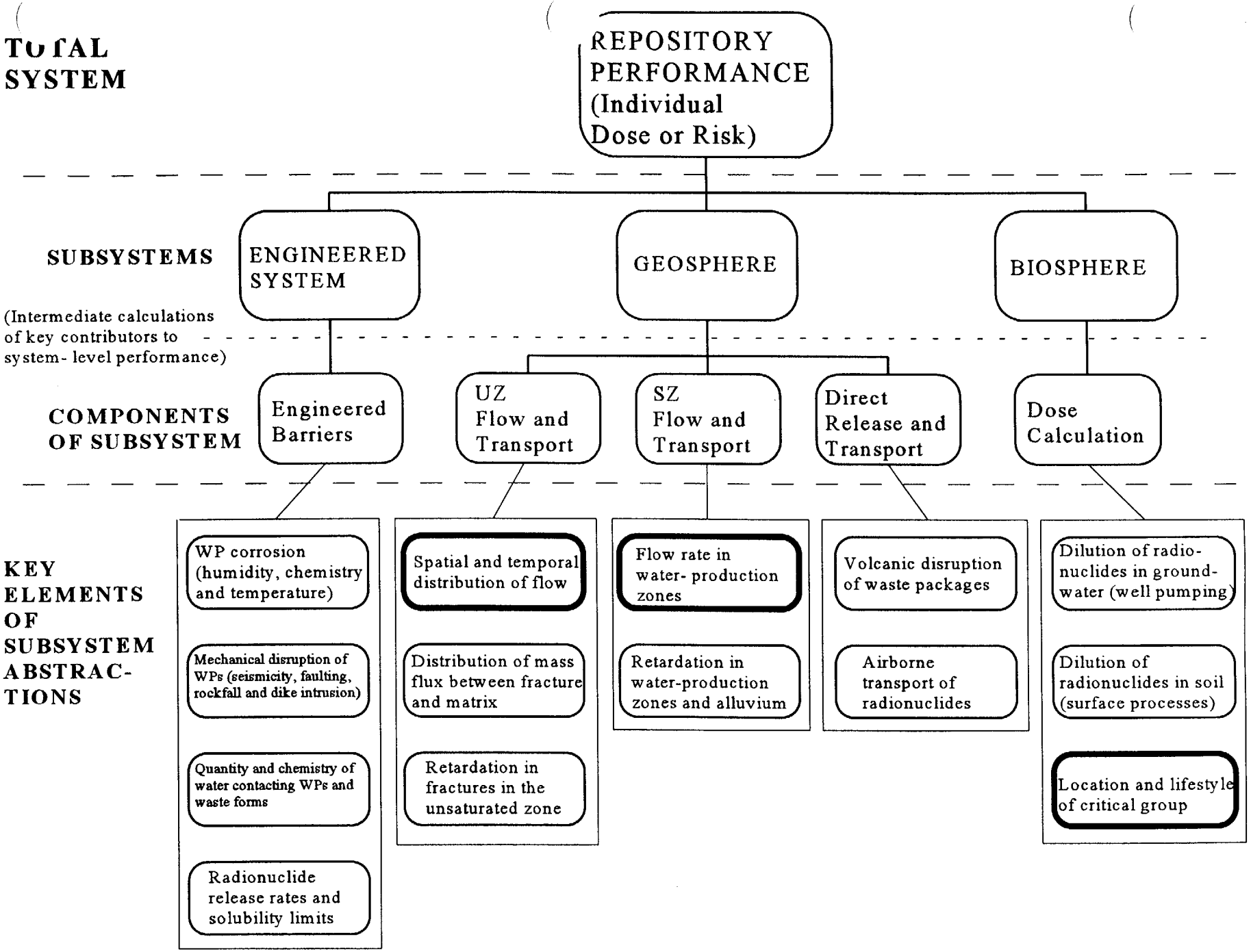

Figure A-1. Flowdown diagram for total system performance assessment. The USFIC subissues on climate change & hydrologic effects provide input to the highlighted elements.

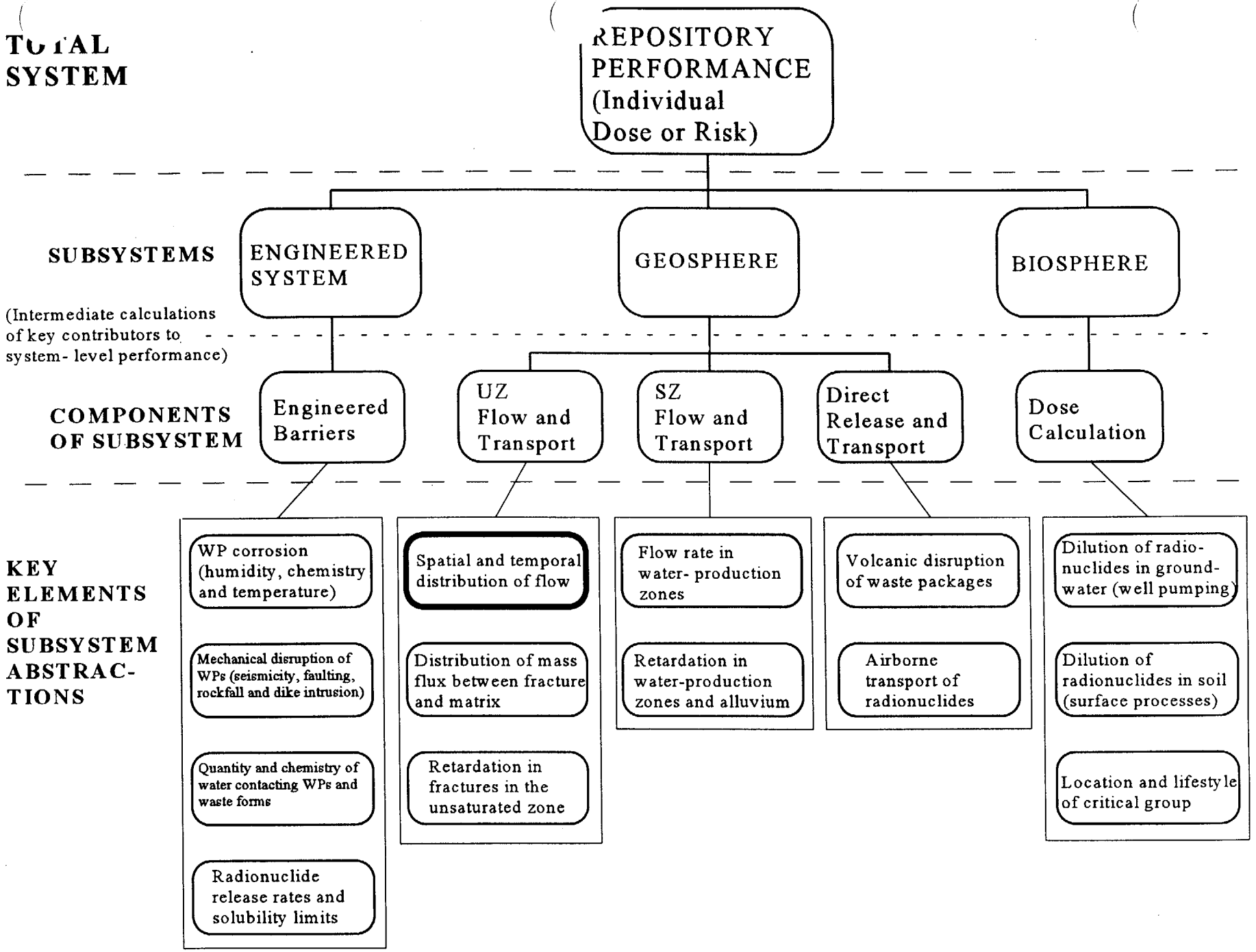

Figure A-2. Flowdown diagram for total system performance assessment. The USFIC subissue on shallow infiltration providesinput to the highlighted elements.

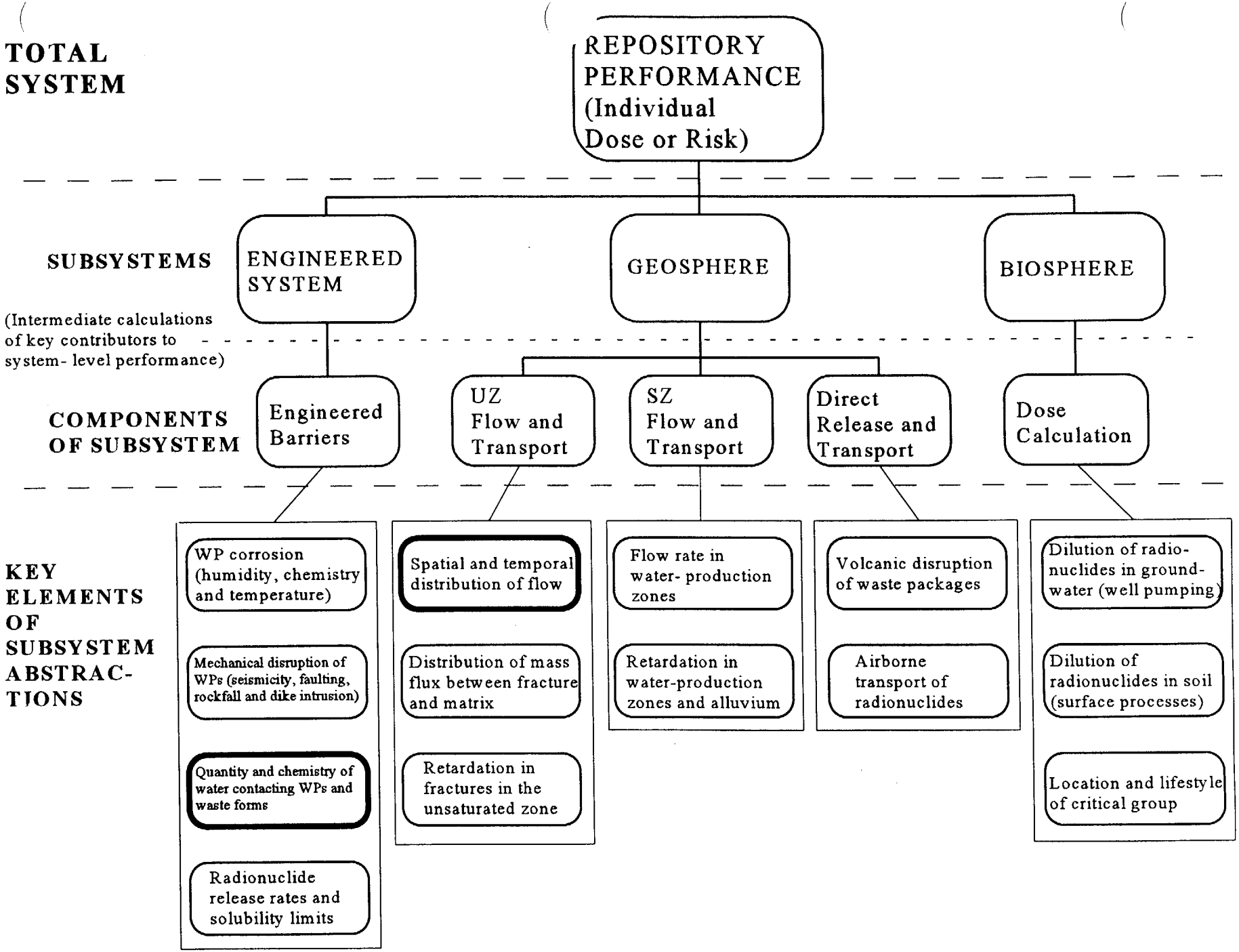

Figure A-3. Flowdown diagram for total system performance assessment. The USFIC deep percolation subissue provides input to the highlighted elements.

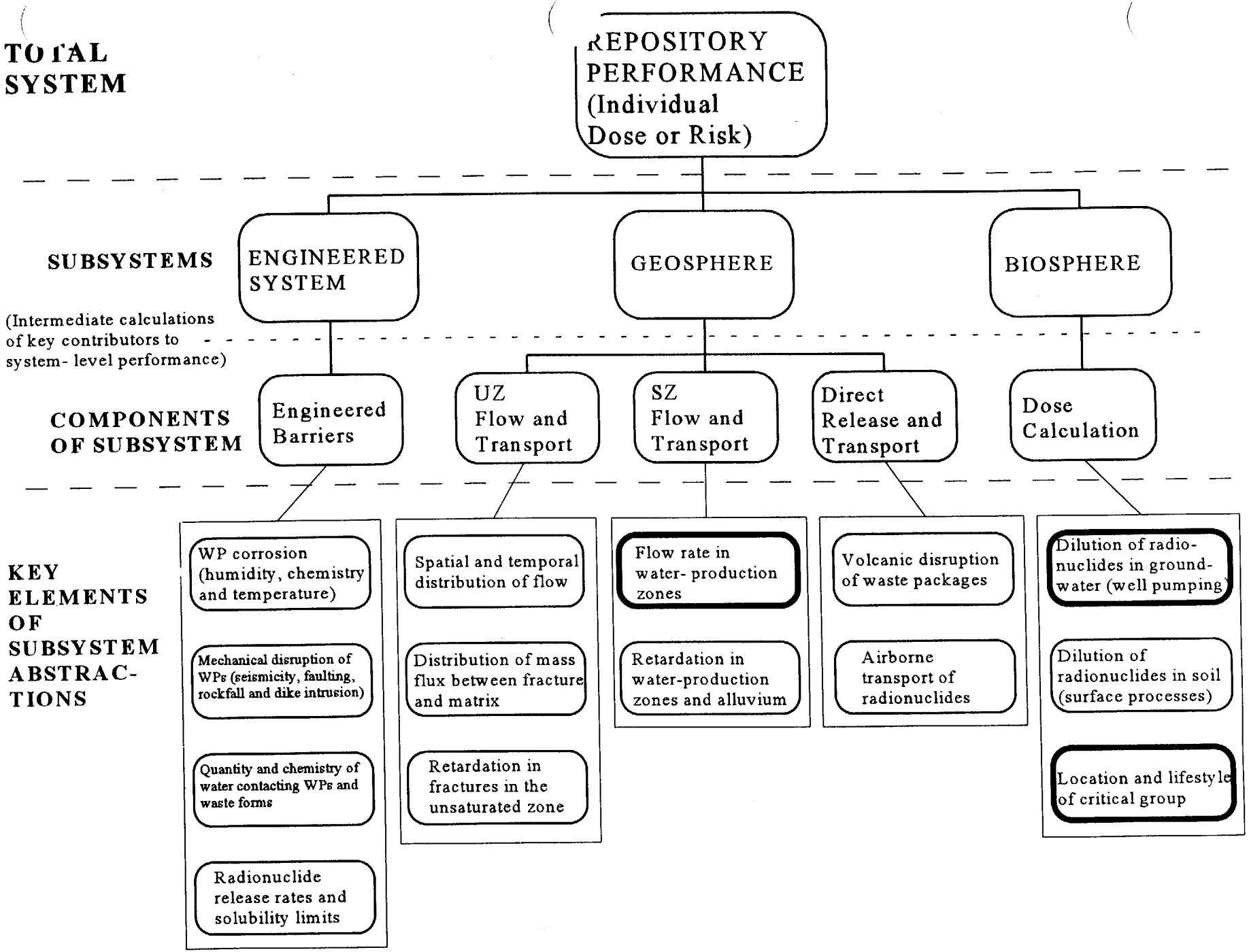

Figure A-4. Flowdown diagram for total system performance assessment. The USFIC saturated zone subissue provides input to the highlighted elements.

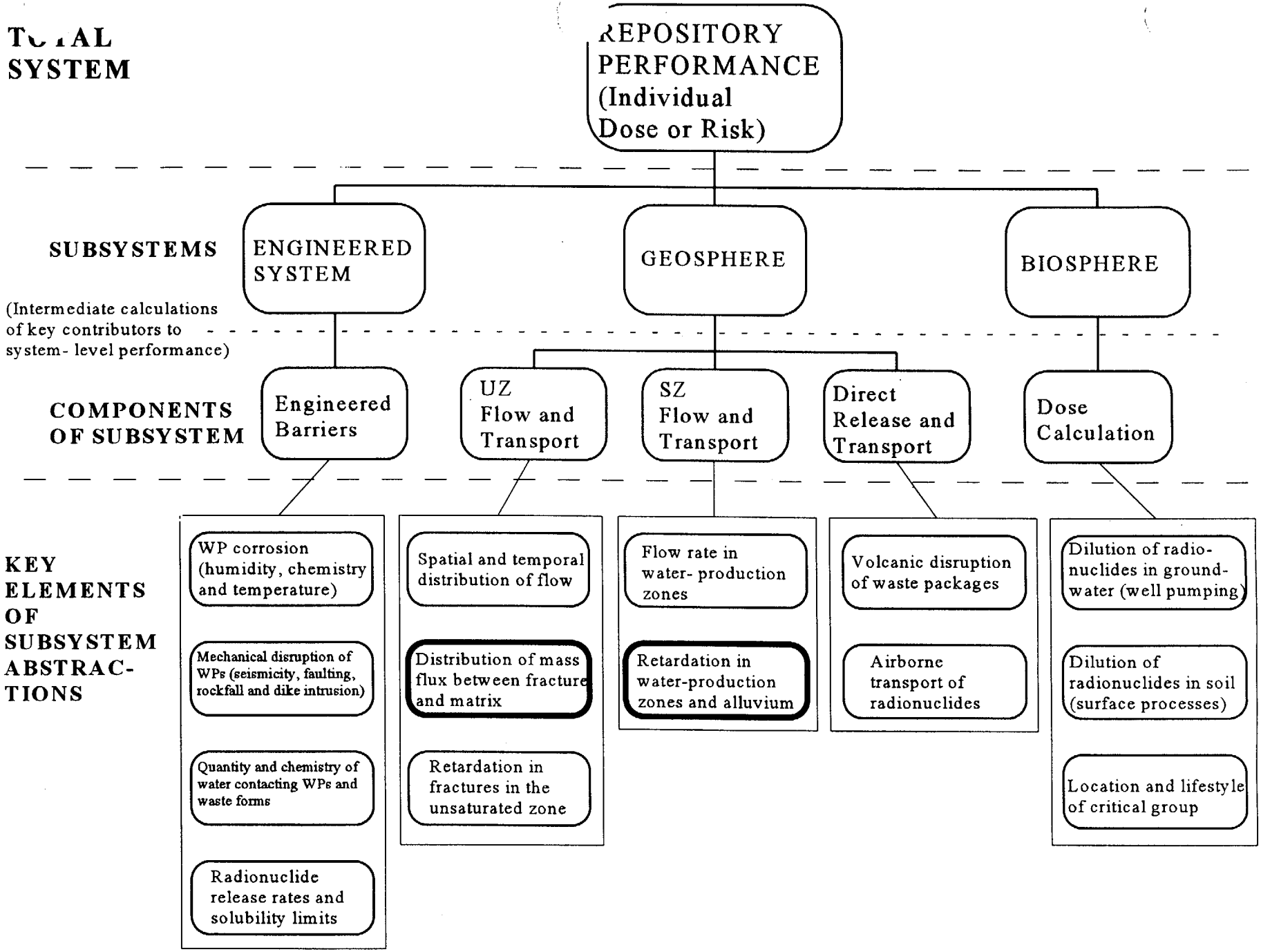

Figure A-5. Flowdown diagram for total system performance assessment. The USFIC matrix diffusion subissue provides input to the highlighted elements.

ENCLOSURE

ACKNOWLEDGMENTS

This report has been prepared jointly by staff from the U.S. Nuclear Regulatory Commission and the Center for Nuclear Waste Regulatory Analyses (CNWRA). Primary authors of the report are, in alphabetical order, Amit Armstrong, Jeff Ciocco, Neil Coleman, Randall Fedors, Latif Hamdan, Stuart Stothoff, David Turner, James Winterle, and Gordon Wittmeyer. The authors offer special thanks to David Brooks, Budhi Sagar, and English Pearcy for their excellent reviews.

Valuable technical assistance was provided by William Murphy, David Ferrill, John Stamatakos, and English Pearcy. Special thanks to Ronald Martin for providing assistance with figures. This report would not have been possible without the assistance of Carrie Crawford, Corky Gray, Annette Mandujano, and Arturo Ramos.

QUALITY OF DATA, ANALYSES, AND CODE DEVELOPMENT

DATA: NRC and CNWRA-generated original data contained in this report meet quality assurance requirements described in the CNWRA Quality Assurance (QA) Manual. Sources for other data should be consulted for determining the level of quality for those data.

ANALYSES AND CODES: The TPA Version 3.1.1 code has been developed following the procedures described in CNWRA Technical Operating Procedure, TOP-018, which implements the QA guidance contained in the CNWRA QA Manual. The code was used to perform the sensitivity studies described in Section 3.

INTERNET WEBSITES

The reader can find informative discussions about the Yucca Mountain Project by visiting internet web sites and associated links. A partial list is provided below. The U.S. Nuclear Regulatory Commission (NRC) web site provides general information about agency programs and nuclear wastes. The U.S. Nuclear Waste Technical Review Board (NWTRB) website in particular provides many additional important links.

U.S. Nuclear Regulatory Commission	http://www.nrc.gov http://www.nrc.gov/ACRSACNW/
U.S. Department of Energy (DOE)	http://www.ymp.gov [and] http://www.rw.doe.gov
U.S. Nuclear Waste Technical Review Board	http://nwtrb.gov
Nevada Nuclear Waste Project Office	http://www.state.nv.us/nucwaste/
Nye County, Nevada	http://site206087.primehost.com/index.htm
Los Alamos National Laboratory	http://ees13.lanl.gov/lees-13y.htm
Lawrence Livermore National Laboratory	http://energy.llnl.gov/Yucca.html
Earnest Orlando Lawrence Berkeley National Laboratory	http://www-esd.lbl.gov/NW/yuccamtn.html
Sandia National Laboratories	http://ntp.nwer.sandia.gov/nwmp/ymp.htm
U.S. Environmental Protection Agency	http://epa.gov/rpdweb00/yucca.index.html

Americium and plutonium were significant contributors to maximum TEDE for a receptor group 5 km away from the repository. This indicates that sorption does not become effective in the model for these radionuclides. Although these radionuclides have a great tendency to sorb to most types of earth minerals, they are experiencing little retardation. This low retardation resulted from modeling assumptions where flow is predominantly through fractures for the 5 km receptor group, allowing little contact with sorbing minerals. Normally, americium and plutonium would not be expected to migrate significant distances unless associated with substantial colloidal transport.

The following aspects were identified as requiring additional characterization and examination: (1) well pumping rates (5 km and 20 km receptor groups); (2) mixing zone thickness (5 km and 20 km); (3) maximum hydraulic head in the SZ; and (4) width of the streamtubes at 20 km. Also, the treatment of matrix diffusion and/or the parameters related to sorption of radionuclides such as americium and plutonium need confirmation. Sorption is addressed in detail in the IRSR on Radionuclide Transport (NRC, 1998d).

4.0 REVIEW METHODS AND ACCEPTANCE CRITERIA

The staff's technical review of DOE's treatment of subissues under unsaturated and saturated flow under isothermal conditions will be based on the completeness and applicability of data and analyses. The staff will determine whether DOE has reasonably complied with the acceptance criteria listed in this section for each subissue.

4.1 CLIMATIC CHANGE

See Section 4.2.

4.2 HYDROLOGIC EFFECTS OF CLIMATE CHANGE

Review methods, acceptance criteria, and technical bases for the subissues (climate change and hydrologic effects of climate change) were provided in a previous version of this IRSR which is attached as Attachment E (NRC, 1997a). The acceptance criteria, with slight modification, are repeated below for the convenience of the reader.

4.2.1 ACCEPTANCE CRITERIA

(1) Climate projections based primarily on paleoclimate data are acceptable for use in performance assessments of the YM site. During its review, the staff should determine whether DOE has made a reasonably complete search of paleoclimate data that are available for the YM site and region, and has satisfactorily documented the results. Staff should determine that, at a minimum, DOE has considered information contained in Forester, et al. (1996); Winograd, et al. (1992); Szabo, et al. (1994); and other reports that may become available.

(2) DOE's projections of long-term climate change are acceptable if these projected changes are consistent with evidence from the paleoclimate data. Specifically, staff

should determine whether DOE has evaluated long-term climate change based on known patterns of climatic cycles during the Quaternary, especially the last 500 ky. The current analysis indicates that these cycles included roughly 100-ky cycles of glacial/interglacial climates, with interglacials lasting about 20 ky. Current information also suggests that past climate conditions were cooler and wetter than today, about 60 to 80 percent of the time.

(3) The staff will not require climate modeling to estimate the range of future climates. If DOE uses numerical climate models, staff will determine whether such models were calibrated with paleoclimate data before they were used for projection of future climate, and that their use suitably simulates the historical record.

(4) Values for climatic parameters (time(s) of onset of climate change; mean annual precipitation (MAP); mean annual temperature (MAT); etc.) to be used in DOE's safety case should be adequately justified. Determine whether appropriate scientific data were used, reasonably interpreted, and appropriately synthesized into parameters such as MAP, MAT, and long-term climate variability. The current knowledge about these parameters, coupled with past climate change, will require that, as a bounding condition, a return to full pluvial climate (higher precipitation and lower temperatures) be considered for at least a part of the 10-ky period (current information does not support persistence of present-day climate for a duration of 10 ky or more). The current interpretations of paleoclimate data indicate an increase in MAP by a factor of 2 to 3 and a lowering of MAT of 5-10 °C (9-18 °F) during the pluvial climate episodes.

(5) If DOE uses expert elicitation to arrive at values of climate parameters, staff will determine whether the guidance in the Branch Technical Position on Expert Elicitation (NRC, 1996a) was followed by DOE.

(6) Bounding values of climate-induced effects (for example water-table rise) based primarily on paleoclimate data will be acceptable. Staff should determine whether DOE has made a reasonably complete search of paleoclimate data pertinent to water-table rise and other effects (for example, changes in precipitation and geochemistry) of climate change that are available for the YM site and region, and has satisfactorily documented the results. In evaluating DOE's analyses, staff should determine whether, at a minimum, DOE has fully considered information contained in Paces, et al. (1996a), Szabo, et al. (1994), Forester, et al. (1996), and other reports that may become available.

(7) It will be acceptable for DOE to use regional and sub-regional models for the saturated zone to predict climate-induced consequences if these models are calibrated with the paleohydrology data. Staff should determine whether DOE's models of the consequences of climate change are consistent with evidence from the extensive paleoclimate data base. Specifically, climate-induced water-table rise is expected to occur in response to elevated precipitation during future pluvial climate episodes, and the staff should determine whether DOE's estimates of climate-induced, water-table rise are consistent with the paleoclimate data. The current estimate of water-table rise during the late Pleistocene is 120 m (394 ft). Staff should determine whether DOE's

assumptions about climate-induced, water-table rise over 10 ky, if different from 120 m (394 ft), are adequately justified.

(8) Based on judgment and analysis, staff will determine whether DOE has adequately incorporated future climate changes and associated effects in its performance assessments. Current information does not support an assumption that present-day climate will persist unchanged for 10 ky or more. The staff should keep in mind that the consequences of climate change may be coupled to other events and processes and therefore the projections of water-table rise that are used in total system performance may be different from those based solely on climate change.

(9) The collection, documentation, and development of data, models, and computer codes have been performed under acceptable QA procedures. If they were not subject to an acceptable QA procedure, they have been appropriately qualified.

4.2.2 Technical Basis for Review Methods and Acceptance Criteria

See NRC (1997a) for a description of the technical basis for review methods and acceptance criteria for the subissues of climate change and hydrologic effects of climate change. An important new paper on Devils Hole was published in 1997, and the main conclusions are presented below. These do not lead the NRC staff at this time to change the previously developed acceptance criteria. Winograd, et al. (1997) examined the Devils Hole paleoclimatic record in light of the widely held view that interglaciations lasted 11 ky to 13 ky and constituted only about 10% of middle-to-late Pleistocene climatic cycles. They concluded that the previous interglacial (Sangamon, or substage 5e) lasted significantly longer, about 22 ky, consistent with the Vostok ice core record which suggests a duration of about 19 ky for this event in Antarctica. The three preceding interglacials in the Devils Hole record (analogs of marine isotopic substages 7e, 9c, and 11c) lasted 20 ky to 26 ky. The warmest intervals of each interglacial in the Devils Hole record indicate apparent climatic stability for periods lasting 10 ky to 15 ky. Winograd, et al. (1997, p. 153) also note that "Phase offsets of thousands of years are likely between different climate proxy records (especially temperature and ice volume) of the same interglaciation." They also speculated about the possible duration of our current interglacial climate, assuming only natural variation. With no anthropogenic warming, Holocene-like temperatures could remain with us for up to another 5 ky, or alternatively, the next millennium could experience steadily lowering temperatures.

NRC (1997a) discussed the fact that, during the Wisconsin, the water table at YM may have risen 10 times higher than at Devils Hole, given the proximity of YM to areas of higher elevation where recharge would have been greater, and also due to higher transmissivities in the Paleozoic carbonate aquifer at Devils Hole. It should also be mentioned that the Wisconsin-age rise of the potentiometric surface at Devils Hole may have been controlled, to some extent, by local topography. The present water table is only 17 m below the land surface (Szabo, et al., 1994). Areas close to Devils Hole occur at lower elevations where surface discharges of groundwater could occur during times of elevated water tables. This could perhaps limit the Wisconsin-age rise of the water table to less than 10 m at Devils Hole, as inferred from calcites in the subterranean Browns Room.

The NRC staff has previously recommended (NRC, 1997a, p. 8) a pragmatic approach to address climate change. Under this approach, the effects of global, enhanced, greenhouse warming would be presumed to last no more than several thousand years, and that, about 3 ky into the future, the climate at YM will resume or continue the global cooling predicted by the Milankovitch orbital theory of climate. Pluvial conditions should be expected to dominate at least several thousand years of the next 10 ky. Current information suggests that past climate conditions were cooler and wetter than today, about 60 to 80 percent of the time.

4.3 PRESENT-DAY SHALLOW INFILTRATION

Review methods, acceptance criteria, and technical bases for the subissue of present-day shallow infiltration were provided in a previous version of this IRSR which is provided as Attachment F (NRC, 1997b). The acceptance criteria, with slight modification, are repeated below for the convenience of the reader.

4.3.1 Acceptance Criteria

(1) Staff shall determine whether DOE has estimated shallow infiltration for use in the PA of YM using mathematical models that incorporate site-specific climatic, surface, and subsurface information. Staff will also determine whether DOE provided sufficient evidence that the mathematical models were reasonably verified with site data. These data would include measured infiltration data and indirect evidence such as geochemical and geothermal data. DOE may choose to use a vertical one-dimensional (1D) model to simulate infiltration. However, in that case, DOE should reasonably show that the fundamental effects of heterogeneities, time-varying boundary conditions, evapotranspiration, depth of soil cover, and surface-water runoff have been considered in ways that do not underestimate infiltration.

(2) Staff shall determine whether DOE has: (1) appropriately analyzed infiltration at appropriate time and space scales; and (2) has tested the abstracted model against more detailed models to assure that it produces reasonable results for shallow infiltration under conditions of interest. Recent studies by NRC (Stothoff, et al., 1996) and the DOE (Flint, et al., 1994; Flint and Flint, 1995; Flint, et al., 1996a) suggest that shallow infiltration is relatively high in areas where rocks are covered with shallow soils or channels and relatively low in areas where soil cover is deep. In addition, infiltration takes place episodically in time with areas having a shallow soil cover contributing more frequently.

(3) Staff shall determine whether DOE has characterized shallow infiltration in the form of either probability distributions or deterministic upper-bound values for PA, and whether DOE has provided sufficient data and analyses to justify the chosen probability distribution or bounding value. DOE's expert elicitation on unsaturated zone flow (Geomatrix, 1997) resulted in various estimates of a related parameter, the groundwater percolation flux at the depth of the proposed repository (see Attachment F of this report, Table C-2). The estimated aggregate mean flux was approximately 10 mm/yr. The panelists estimated the 95th-percentile percolation flux over a range from 10 to 50 mm/yr, with an aggregate estimate of 30 mm/yr. An independent staff assessment of an

upper bound for yearly shallow infiltration under present climatic conditions is about 25 mm, which is somewhat less than the aggregate 95th percentile flux estimated by the expert panel.

(4) DOE's estimates of the probability distribution or upper bound for present-day shallow infiltration need not be refined further if DOE demonstrates through TSPA and associated sensitivity analyses that such refinements will not significantly alter the estimate of total-system performance.

(5) If used, expert elicitations should have been conducted and documented using the guidance in the Branch Technical Position on Expert Elicitation (NRC, 1996), or other acceptable approaches.

(6) Staff will determine whether the collection, documentation, and development of data, models, and computer codes have been performed under acceptable QA procedures. If they were not subject to an acceptable QA procedure, they have been appropriately qualified.

4.3.2 Technical Basis for Review Methods and Acceptance Criteria

See NRC (1997b) for a description of the technical basis for review methods and acceptance criteria for the subissue on present-day shallow infiltration.

4.4 DEEP PERCOLATION (PRESENT AND FUTURE)

The staff's technical review of DOE's treatment of deep percolation will be based on an evaluation of the completeness and applicability of the data and evaluations presented by DOE. It is expected that DOE will summarize or document the results of all significant-related studies that have been conducted in the YM vicinity. The staff will determine whether DOE has reasonably complied with the acceptance criteria listed below.

4.4.1 Acceptance Criteria

(1) It will be acceptable for DOE to estimate present-day deep percolation by using (1) a reasonable upper bound based on available data; or (2) through a demonstration in TSPA and associated sensitivity analyses that further refinement of the estimate will not significantly alter the estimate of total-system performance. In the latter case, the staff will conduct an independent analysis to judge the appropriateness of the estimate. In the VA analysis, it will be acceptable to use the aggregate distribution for areally averaged percolation flux estimated through the expert elicitation (i.e., Geomatrix, 1997). DOE's current infiltration map (e.g., Flint, et al.,1996a) may be used to account for spatial variations in percolation.

(2) DOE's estimate of future percolation will be acceptable if it provides a reasonable basis for assumed long-term average net infiltration and percolation flux. It will be acceptable to apply spatial- and temporal-average values of deep percolation through the use of an abstracted deep percolation model in PA. In arriving at spatial- and temporal-average values: variability is appropriately considered; model parameters are averaged over

appropriate time and space scales; and the abstracted model is tested against more detailed models and field observations to assure that it produces reasonably conservative dose estimates. The current understanding is that a vertical one dimensional (1D) model, capable of considering heterogeneities and time-varying boundary conditions at the ground surface, may be sufficient for such calculations above the repository, while a vertically oriented, two dimensional (2D) model or three dimensional (3D) model may be necessary below the repository.

(3) It will be acceptable for DOE to conservatively assume that the fraction of deep percolation that intercepts disposal drifts also drips onto waste packages. Technical bases should be provided for deep percolation that is considered to bypass emplacement drifts. These technical bases should use field observations, experimental data from the ESF facility, calculations based on mass balance, tracer studies, and data from natural analog sites. Likely changes in percolation rates and patterns due to climate change should also be considered. Also, the abstracted model used in PA should be tested against more detailed models and field observations to assure that it produces reasonably conservative dose estimates. It is known that the amount of deep percolation into the waste emplacement drifts is sensitive to fast flow in fracture zones. Such flow paths need to be considered in DOE's calculations.

(4) It will be acceptable for DOE to conservatively assume that all deep percolation below the repository level bypasses the bulk of the units of the CHn formation, either by lateral movement above the units or through vertical flow through fractures and faults. Technical bases should be developed for any deep percolation considered to flow vertically through the matrix of the nonwelded zone. Such technical bases should consider spatial and temporal variability and the scales at which model parameters have been averaged. Also, the abstracted model has been tested against more detailed models and field observations to assure that it produces reasonably conservative dose estimates.

(5) If used, DOE's expert elicitations should have been conducted and documented using the guidance in the Branch Technical Position on Expert Elicitation (NRC, 1996), or other acceptable approaches.

(6) Staff will determine whether the collection, documentation, and development of data, models, and computer codes have been performed under acceptable QA procedures. If they were not subject to an acceptable QA procedure, they have been appropriately qualified.

4.4.2 Technical Basis for Review Methods and Acceptance Criteria

- **Definitions**

To ensure clarity, the staff have developed definitions for various terms related to deep percolation. The terms infiltration, shallow infiltration, net infiltration, percolation, seepage, and recharge refer to flow across a boundary or datum. The NRC staff associates the term infiltration with near-surface processes and the term percolation with processes deeper in the

unsaturated zone. Emphasis is placed on the types of processes as well as on the vertical delineation in the following definitions:

Shallow Infiltration Flux - The liquid-water flux that has moved beyond the zone of evapotranspiration and remains in the rock is called shallow infiltration. In other words, this is the fraction of precipitation that has penetrated the ground surface and moved just below the zone of evaporation and the zone of plant roots. Relative to the entire UZ column, shallow connotes both a spatial delineation and a distinction of the type of processes affecting flow. Shallow infiltration incorporates the surface and near-surface processes of precipitation, runoff, heat flux, and evapotranspiration. These processes impact groundwater flow in the colluvial and alluvial sediments as well as the top few meters of bedrock. Although there may be evaporation from the fracture system down to the PTn and further, especially as suggested by the high air permeability in the TCw, the amount is not considered significant with respect to the MAI. Net infiltration is used interchangeably with shallow infiltration.

Deep Percolation Flux - The liquid-water flux below the zone of shallow infiltration that moves downward through the UZ is called deep percolation flux. Excluding lateral flow, the upper bound for the magnitude of average vertical deep percolation flux is the average shallow infiltration flux. The zone of deep percolation covers the 500 to 700 meters of the unsaturated domain below the shallow infiltration zone down to the water table. Percolation is governed by flow processes in the fractured bedrock comprising the portion of the UZ below the impact of evapotranspiration, hence the deep portion of the unsaturated column. The study of deep percolation addresses flow processes above, near, and below the repository horizon, including lateral flow, perched water formation, and matrix/fracture interaction.

Seepage Flux - The fraction of the deep percolation at the repository horizon that enters the drifts is the seepage flux. The physics of flow at the interface of the bedrock and the drift, such as capillary diversion of matrix flow around the drift and the spatial relationship between fractures and drift, determine the fraction of percolation flux above the drifts that becomes seepage flux into the drift.

Recharge - The downward liquid-water flux across the boundary delineated by the water table.

Under the assumptions of steady state and downward flow with no lateral component, all of these flux values are equal in magnitude. At YM, the assumptions are not likely valid at the drift boundary and below the repository.

Evaluation of the following topics provided key support for review methods and acceptance criteria for deep percolation.

General discussion about deep percolation
Measurements and modeling related to deep percolation at YM (Bodvarsson, et al., 1997a)
Conceptualization of site-scale flow from the near surface to the water table (Geomatrix, 1997)
Conceptualization of small-scale flow in fractures and fracture/matrix interactions
Estimates of deep percolation from geochemical, thermal, and water distribution data (Bodvarsson, et al., 1997a)

Estimates of deep percolation based on numerical simulations (Bodvarsson, et al., 1997a)
Past evidence and impact of future climate changes on deep percolation (NRC, 1997b)
Pneumatic responses at YM (Ahlers, et al., 1996; 1997)
Evidence for fast pathways (Fabryka-Martin, et al., 1997)
Calculated distribution of percolation at the repository horizon (Flint, et al., 1996a; NRC, 1997b)
Summary of deep percolation topics that warrant further analysis

4.4.2.1 General Discussion About Deep Percolation

It can be simply (and conservatively) assumed, for the purposes of PA, that all net shallow infiltration (i.e., water entering the subsurface below the root zone) within and updip of the repository footprint enters the waste packages (WP) and contacts waste. However, this assumption is not realistic. Geometric arguments alone suggest that only a small fraction of this total flux should be intercepted by the emplacement drifts because the area occupied by drifts is a small fraction of the area of the repository footprint. There are several additional ways that the fraction of shallow infiltration contacting waste may be reduced or that some portion may bypass the WPs, including

- Evaporation from below the root zone
- Lateral diversion due to capillary or permeability contrast, such as might occur at the Paintbrush Tuff nonwelded (PTn) unit
- Local lateral diversion due to capillary or permeability contrast, such as might occur at the rock/drift interface
- Lateral diversion within the drift (e.g., by drip shields or other engineered systems)

On the other hand, some heterogeneities such as fracture and fault zone may focus the infiltration into flow paths that may carry a larger fraction of flux than would normally be expected from geometric arguments alone.

If flow is predominately within the matrix, the drifts would tend to be protected through capillary-barrier effects, and migration through the UZ would tend to be quite slow (e.g., assuming 1 mm/yr fluxes and 10 percent average moisture content, water travel times for 100 m would be 10^4 yr and sorption processes might retard many radionuclides further). The relatively low permeabilities of the matrix at the repository horizon would tend to require large saturations everywhere in space and many drifts might be affected by matrix fluxes. On the other hand, if flow is predominantly through the fractures, the drifts would be less well-protected through capillary-barrier effects and travel times to the water table would be drastically reduced. Also, as permeabilities of the fractures are rather large relative to the current estimates of percolation flux, it is possible that relatively few fractures might carry the bulk of the water and only a few drifts would be contacted by a flowing fracture. Accordingly, it is important to characterize percolation flux in terms of the capacity for driving fracture flow at and below the repository horizon.

Net vertical infiltration from the ground surface is the predominant source of moisture for deep percolation, with the water table potentially contributing a small amount of water through capillary rise and vapor redistribution due to the geothermal gradient. Deep percolation patterns can be strongly dependent on the nature of infiltration due to the intermittent pattern of precipitation in arid and semiarid climates. For example, consider a homogeneous fractured welded tuff with a matrix saturated hydraulic conductivity (K_{sat}) of 10 mm/yr and a fracture K_{sat} of 10^4 mm/yr. If a source of water is applied at a steady rate of 5 mm/yr, then the fractures will not be active due to capillary effects. On the other hand, if the same total volume of water is due to an extreme precipitation event and is applied over a short period, for example 1 month out of every 10 yr, the average flow during that month is equivalent to 600 mm/yr and, at best, the matrix can carry 1.7 percent of the total flux, leaving the remainder to the fractures. Higher flux rates may occur, as a significant rainfall might be 1 cm over a period of a day (equivalent to 3,650 mm/yr). Even larger proportions of total flux may be carried in the fractures if the same total inflow is focused into small areas, such as stream channels. If the pulses are not attenuated with depth, one would expect flows at the repository horizon to be episodic and dominated by fracture flow. On the other hand, if the pulses are strongly attenuated with depth, such that average infiltration rates are sufficiently low, flows would tend to be matrix-dominated at the repository horizon. Accordingly, the episodicity of infiltration, the localization of influx, and the ability of the vertical profile to attenuate the wetting pulses are issues that should be appropriately evaluated in order to characterize the behavior of deep percolation. The use of steady-state percolation fluxes may significantly misrepresent the partitioning of deep percolation into matrix and fracture fluxes.

The ability of any method to estimate deep percolation under climatic variation is another issue to be considered. This issue is only briefly discussed in this IRSR. However, the performance of the potential repository should be assessed over periods of time long enough that climatic variation will be a factor. Percolation flux changes in response to climatic variations may be translated from changes to shallow infiltration and may primarily be reflected both in magnitude and distribution of flux. Therefore, methods for estimating deep percolation that are suitable for such long time periods are more useful for PA than methods that can only be applied for current climatic conditions.

4.4.2.2 Measurements and Modeling Related to Deep Percolation at Yucca Mountain

A wide variety of methods are used to model the movement of water in fractured porous media. Good overviews of some of the more common methods to study rock fractures and fluid flow are presented in Evans and Nicholson (1987), Bear, et al. (1993), and National Research Council (1996). Prior to the intensive work at YM, unsaturated flow in fractured porous media received little attention. Saturated fractured porous media received more attention due to topics of water supply, petroleum, and potential nuclear repository sites in other countries (Canada, Sweden, France). The development of methods to study unsaturated flow in fractured rock domains was primarily driven by YM as evidenced by the appropriate sections of Evans and Nicholson (1987), Bear, et al. (1993), and National Research Council (1996) on unsaturated flow. The methods have evolved as new information was gained. As such, the following sections contain descriptions of the current status of methodologies applied to YM, which taken as a whole, present a convergence of estimates for percolation for present day

conditions. However, specific aspects of flow at YM remain unclear thus necessitating a close review of the methods used; appropriate comments are discussed in each section.

The primary source of integrated information for UZ flow at YM is the work on the site-scale model by Lawrence Berkeley National Laboratory (LBNL). The LBNL UZ model of YM (Wittwer, et al., 1995; Bodvarsson and Bandurraga, 1996; Bodvarsson, et al., 1997a) is an ongoing synthesis of data focused on the development of numerical models that capture the important features of flow both at the site scale and at the smaller drift scale. Concurrent studies of site scale processes at Sandia National Laboratories (SNL) (Arnold, et al., 1995; Altman, et al., 1996) and at Los Alamos National Laboratory (LANL) (Robinson, et al., 1997) focus on groundwater velocities and transport of radionuclides through the UZ. Concurrent drift-scale experiments (niche and alcove) and modeling is being done by Lawrence Livermore National Laboratories (Nitao, 1997) and LBNL (Wang, et al., 1998; Birkholzer, et al., 1997a).

- **Unsaturated Zone Hydrostratigraphy**

The LBNL site-scale UZ hydrogeologic model of YM (Bodvarsson, et al., 1997a) has been the primary mechanism of data synthesis for numerical simulations. Recently the Geologic Framework Model (GFM) ISM2.0, created by the Management and Operations (M&O) contractors at YM, became the standardized model.

Following Montazer and Wilson (1984), the primary hydrostratigraphic units consist of alternating zones of moderately to densely welded, highly fractured tuffs and non- to partially-welded, highly porous tuffs. From highest to lowest, these units are:

- The Tiva Canyon Welded (TCw) unit, consisting of the moderately to densely welded portions of the Paintbrush Group.
- The PTn unit, consisting of the partially welded to nonwelded portions of the Tiva Canyon Tuff underlying the TCw, alternating layers of bedded tuffs of the Yucca Mountain Member and Pah Canyon Member and the partially welded to nonwelded portions of the Topopah Springs Tuff.
- The Topopah Springs Welded (TSw) unit, consisting of the moderately to densely welded portions of the Topopah Spring Tuff.
- The CHn unit consisting of the formations underlying the basal vitrophyre of the TSw and including the nonwelded to partially welded portions of the lower part of the Topopah Spring Tuff, the Calico Hills formation, the Prow Pass Tuff of the Crater Flat Group, and the nonwelded to partially welded portion of the Bullfrog Tuff of the Crater Flat Group.
- The Crater Flat Undifferentiated (CFu) units consisting of the lower Bullfrog and Tram Tuffs of the Crater Flat Group (only found in the UZ below Yucca Crest south of the repository).

Table 1, taken from Hinds, et al. (1997), illustrates the relationship between the hydrostratigraphic units and the geologic units as delineated by Buesch, et al. (1996). The geologic units are illustrated in cross-sections (Figure 2) from Hinds, et al. (1997). Detailed geologic descriptions of the PTn subunits are in Moyer et al. (1996) with the description of the fracture characteristics in Sweetkind, et al. (1995, 1997). Descriptions of the CHn and Prow Pass Tuff are found in Moyer and Geslin (1995) and Loeven (1993). Measurements of core samples including porosity, saturation, bulk density, and permeability for the major hydrostratigraphic units are reported in Flint (1997). A synthesis of the stratigraphic and fracture data, as combined with a geologic site-scale model into a hydrostratigraphic model, is described in Bandurraga and Bodvarsson (1997) and Sonnenthal, et al. (1997a).

In general terms, the nonwelded bedded tuffs have high porosities and low fracture frequencies, whereas the welded tuffs typically have low matrix porosities and high fracture frequencies (Hinds, et al., 1997). In terms of fracture data, there is a high density of fractures near vitric (both crystal-rich and crystal-poor) and nonlithophysal units, relatively high fracture density within nonlithophysal as compared to lithophysal units, relatively lower fracture density within the nonwelded PTn, and very low fracture density within the CHn. Features that increase matrix porosity and hydraulic conductivity are a lower degree of welding and the presence of lithophysae in the welded units.

The TCw hydrostratigraphic unit is subdivided into 3 model layers (Table 1) for the LBNL site-scale model. As an indication of the importance of fracture flow in the TCw, the delineations preserve units of generally similar fracture characteristics (Sweetkind, et al., 1997). As the uppermost unit, the TCw varies in thickness based on erosional features. The PTn

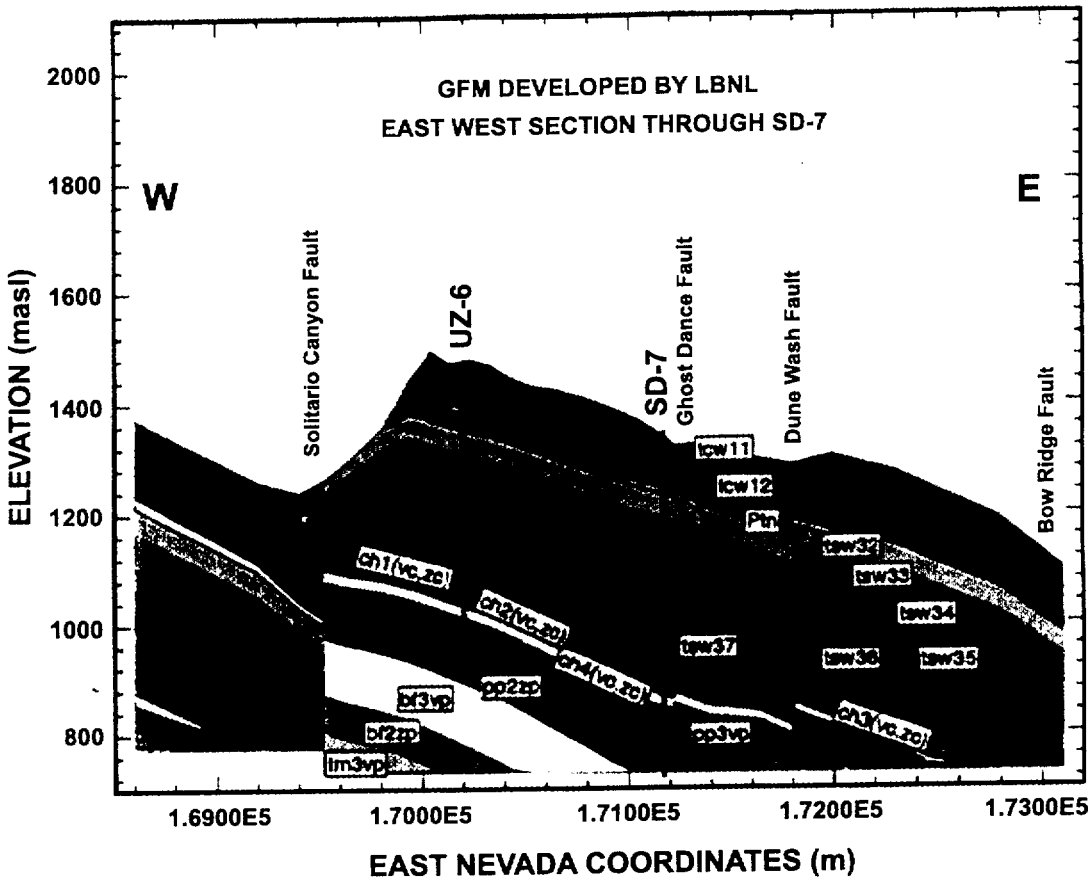

Figure 2. East-west geologic cross-section across the repository from Hinds, et al. (1997).

Table 1. Relationship between model hydrogeological units and geological formation (Lawrence Berkeley National Laboratory geological model from Hinds, et al., 1997)

Geological Unit	Welding Intensity/Formation Name (Buesch, et al., 1996)	Model Layer Name	Hydrogeological Unit
Paintbrush Group			
Tiva Canyon Tuff	M,D[1] (Tpcxxxx)	tcw11 tcw12	Tiva Canyon
	D-Basal vitrophyre (Tpcpv3) M (Tpcpv2)	tcw13	
	N,P (Tpcpv1)	ptn21	Paintbrush
Bedded Tuff	N (Tpbt4)		
Yucca Mountain Tuff	N,P,M (tpy)	ptn22	
Bedded Tuff	N (Tpbt3)	ptn23	
Pah Canyon Tuff	N,P,M (Tpp)	ptn24	
Bedded Tuff	N (Tpbt2)	ptn25	
Topopah Spring Tuff	N,P (Tptrv3)		
	M (Tptrv2) D-Upper vitrophyre (Tptrv1)	tsw31	Topopah Spring
	M,D (Tptrn)	tsw32	
	M,D,L[2] (Tptrl) M,D,L (Tptpul)	tsw33	
	D (Tptpmn)	tsw34	
	M,D,L (Tptpll)	tsw35	
	D (Tptpln)	tsw36	
	D-Basal vitrophyre (Tptpv3)	tsw37	
	N,P,M; may be altered (Tptpv1, Tptpv2)	ch1(vc or zc)	Calico Hills
Bedded Tuff	N; may be altered (Tpbt1)		
Calico Hills Formation	N; unaltered (Tac-vitric)	ch2(vc or zc)	
	N; altered (tac-zeolitic)	ch3(vc or zc)	

Geological Unit	Welding Intensity/Formation Name (Buesch, et al., 1996)	Model Layer Name	Hydrogeological Unit
Bedded Tuff	N; may be altered (Thtbt)	ch4(vc or zc)	
Crater Flat Group			
Prow Pass Tuff	N; may be altered (Tcp) Unit 4[3]		
	P,M Unit 3	pp3vp	
	N,P; generally altered Units 2,1	pp2zp	
Bedded Tuff	N; generally altered (Tcpbt)		
Upper Bullfrog Tuff	N;P; generally altered (Tcb)		
Middle Bullfrog Tuff	P,M	bf3vp	
Lower Bullfrog Tuff	N,P; generally altered		Crater Flat Undifferentiated
Bedded Tuff	N; generally altered (Tcbbt)	bf2zp	
Upper Tram Tuff	N,P; generally altered (Tct)		
Older tuffs and lavas	Generally altered (Tct)	tr3zp	
		tr2zp	

[1]Welding Intensity N=Non P=Partially; M=Moderately; D=Densely
[2]L=Lithophysal Zone
[3]Units per Moyer and Geslin (1995)

hydrostratigraphic unit is subdivided into 5 model layers that generally correspond to both the lithostratigraphic units of Buesch, et al. (1996) and the delineations based on pneumatic testing (Sweetkind, et al., 1997). The overall thickness of the PTn varies from about 20 m in the south to 170 m in the north in the area of the LBNL site-scale model (Wittwer, et al., 1995). The 7 model layers of the TSw hydrostratigraphic unit correspond to lithostratigraphic units of Buesch, et al. (1996). The delineations correspond to variations in porosity, saturation, and capillary pressure measurements. The overall thickness of the TSw is greatest in the center of the LBNL site-scale model area and decreases to the north, varying from 340 m to 50 m thick (Wittwer, et al., 1995). The Calico Hills hydrostratigraphic unit is divided into 7 model layers of which the top 4 model layers may transition from vitric to zeolitic. The Calico Hills hydrostratigraphic unit includes a portion of the basal TSw vitrophyre, the Calico Hills Formation, Prow Pass, and upper portion of the Bullfrog Tuffs. The thickness of the Calico Hills

Formation ranges from about 30 m in the southwest to 300 m in the north, whereas the Prow Pass Tuff varies from about 200 m in the east to 80 m in the west (Moyer and Geslin, 1995).

The LBNL and the ISM2.0 models correlate well except for several instances of grouping of layers in the latter model, and for the delineation of units below the TSw (Hinds, et al., 1997). The Calico Hills hydrostratigraphic unit is a zone of the geologic section that is particularly important to repository performance. The LBNL model uses altered zones as a basis for sublayering and delineates a transition within each sublayer based on a threshold zeolite weight percent. The LBNL model follows the Moyer and Geslin (1995) interpretation that describes a gap in the alteration in the southwest portion of the repository that extends through all sublayers of the CHn. However, Chipera, et al. (1997) state that there is no gap in the alteration. LANL site-scale modeling (Robinson, et al., 1997) uses the ISM2.0 geologic framework model and adds a mineralogic model that modifies CHn sublayer properties in order to incorporate hydrologic properties of zeolites in the CHn unit. In contrast, the LBNL modeling (Hinds, et al., 1997) assigns appropriate hydrologic property values to zeolitic and to vitric model sublayers of the CHn. This topic is discussed in more detail in a later section.

Structural features of importance to flow in the UZ are faults, fractures, joints, and bedding planes. These discontinuities form interconnected networks at varying scales. The central part of YM is a relatively undeformed block of Miocene tuff bounded on the west by the Solitario Canyon Fault (SCF) and by the Bow Ridge fault (BRF) located about 3.5 km to the east (see Figure 2). These block-bounding faults have predominantly dip-slip separations with cumulative displacements between 100 and 1000 m (Day, et al., 1997; Scott, 1990). Both dip moderately to steeply to the west (Day, et al., 1997). Within the YM block are north-south striking normal and northwest-southeast striking dextral strike-slip faults. These secondary faults are often discontinuous or *en echelon* and have displacements between 1 and 50 m. The Ghostdance Fault (GDF) is one of the largest intrablock faults, having up to 25 m of dip-slip offset separation. It is discontinuous at the surface. The Sundance (SDF) and Drill Hole Wash (DHW) faults are two of the better known strike-slip faults. Because of localized fracturing and the possible connectivity through numerous thermal mechanical units associated with the structures, these faults can be important to groundwater flow in the UZ. On a smaller scale, the fracture and joint systems and bedding planes are also important to groundwater flow in the UZ. Fracture systems may cross or interfinger across lithologic and thermal-mechanical boundaries. Cooling joint systems are generally confined within thermal-mechanical units (e.g., Sweetkind, et al., 1997). Each thermal-mechanical unit has a characteristic set of fracture and joint attributes, including orientation, distribution, intensity, and length (e.g., Sweetkind and William-Stroud, 1996). Lateral flow along sub-horizontal cooling joints, fractures, and bedding planes can be locally important to flow in the UZ. Layering in the fault blocks dip 5 to 15 degrees to the east (Day, et al., 1997). Details of the important structural features and lithologic and thermal mechanical layering of YM are summarized in the Structural Deformation and Seismicity (SDS) IRSR (NRC, 1998a).

4.4.2.3 Conceptualization of Site Scale Flow from the Near Surface to the Water Table

The NRC conceptual model of flow from the near surface to the water table is broadly similar to the conceptual model proposed by Montazer and Wilson (1984). The Montazer and Wilson (1984) conceptual model has been generally supported by subsequent field studies and

modeling. The work presented by Bodvarsson and Bandurraga (1996) and Bodvarsson, et al. (1997a), using available field observations to calibrate 1D, 2D, and 3D models, provides updated support for the Montazer and Wilson (1984) conceptual model. The conceptual models and measurements were reviewed by an expert-elicitation panel (Geomatrix,1997), reinforcing the general agreement on conceptual models and elucidating disagreements. The following discussion presents the NRC conceptual model.

Water that flows through the zone of potential evapotranspiration, thus becoming net shallow infiltration, is believed to proceed via rapid flow through the highly fractured and relatively impermeable TCw matrix to the less fractured but highly porous and permeable PTn unit. The notion that fast flow occurs through the TCw is supported by the extensive presence of bomb-pulse ^{36}Cl throughout the TCw and into the top of the PTn. Pneumatic pulses are minimally attenuated within the TCw, suggesting that fast pathways are available for moisture flow as well. Rapid changes in gas pressure and temperature in boreholes, attributed to a pulse of water from a previous season (Bodvarsson and Bandurraga, 1997), are additional evidence suggesting that water moves quickly through the TCw. Velocities in the TCw may be as high as tens of meters per year based on the ^{36}Cl, temperature and gas pressure data. Once water moves below the rooting zone, some removal of vapor is believed to occur due to air flow within the TCw bedrock. Estimates for vapor removal, in terms of water flux, range from 0.1 mm/yr for a local value (Rousseau, et al., 1996) to 0.02 mm/yr (E. Weeks, presentation at the Unsaturated Zone Expert Elicitation Workshop, February 4, 1997).

As the water enters the PTn unit, the rate (and perhaps direction) of flow changes. Capillarity and the large storage capacity of the PTn may strongly dampen infiltration pulses, as is shown by numerous modeling studies. Depending on the fluxes from infiltration and the hydraulic properties of the PTn, water may pass through the PTn to the TSw unit through several pathways:

- Predominantly vertical movement through the matrix of the PTn, thereby strongly damping out infiltration pulses.
- Predominantly vertical movement through the PTn, with some local lateral flow focusing water into slump faults, thereby damping out infiltration pulses to a lesser extent.
- Predominantly vertical movement through local fast pathways formed by small-scale heterogeneities in the PTn matrix, thereby bypassing the bulk of the matrix and not strongly damping out infiltration pulses. In modeling exercises, this component of movement is termed fracture flow, but field observations do not support significant fracture flow *per se*.
- Lateral movement downdip at a permeability barrier at the base of the PTn, thereby damping pulses but perhaps significantly redistributing water to the east. The redistributed water may be focused into larger faults or may move into the fracture system to the west of the Ghost Dance Fault. Infiltration pulses are expected to be strongly dampened.

- Lateral movement downdip at the capillary barrier at the base of the TCw, again with a potential for focusing flows into larger faults or the fracture system. TCw matrix waters are likely to move downdip at a steady state, but only a small component of flux is likely to be involved. TCw fracture waters are likely to move downdip in (possibly large) transient pulses if the stratabound TCw fractures are not well connected to the PTn matrix.

There is substantial evidence suggesting that fast flow paths exist through the PTn (e.g., geochemical and bomb-pulse data below the PTn). These fast flow paths may carry a substantial portion of the entire infiltration flux. The actual pathways by which flow bypasses the PTn have not been determined. Most current DOE modeling efforts predict that bypass flows are predominantly vertical, as does expert elicitation (Geomatrix, 1997).

As with the TCw unit, flow in the TSw is believed to be predominantly in the fracture and fault systems. Strong damping of wetting pulses in the PTn would cause all flows below the PTn to be approximately steady state. The TSw matrix is likely to be approximately at a steady state regardless of the PTn, due to its low matrix permeability. If bypass fluxes are minimally damped, TSw fracture flows may be transient. The TSw matrix water contents are near saturation values, with little capacity for capillary action, and thus minimal fracture/matrix interaction is expected. The disparity between geochemical signatures of pore waters and perched waters further suggests that the matrix has little connection with fast paths. The fine pores of the TSw matrix are likely to provide a strong capillary barrier to entry into mined cavities, even if backfill were to be emplaced, so that water in the matrix is likely to be diverted around the cavities. On the other hand, TSw fracture flows have less of a capillary barrier to overcome in order to enter mined cavities, particularly if backfill were emplaced, so that the dominant mode of water entering drifts is likely to be through TSw fracture flow.

Portions of the vitric non-welded tuff in the Calico Hills formation have been altered into zeolitic horizons. These zeolitic horizons may represent the single most effective barrier for radionuclides between the repository horizon and the water table. Combined with the hydraulic barrier represented by low fracture densities and low matrix permeability, the large adsorptive capacity of these zeolitic horizons provides a significant geochemical barrier to radionuclide transport (RT), realized only if flows do not bypass the bulk of the zeolitic horizons through vitric horizons or fast pathways. Perched-water bodies are present in portions of the repository footprint where significant zeolitization is present, suggesting that vertical percolation is slow in these areas. The absence of perched water bodies where the vitric units have not been zeolitized suggests that any percolation fluxes entering these zones can be accommodated through vertical percolation. Further, lateral flow from the perched water bodies may divert substantial quantities of water away from the zeolitic units into vertical flow through the vitric units. There may also be substantial lateral flow into faults such as the GDF, or downdip to the east of the GDF. If lateral flow is significant along the top of zeolitic units, the volume of the perched water bodies may be controlled by geometric factors (e.g., particular perching height may be required to encounter a lateral fast pathway) rather than by the hydrostatic pressures required to force waters through low-permeability zeolitic zones. If any of these potential lateral-flow pathways carry significant quantities of water, rapid transport to the water table may be considerably facilitated.

The factors affecting deep percolation most, from the standpoint of repository performance, are related to initiation and sustenance of fast-pathway flow. Transport of radionuclides from non-backfilled drifts is likely to be minimal if there is not significant fracture flow in the TSw. Transport from the repository to the water table is likely to be very slow for pathways significantly occurring within the matrix. Accordingly, later sections address issues regarding fast pathways and fracture/matrix interactions in some detail.

4.4.2.4 Conceptualization of Small-Scale Flow in Fractures and Fracture/Matrix Interactions

Flow through an unsaturated, fractured rock involves two systems - matrix and fracture - that exhibit greatly different hydraulic behavior. Assuming isothermal conditions, liquid flow is governed by capillary, gravity, and viscous forces. As these effects are relatively well understood in the porous media representation of the matrix, most of the uncertainty in combined systems is associated with describing flow in the fractures. In contrast to porous media flow and transport theories, there are no widely acceptable theories for the study of fracture flow under unsaturated conditions (Bagtzoglou, et al., 1994). The flow process that dominates repository performance, flow in the fracture system, is also the process with the most uncertainty. Four issues pertinent to fracture flow in the UZ will be discussed in this section: flow in small-aperture fractures, flow in large-aperture fractures, matrix/fracture interaction, and the distinction between discrete fracture and dispersed fracture flow.

The classical view of flow in unsaturated, fractured rocks is that flow will not occur in fractures unless the matrix is saturated. Unsaturated fractures were viewed as barriers to flow because of capillary forces that preferentially draw water into finer matrix pores. Given low estimates of average annual infiltration rates for YM, minimal flow in fractures would be expected due to the capillary forces. Another model of flow in fractured rocks is based on transient wetting pulses in the fractures, occurring due to precipitation events that promote fracture saturation at the ground surface. The wetting front in the fractures is not likely to coincide with the front in the matrix unless the matrix and fractures are strongly coupled. A pulse initiated near the ground surface penetrates to depth based on the connectivity of the fracture system and the properties and conditions of the pathway. These two views of flow in fractured rocks can be considered as modes corresponding to different stresses at the ground surface (National Research Council, 1996).

Fractures are void spaces. An understanding of the control that void space geometry plays on hydraulic flow properties is important in ascertaining the appropriateness of models developed to match conditions or predict future behavior. Fractures are often visualized as parallel plates separated by a gap, the fracture aperture. A more accurate and meaningful conceptualization accounts for areas where surfaces are in contact and areas with no contact, which can also be viewed as large-scale differences in roughness between the two sides of the fracture (National Research Council, 1996). The points of roughness between the two sides of the fracture will lead to partial saturation of the fracture as the matrix saturation is increased. Following the model of Peters and Klavetter (1988), flux in the fracture begins to exceed the flux in the matrix as the matrix becomes saturated. Any amount of percolation above the transmission capacity of the matrix will be in fractures. Often used for quick estimates, transmission capacity of the matrix is generally taken as a direct function of the effective conductivity at the steady state

matrix saturation; the limiting case, assuming no ponding above the matrix, is a unit gradient under saturated conditions.

The voids of a fracture form a planar interconnected network, thus the analogy with porous media. However, the fracture voids are limited to a 2D (albeit not necessarily smooth) plane, thus increasing the possibility of phase interference over that of 3D porous media. Phase interference, or capillary exclusion, occurs when one phase in the plane of the fracture creates barriers to flow of the other phase. Fine fractures imbibe water, which then has the potential to block further water movement because of capillary effects in small apertures. In large-aperture fractures, film flow may occur that is impacted not by capillary forces across the width of the fracture but rather by the roughness of the fracture wall on which flow is occurring (Brown, 1987). For unsaturated flow in fractures, therefore, the geometry of the flowing pulse may differ from the aperture geometry (Glass, et al., 1996).

Transient, nonequilibrium flow in response to surface infiltration processes is another mechanism that initiates and sustains fracture flow. Flint, et al. (1996a) suggested that significant infiltration events occur at YM, on the average, once every 5 yr, noting that there were major runoff events in 1969, 1983-84, 1991, and 1995. Based on watershed modeling in Solitario Canyon using historical precipitation data, Woolhiser, et al. (1997) suggest that large runoff events, and hence large possible infiltration events, occur once or twice every 10 yr. A large pulse of water entering the fracture system near the ground surface may percolate at a high rate in large open fractures as sheet or rivulet flow. Fracture flow in this situation will be driven by a combination of viscous and gravity forces, and the 2D pore structure of the fracture.

Factors which affect the depth to which transient pulses of water may travel are the matrix saturation adjacent to the fracture, the water sorptivity of the matrix, the presence of fracture coatings, and the fracture aperture. Near-saturation matrix water contents, low matrix sorptivity, and low-permeability fracture coatings will all promote penetration of transient pulses to greater depths. Measurements by Thoma, et al. (1992) and simulations by Soll and Birdsell (1998) illustrate the strong impact that fracture coatings have on imbibition into the matrix. Small-aperture fractures would have the tendency to produce more tortuous paths and a higher possibility of phase interference due to capillary forces; if positive pressure heads drive the pulse, however, the impact of capillarity is lessened. If the flow of water is along rivulets in the rough-surfaced fractures rather than as sheet flow along smooth fractures (Kapoor, 1994), pulse penetration to greater depths is supported by reduction of the surface area available for imbibition. Measurements and observations by Tokunaga and Wan (1997) demonstrate that water preferentially flows in fractures with rougher walls. Flow in rough-walled fractures has been numerically simulated by Preuss and Tsang (1990), Tsang (1984), Tsang, et al. (1988), Brown (1987), and Silliman (1989). Coatings on the footwall and not the hanging wall of some fractures or faults at YM indicate that sheet or rivulet flow occurs in at least some fractures or faults at YM.

Paces, et al. (1998a) describe the distribution and isotopic composition of hydrogenic minerals in fractures and cavities in the ESF. The presence or absence of coatings in fractures may not be a good indicator of which fractures would likely carry flow. The chemistry of the fluids migrating down the fracture system would be expected to control whether precipitation or flushing (dissolution) is occurring. The fluids could either be undersaturated or oversaturated with respect to the minerals in the coatings. For example, percolating water that is

undersaturated with respect to calcite would not lead to precipitation of calcite along the water pathways, and hence, the fractures with no coatings would be expected to carry the percolating water. If the percolating water is oversaturated with respect to calcite, then calcite would be precipitated along the flow path, and hence, the fractures with coatings would be expected to carry the percolating water. Another possibility is that the percolating water is initially undersaturated with respect to calcite, but evaporation along the pathway causes the water to become oversaturated. Coatings on open fractures in the ESF imply that the percolating sheet flow was either oversaturated initially or became oversaturated due to evaporation. For the latter case, the strong air connectivity of some large fault features to the atmosphere at the surface may allow for evaporation to be significant even at large depths. If a significant amount of the percolation occurs in large aperture fractures, where coatings occur on the footwall, the implication for fracture/matrix interaction is that the portion of the fracture surface across which flow to the matrix may occur could be reduced. Dependent on the hydraulic properties of the coatings, they may restrict or enhance fracture/matrix interaction. Since the water chemistry of percolating water is poorly constrained at YM, it is prudent to consider that all possibilities of water chemistry occur, and therefore, all fracture pathways should be considered.

Approaches used to model fracture flow and matrix/fracture interaction draw on classic porous flow concepts. Parameters used for the modeling are briefly described below along with brief mention of some of the limitations due to molding classic porous media concepts to fracture flow. Under the assumption that the fractures can be modeled as a classic porous media continuum, hydraulic properties valid for a representative elementary volume of fractures are needed. Air-permeability tests are used to infer indirect information on, and constrain the range of values for, the unsaturated constitutive relationships for water retention and relative permeability. However, inverse modeling is relied upon for their determination for each sublayer in the LBNL model (Bandurraga and Bodvarsson, 1997). Conceptually, the step from air permeability to constitutive relations is through variability of fracture spacing and fracture apertures. The constitutive relationships used for porous media are applied to estimate the fracture-continuum properties. No measurements of unsaturated-fracture constitutive relationships have been made at YM, although they may be highly variable given the range of fracture geometries and the nature of unsaturated flow in rough-walled fractures. Glass, et al. (1996) demonstrated that air entrapment in fractures can lead to prominent hysteresis in the constitutive relations. Reitsma and Kueper (1994) illustrate a technique to measure water retention curves on a single fracture; however, they noted that the Brooks-Corey relation was more applicable than the van Genuchten relation (which is usually used at YM) due to the physics of water entry into fractures. Given the small amount of hydrologic data on fractures at YM, the unsaturated parameters are primarily determined by inverse modeling (Bandurraga and Bodvarsson, 1997).

Two parameters have been introduced into unsaturated zone modeling at YM to link flow in the tuff matrix to flow in the fracture system. The first factor, matrix/fracture conductance, is essentially the fracture surface area multiplied by an imbibition rate into the matrix. Model calibrations suggested that the potential conductance was too large to match the data (Bandurraga and Bodvarsson, 1997). Accordingly, the fracture surface area fraction became a calibration parameter, justified by qualified observations of channeling or rivulet flow in fractures. A second factor, satiation, was included in models using similar arguments of difficulty in matching model results to field observations. Capillary theory dictates that flow from the matrix into a fracture will not occur until the matrix is fully saturated (Bear, et al., 1993). The

term satiation was introduced to account for flow initiating in the fractures at pressure heads slightly less than atmospheric. In measurements of flow along fractures in the nonwelded Bishop tuff, Tokunaga and Wan (1997) found that film flow in the fracture had velocities of 2 to 40 m/d at -250 Pa, although the volumetric rate may not be significant. Tokunaga and Wan (1997) note that similar behavior may occur at much greater suctions in welded tuffs. Three reasons can be used to justify using a satiation value less than full saturation. The first argument is based on small-scale heterogeneities leading to local areas of saturated matrix adjacent to fractures even though the larger-scale average of matrix saturation is less than one. A second argument is nonequilibrium of the matrix in the vicinity of the fracture. Matrix saturations may reach full saturation adjacent to the fracture, but the rest of the matrix, some distance from the fracture, remains relatively drier. The third argument addresses the conceptualization of fractures as smooth parallel plates. Small-scale surface roughness on the fractures, or heterogeneities of the fracture surface leading to "point connections" (Glass, et al., 1996), may lead to wetted regions and contact points where water may enter the fracture.

The NRC staff considers that spatial and temporal variations in flux through the YM unsaturated flow system are dominated by the fracture flow system, particularly in welded and altered layers. Defining the flow system requires either detailed data on the fractures, especially those that dominate the flow system, or detailed information on the hydrologic response. At YM most of the available fracture data for the UZ has been obtained from the ESF. The east-west drift (enhanced characterization of the repository block, or ECRB) will likewise add to the fracture data base. However, it is difficult to directly evaluate modes and rates of water flow through fractures and faults in unsaturated rocks. In addition, little is known about the mechanisms and parameters that control flow: (i) between matrix and fracture; (ii) in open and coated fractures; (iii) in capillary films, sheets, or rivulets in open fractures; and (iv) along fracture planes and intersections. When insufficient data are present, the necessary fracture flow parameters can be estimated by inverse modeling given the constraints of other information at YM such as thermal and geochemical data and the presence and extent of perched water bodies. Groundwater tracers such as ^{36}Cl and ^{3}H are especially useful for detecting zones of enhanced downward flow in the UZ. Given the uncertainty, field observations and measurements should be a critical part of validating both site-scale and drift-scale models.

4.4.2.5 Estimates of Deep Percolation Based on Geochemical, Thermal, and Water Distribution Data

There is a wide variety of information and approaches for estimating deep percolation at YM. Geochemical, thermal, and water saturation conditions can potentially be used to indirectly estimate residence times, percolation rates, or volumetric flux rates. Table 2 contains a partial list of shallow infiltration and percolation flux estimated using different methods. Here, percolation flux is taken to be equal to the shallow infiltration rate under the assumptions of steady state, vertical flow. Most estimates prior to 1990 were less than 5 mm. Over time the estimates have increased, with an apparent convergence on the range 1 to 10 mm/yr for an areally averaged mean annual rate of percolation. Locally, infiltration and deep percolation can exceed this average range or can approach zero.

Table 2. Estimates of shallow infiltration and deep percolation rates under current climatic conditions using different methods (in approximate chronologic order).

Estimate (mm/yr)	Location	Methodology	Source
1.5	YM	elevation & precipitation	Rush (1970)
2	Yucca Flat	parameter values	Winograd (1981)
1 to 10	YM	drill hole geothermal	Sass and Lachenbrush (1982)
4	YM	elevation & precipitation	Rice (1984)
0.5	YM	matrix Ksat data	Sinnock, et al. (1984)
0.5 to 2	YM	elevation & precipitation	Czarnecki (1985)
0.1 to 0.5	UZ-1	core & *in situ* data	Montazer, et al. (1988)
2 to 5	YM	drill hole geothermal	Sass, et al. (1988)
0 to .001	H-1	core data	Gauthier (1993)
4 to 35.1	UZ-4,5,7	Tritium and ^{14}C	Kwicklis, et al. (1993)
0.6 to 1.9	YM	1D modeling	Long and Childs (1993)
0 to 5.4	YM	Cl mass balance	Fabryka-Martin, et al. (1994)
6 to 15	YM channel	bomb-pulse ^{36}Cl	Fabryka-Martin, et al. (1994)
0 to 13.2	YM	outcrop Ksat data	Flint and Flint (1994)
0.001 to 0.5	YM	3D UZ site-scale	Wittwer, et al. (1995)
0.1 to 10	YM	inverse modeling	Bodvarsson and Bandurraga (1996)
1.7	YM	1D modeling	EPRI (1996)
6.5	YM	100-yr 1D modeling	Flint, et al. (1996)
0.1 to 18	north YM	heat flux	Rousseau, et al. (1996)
0.001 to 0.29	north YM	perched water balance	Rousseau, et al. (1996)
1.8 & 3.4	ESF	fracture coatings	Marshall, et al. (1998)
1 to 15	YM	3D UZ site-scale	Wu, et al. (1998)
3.9 to 21.1	YM	expert elicitation	Geomatrix (1997)

Some of the methods provide only indications of pathways whereas other methods provide flux estimates that may be reflective of bulk response of the system. Percolation rate is taken to be a Darcy flux, the average flow perpendicular to a cross-sectional area. Pore-water velocity, particle velocity, and seepage velocity all refer to the velocity of a solute or water particle from one point to another point. The Darcy flux is related to the particle velocity by an effective porosity, or water content if unsaturated, through which the flow occurs. The effective porosity, or water content, may be difficult to determine, especially for the individual portions of dispersed fracture and fast-pathway fracture flow. The presence of environmental tracers at different depths at YM provides indications of pore-water velocity along a pathway with no indication of the amount of flow between two locations unless a mass balance can be developed, or it can be shown that the environmental tracer moved in all the fractures pathways, not just a portion.

The following subsections focus on various approaches for estimating rates of deep percolation. Key citations are noted.

In Situ Observations and Measurements (Wang, et al., 1997)

Net Shallow Infiltration Related to Deep Percolation (Flint and Flint, 1994; Flint, et al., 1996a).

Temperature Gradients and Heat Fluxes (Sass, et al., 1988; Wittwer, et al., 1995)

Isotopes (Fabryka-Martin, et al., 1997; Yang, et al., 1996b)

Chloride Mass Balance (Fabryka-Martin, et al., 1997)

Saturation and Water Potential (Flint, 1997)

Fracture Coatings (Paces, et al., 1996b; Marshall, et al., 1998)

Perched Water (Wu, et al., 1996)

- ***In Situ* Observations and Measurements**

Damp fractures or joints that quickly evaporate due to the required ventilation have been observed at the ESF. Seeps in niches and alcoves of the ESF also evaporated rapidly when exposed to the ventilation. Closing off niche 3566 (near the SDF) after finding a seep allowed re-equilibration of the relative humidity in the niche but no visual rewetting of the seep, reported Wang, et al. (1997). Damp features have also been noted in niche 3650 and the ESF directly. At the Expert Elicitation for Unsaturated Flow (Geomatrix, 1997), reference was made to an estimate of deep percolation based on vapor flow and the shutdown of the ventilation system on weekends. It was established that the average moisture flux from the rocks into the ESF was 50 mm/yr (Geomatrix, 1997). The ambient percolation flux within the rock does not exceed the transfer rate with the ESF in place, hence the 50 mm/yr would be an upper limit.

Given its close proximity and similar lithology, Rainier Mesa is considered a possible analog site for YM. Percolation estimates from seepage into the tunnels at Rainier Mesa are approximately 24 mm/yr under current mean annual precipitation of 320 mm (Russell, et al., 1987; Wang, et al., 1993), or about 8 percent of the precipitation.

- **Net Shallow Infiltration Related to Deep Percolation**

Infiltration is the source of virtually all deep groundwater flux in the UZ. This section summarizes, for completeness, the detailed discussion of infiltration modeling approaches of both NRC and DOE at YM that was provided by NRC (1997b). Models of infiltration processes provide information on the spatial and temporal variation of net infiltration, which can then be used as boundary conditions in models of deep subsurface processes. Infiltration models and deep subsurface models consider time scales so disparate that it would be computationally infeasible to consider infiltration processes and deep subsurface processes simultaneously. There are sufficient uncertainties arising from the use of infiltration models, including lack of understanding of flow processes, lack of knowledge of parameters, and lack of resolution, that infiltration models cannot be relied on to provide accurate estimates of infiltration magnitudes without significant corroborating evidence. Infiltration models can provide estimates of the spatial distribution of relative magnitudes and frequencies of wetting pulses. Most importantly, infiltration models may provide the primary source of information regarding infiltration and deep percolation under future climates.

The infiltration maps provided by Flint, et al. (1996a) (based on detailed 1D numerical modeling) have superseded the maps by Flint and Flint (1994) (based on matrix properties of bedrock outcrops) for use in boundary conditions in DOE site-scale and cross-sectional studies (Bodvarsson and Bandurraga, 1996; Bodvarsson, et al., 1997a; Robinson, et al., 1997). The Flint, et al. (1996a) map is derived from sequences of 50 to 100 yr of weather, applied with a daily time step, using a 30-m by 30-m grid of independent 1D infiltration simulations. The 1D bucket model for each grid element considers evapotranspiration but not lateral redistribution.

The Flint, et al. (1996a) map is generally supported by neutron-probe observations during the period of October 1984, through April 1995, which Hudson and Flint (1996) used to create an infiltration map based on regressions taking into account precipitation, elevation, geomorphic class, and soil thickness. These maps suggest that infiltration occurs primarily on ridgetops and sideslopes, where surficial materials are shallow, and little infiltration occurs where alluvium is deeper than 1 to 2 m. The base infiltration map used by Bodvarsson, et al. (1997b) provides 6.7 mm/yr infiltration over the repository footprint and 4.9 mm/yr over the site-scale model.

The NRC model (Bagtzoglou, et al., 1997; NRC, 1997b), based on abstractions of detailed nonisothermal 1D simulations, predicts roughly three times as much infiltration as does the Flint, et al. (1996a) model, but is broadly in agreement with USGS predictions of the spatial distribution of mean annual infiltration (MAI). The NRC model neglects transpiration but has much finer spatial and temporal resolution than the USGS model. The agreement between the USGS and NRC models is not unexpected, as both are based on 1D approaches and both neglect lateral redistribution.

- **Temperature Gradients and Heat Fluxes**

This section outlines the use of borehole temperature measurements at YM to estimate percolation. Solution of the conduction equation using borehole temperature measurements to infer temperature gradients, heat conductivity of each unit, estimates of heat flux, and the assumption that the heat flow in YM is controlled by conduction, leads to a temperature profile

which differs from the actual profile. The difference is interpreted to be due to either downward flux of cool water or upward flux of vapor.

Temperature data from boreholes, reported by Sass, et al. (1988) for a regional study, and by Rousseau, et al. (1996) in an area near the North Ramp of the ESF, were compared by those authors to predictions from models using the conductive heat equation. Although most of the heat flux could be explained by the conductive model, vertical heat-flux deficits were present that could be explained either by percolating water or by evaporation of water. Sass, et al. (1988) estimated that either 2 to 5 mm/yr percolation through the PTn and into the TSw or 0.1 mm/yr vaporization with 15 m/yr upward air discharge would account for the apparent deficits. The spatial distribution of infiltration rates estimated by Sass, et al. (1988), using the approach outlined above, is generally consistent with infiltration maps produced by Flint, et al. (1996a). Although vaporization and advective transport of vapor may be locally important in the highly fractured, densely welded tuffs such as the TCw, site-scale numerical modeling suggests that these effects are secondary to the effects of percolation (Rousseau, et al., 1996), particularly below the pneumatic barrier represented by the PTn. Temperature data from boreholes UZ#4 and UZ#5, in Pagany Wash, suggest that percolation may be on the order of 10 to 20 mm/yr (Rousseau, et al., 1996). In both studies, an average heat flux for the area was assumed in order to estimate percolation. Sass, et al. (1988) noted that the actual heat fluxes used in the analysis are difficult to measure.

Bodvarsson, et al. (1997c) re-analyzed the borehole data without assuming an average heat flow for the area. Percolation fluxes were estimated by matching the borehole temperature data with predictions from analytical solutions for the layered system, using both constant heat flux and constant temperature lower boundary conditions. Estimates ranged from 0 to 63 mm/yr. Low heat-flux boreholes appeared to be affected by vapor transport in the TCw, and high heat-flux boreholes appeared to be affected by proximity to fault zones. In both cases, the assumptions for the analytical solution are violated. For the remaining 18 boreholes, percolation estimates ranged from 0 to 15 mm/yr.

The thermal properties of the welded and nonwelded tuffs used in the studies are summarized by Wittwer, et al. (1995), Rautman, et al. (1995), and Rautman and McKenna (1997). Heat flux modeling by Rousseau et al. (1996) and by Bodvarsson, et al. (1997c) found that the regression equation of Rautman, et al. (1995) for thermal conductivity of the welded and nonwelded lithologies as a function of porosity, temperature, and saturation worked well in their modeling of the temperature profiles.

The different thermal properties and heat flow in the TCw, TSw, and CHn are reflected in the temperature profiles and subsequent percolation estimates. Estimates of percolation flux through the CHn are less than those estimated for the TSw (Bodvarsson, et al., 1997c). The temperature gradient through the CHn is much larger than that of the TSw, which, in part, may be explained by the lower effective thermal conductivity of the CHn. Another possible explanation is lateral flow above the zeolitic horizons of the CHn. The thermal conductivity of the CHn varies depending on the vitric or zeolitic content of the layer as well as the degree of welding and the water content. Temperature gradients and heat flux estimates in the TCw may be problematic due to the effects of vapor flow on the temperatures.

An indication of the temporal aspect of a percolating pulse was noted by Sass, et al. (1988). In 1983, about 15 months after the previous reading, temperature perturbations were observed in UE-25a#7 following a major storm. Borehole UE-25a#7 lies on or near the Drillhole Wash fault zone. The temperature response was recorded to a depth of 150 m, which Sass, et al. (1988) assessed as possibly attributable to perturbation along the borehole-annulus. If temperature fluxes along the annulus of UE-25a#7 were significant, the temperature anomalies are meaningless. Since the temperature anomaly persisted for at least 1 yr and was different from previous conditions, the anomaly may represent an infiltration event moving through the fault. If so, the moisture penetrated 47 m of alluvium, 4 m of TCw, 42 m of PTn, and 58 m of TSw in about 15 months.

- **Isotopes**

Environmental isotopes ^{36}Cl, ^{14}C, and $^{87}Sr/^{86}Sr$ have been used to estimate percolation rates and residence times as well as to confirm the presence of fast pathways at YM. As discussed by Tyler and Walker (1994), the use of bomb-pulse tracers, however, can overestimate recharge by an order of magnitude or greater when the impact of transpiration on the flow velocities is neglected.

Elevated levels of ^{36}Cl in the ESF and in boreholes at YM are traceable to global fallout in the nuclear tests from 1952 to 1958 (Levy, et al., 1997). A report by Fabryka-Martin, et al. (1997) contains the currently available set of ^{36}Cl measurements from boreholes and the ESF. Of 247 samples from the ESF, 13 percent had an unambiguous bomb pulse signal. In a straightforward approach, the presence of unambiguous bomb pulse ^{36}Cl in the ESF suggests pore-water velocities on the order of 7.5 m/yr assuming a depth of 300 m and onset of testing as 40 yr ago. However, these pore-water velocities may only represent a fraction of pathways, those that are faster preferential pathways, and may not be directly used to estimate percolation rates even for the fast pathways, since the effective porosity (or water content) for fast pathways is also unknown.

Another environmental tracer, ^{14}C, has been used not only for calculation of residence times of water but has also been used to infer velocities. Interpretation of the ^{14}C data is complex because of its transport mechanism, movement both in the aqueous and vapor phases, and carbon exchange with older calcite or younger gas. Yang, et al. (1996b) report a wide range of isotopic dates from ^{14}C data in the CHn that may support multiple origins for the perched water. The ambiguity of ^{14}C dating carries over to estimates of percolation rates. From data at a depth of 100 m in borehole UZ-25, Murphy (1995) estimated pore-water velocities of 20 to 100 mm/yr. Flow and transport models with varying degrees of geochemical complexity incorporated have been used to model borehole ^{14}C data. Using tritium and ^{14}C data, estimates are 35.1 and 20 mm/yr for UZ-4 and 4 mm/yr for UZ-5 (Kwicklis, et al., 1993). Moridis, et al. (1997) used optimization of two 1D models for wells UZ-1 and UZ-14 to determine a percolation rate of 4.2 mm/yr.

Strontium isotope ratios in pore waters are a function of dissolution and exchange with the rock as well as total strontium concentration and water percolation rates. Strontium geochemistry and isotopic ratios have been measured at only a few boreholes. Based on the analysis at one

borehole (SD-7), using the dissolution rate from fractured basalts, an estimate of percolation based on $^{87}Sr/^{86}Sr$ ratios ranges from 0.5 to 5 mm/yr (Sonnenthal, et al., 1997b).

- **Chloride Mass Balance**

The percolation flux at depth can be estimated by a meteoric chloride mass balance method by using the average precipitation rate, Cl^- concentration corresponding to the typical near-surface infiltrating water, and Cl^- concentration in a well-mixed reservoir at depth (Fabryka-Martin, et al., 1997). This method assumes that precipitation, net infiltration, and chloride deposition rates have been constant for sufficient time to reach steady state and further assumes that matrix and fracture waters have fully mixed. The chloride mass balance approach also assumes piston-like flow, a uniformly downward movement of water that displaces the initial water in the profile (Scanlon, et al., 1997). This assumption may not be valid at YM because of the potential for preferential fast flow paths in the unsaturated zone.

Estimates of percolation tabulated by Fabryka-Martin, et al. (1997, Table 5-2) were calculated using the geometric mean of Cl^- values for hydrostratigraphic units in six wells, 170 mm/yr for precipitation, and a Cl^- concentration of 0.62 mg/L for near-surface infiltrating water. Percolation estimates calculated using the Cl^- mass balance method described above for the PTn range from 1.1 to 3.4 mm/yr with an average of 2.0 mm/yr. Similarly calculated percolation estimates for the CHn range from 2.2 to 5.3 mm/yr with an average of 3.9 mm/yr, while estimates for the perched water range from 11 to 23 mm/yr with an average of 16 mm/yr. Assuming unit gradients and values of saturated hydraulic conductivity of 0.9 and 1.9 mm/yr for the TCw and TSw units, respectively, it is noted that percolation in the units above the PTn and CHn exceed their transmission capacity, the difference being indicative of the portion of total flow due to flow in fractures. Higher fractions due to fracture flow would result if effective conductivity was used instead of saturated hydraulic conductivity. Another important observation is that the perched water has lower concentrations of Cl^-, and, hence, larger percolation estimates, than the PTn. The implication is that the water reaching the perched zone either bypassed the PTn or percolated quickly through the PTn through fast paths, possibly as nonuniform fronts.

Yang, et al. (1996b) report Cl^- concentrations in perched water of 4.1 to 15.5 mg/L, with 15 of the 17 reported values no greater than 8.3 mg/L and a Cl^- concentration of 7 mg/L at NRG-7a (the nearest borehole to UZ-4 and UZ-5 with a reported perched-water sample). Using the same precipitation rate (170 mm/yr) and Cl^- concentration for near-surface infiltrating water (0.62 mg/L) as Fabryka-Martin, et al. (1997) and assuming that the perched water is well mixed with the matrix waters, calculated net infiltrations are 25.7, 12.7, and 6.8 mm/yr for concentrations of 4.1, 8.3, and 15.5 mg/L, respectively. A percolation value of about 26 mm/yr would represent an upper bound based upon the perched-water chloride data; if the matrix waters do not mix completely with the perched water, percolation values may be lower. The estimated percolation values are more consistent with the shallow infiltration estimates than the estimates from the pore-water of the PTn (NRC, 1997b), suggesting that a considerable portion of the percolating water may bypass the PTn matrix.

- **Saturation and Water Potential**

Observations of both saturation/water content and water potential can yield independent estimates of water fluxes, in addition to providing calibration data for numerical simulators. When the hydraulic characteristics of a matrix sample are known, saturation, water content, and water potential each can be used to estimate the unsaturated hydraulic conductivity. Knowing the unsaturated hydraulic conductivity at a particular water content and assuming gravity drainage, the percolation rate is directly calculated using Darcy's law. If capillary effects are negligible, so that the assumption of gravity drainage is appropriate, the vertical flux is numerically equal to the unsaturated hydraulic conductivity.

The question of whether or not gravity drainage is an appropriate assumption was addressed by Rousseau, et al. (1996) who presented *in situ* water potential measurements from five boreholes (UZ-1, UZ#4, UZ#5, NRG-6, and NRG-7a). None of the profiles had unequivocally returned to initial conditions in the time frame examined (several months to years), but, generally, it appears that, upon equilibration, all five boreholes will exhibit minimal vertical variation in water potential (implying gravity drainage) and no profile will be drier than five bars of suction. In boreholes UZ#4 and UZ#5, available core sample potentials are scattered within one or two bars of the *in situ* values; overall, the core values tend to be wetter than the *in situ* values.

The expert elicitation process (Geomatrix, 1997) revealed limitations on the use of water content and potentials for estimating percolation rates. There are two primary sources of saturation and water potential data: (1) measurements from core samples obtained during drilling; and (2) *in situ* measurements. A great number of core-sample measurements were obtained during drilling the more recent boreholes (Flint, 1997). Although care was taken during sampling to preserve *in situ* conditions in the core, some drying apparently occurred during sampling and the resulting data should be considered suspect (L. Flint, 1997, presentation to Site-Scale Unsaturated-Zone Flow Model Expert Elicitation Panel). Drying becomes more of an issue as the degree of welding increases, as the same amount of evaporation distorts the data more by removing a larger fraction of the available moisture. Independent estimates of fluxes obtained from these potentials are dependent on the independent estimates of hydraulic properties, particularly saturated hydraulic conductivity and van Genuchten α. A factor of two change in van Genuchten α (which is small compared to the uncertainty associated with the parameter) may change estimates of relative permeability by an order of magnitude. Accordingly, estimates of flux obtained from *in situ* saturations or water potentials are not considered reliable.

- **Fracture Coatings**

The percolation flux can be estimated from fracture coatings of calcite and silica (e.g., opal). It has been proposed that all of the fracture coating in the UZ was precipitated from downward percolating waters (Johnson and DePaolo, 1994). The finely layered coatings suggest periodic deposition with no textural indication of chemically undersaturated water from large pulses to dissolve the coating (Paces, et al., 1996b). In the ESF, Paces, et al. (1996b) noted that fracture coatings occurred exclusively on the footwall, that the thickest deposits were in the low-angle fractures, and that coatings occurred where apertures generally exceeded several millimeters.

Paces, et al. (1996b) and Marshall, et al. (1998) provide preliminary estimates of the percolation fluxes required to deposit calcite and opal in the form of fracture fillings and lithophysae coatings at YM. Assuming that the fracture characteristics and filling patterns observed in the ESF are representative of the entire UZ, all cations are deposited within the UZ, and infiltrating water has the composition observed under current conditions, the average percolation flux rate required to match the observed patterns is calculated to be 2.1 mm/yr for calcite and 0.3 mm/yr for opal (Paces, et al., 1996b). Marshall, et al. (1998) updated these to 3.4 and 1.8 mm/yr, respectively. As noted by Paces, et al. (1996b), these are minimum estimates, as almost certainly not all calcium and silica in the percolating water is deposited as coatings.

Dating of fracture coatings using ^{14}C measurements range from 16 to 44 kya, whereas, the ages calculated using $^{230}Th/U$ measurements range from 28 to over 500 kya (Simmons, 1996; Paces, et al., 1996b). However, sampling difficulties due to the fine layering make interpretations of the fracture coating ages using isotopic measurements difficult. The older ages for the coatings may be consistent with calcite deposition models that suggest that deposition will only occur where flux is slow. Fast moving pulses of water in the fractures might be expected to dissolve the existing calcite. The use of isotopes to date layers of fracture coatings does not appear to have produced reliable information. This may be a result of apparent ages of fracture coatings being representative of mixtures of older and younger minerals, or representative of precipitation, dissolution, and re-precipitation along flow paths.

- **Perched Water**

A summary of perched water data from YM is provided by Wu, et al. (1996). The presence of perched water in and immediately above the CHn unit can be used as a lower constraint for estimation of percolation flux. Estimates of residence times, volume estimates, material properties, and head gradients can be used in this regard. Volume of perched water is also an important constraint on calibrating the site-scale model, as noted by Wu, et al. (1997); adjustment of rock properties in the layers in and adjacent to the perched zones was required to match the volumes of water in the perched zone.

A flux estimate required to form and sustain perched water above the CHn in the vicinity of UZ-14 was made by Rousseau, et al. (1996). Seepage rates both laterally along and through the perched zone and seepage rates through adjacent vitric zones were weighted by their areal distribution to estimate the percolation through the TSw in the combined areas of the vitric and the perched zones. In addition to the residence time data, estimates of head gradient, permeability, perched water volume, and area were required. Flux through the vitrophyre below the perched zone was estimated to range from 0.0014 to 0.29 mm/yr, a range corresponding to effective porosity values between 0.001 to 0.10 (Rousseau, et al., 1996). However, since the origin of the perched water is not clear and the presence of two distinct waters in the CHn is indicated by geochemical data (Yang, et al., 1996a), estimates of percolation flux may not be reliable.

- **Summary of Deep Percolation Estimates**

There is a wide range of flux estimates, based on various methods and assumed climatic conditions. Concurrence of values from widely different approaches leads to confidence in the

estimates, leaving the extreme values as an indication of less reliability. The UZ Expert Elicitation Panel provided estimates of deep percolation, considering all presented approaches, with estimated mean values ranging from 4 to 21 mm/yr (Geomatrix, 1997).

The use of tracers to robustly estimate percolation rates in the YM area is limited. Difficulties with estimating the impacts of lateral flow and multiple pathways would appear to limit their use over most of the repository footprint. Nevertheless, unambiguous bomb pulse signatures observed at depth in the ESF are interpreted as occurring where high infiltration occurs over a zone having a fault that provides a fast pathway through the PTn unit (Levy, et al., 1997). The bomb pulse data were instrumental in demonstrating that fast pathways exist and, by implication, that, at least locally, there are areas where infiltration might be much higher than previously thought.

Despite the limitations on tracer methods, the chloride mass balance technique does provide a means of estimating an upper bound for net infiltration. The upper-bound value obtained by chloride mass balance on perched water, 26 mm/yr, is remarkably consistent with the upper-bound value obtained by geothermal heat-flux calculations.

Collectively, the geochemical, thermal, and water distribution data suggest that flow in the UZ is better represented by conceptual models that consider fast pathways and limited matrix/fracture interactions than by models which consider predominantly matrix flow. The NRC staff review should ensure that fast pathways and limited matrix/fracture interaction are reasonably represented by DOE numerical models.

4.4.2.6 Estimates of Deep Percolation Based on Numerical Simulations

Numerical modeling of flow processes at YM is unavoidable due to the large spatial and temporal scale of the repository performance relative to the scope of conceivable investigation. Numerical modeling enables observations at limited observational points and times to be extended in time and space. In modeling flow through the UZ at YM, it is important to capture both fracture flow and matrix flow processes. However, fracture flow may be more important from the perspective of PA, as releases and transport are apparently more strongly affected at YM by fracture flow than matrix flow.

A wide variety of methods and formulations have been applied to site- and drift-scale modeling at YM. Current estimates of the spatial distribution of percolation using the site-scale model of LBNL (Bodvarsson, et al., 1997a) are developed using separate, but interacting, continua for matrix and fracture systems. For drift-scale modeling, no definitive choice has been made (TRW Environmental Safety Systems, Inc., 1997a), although Birkholzer (1998) recently presented a fracture continuum model. Inherent in both scales of modeling are the estimates of physical and hydraulic parameters. As such, the first portions of this section discuss issues related to parameter estimation for matrix and fracture systems. The last portion of this section discusses alternative methods and formulations for modeling flow at YM.

- **Matrix Properties and Parameter Estimates**

A large database of bedrock physical and hydraulic properties for units at YM has been collected, correlated to lithologic structure, and analyzed for spatial trends, using samples collected from outcrops and from boreholes (Peters, et al., 1984; Klavetter and Peters, 1986; Flint and Flint, 1990, 1994; Rautman and Flint, 1992; Istok, et al., 1994; Cromer and Rautman, 1995; McKenna and Rautman, 1996; Rautman, et al., 1995; Schenker, et al., 1995; Flint, et al., 1996b; Moyer, et al., 1996; Rousseau, et al., 1996; Flint, 1997; Rautman and McKenna, 1997). Easily measured physical properties (i.e., porosity and bulk density) have been collected for most of these samples, but hydraulic properties have only been sparsely collected. Rautman and McKenna (1997) summarize the available data, much of which is described by Flint (1997) in greater detail, and extrapolate the data to model grids. Bodvarsson and Bandurraga (1996) and Bodvarsson, et al. (1997a) use much of this information to constrain values of grid-block-scale hydraulic parameters derived through inverse modeling.

Porosity is generally used as a surrogate variable for K_{sat} (Flint, 1997; Rautman and McKenna, 1997), because: (1) porosity has been measured on virtually all core samples; (2) values of other hydraulic properties have not been determined for most core samples; and (3) porosity appears to be fairly well correlated to hydraulic properties. Interestingly, a staff comparison of *in situ* water saturation and core-sample K_{sat} suggests that saturation may be a better predictor of K_{sat} than porosity. This correlation may warrant further study. In addition to K_{sat}, the van Genuchten parameters for the UZ constitutive relations are required for UZ flow modeling. Matrix retention parameters require the most effort to obtain and, therefore, have only been determined for a small number of core samples; many of the measurements exhibit a great deal of scatter both within units and for similar rock types. Accordingly, estimates of matrix retention parameters have a great deal of uncertainty.

Measurements from core samples are at a much smaller scale than typical model grid blocks (i.e., several cubic centimeters as opposed to grid blocks 1 to 100 m on a side, which is at least 8 orders of magnitude difference). One way to reconcile the disparity in scales is through inverse modeling to obtain effective properties [e.g., the LBNL 3D site-scale model approach (Bodvarsson and Bandurraga, 1996; Bodvarsson, et al., 1997a)]. Since inverse modeling approaches are inherently mathematically ill-posed and nonunique, it is most effective when only a few parameters need to be determined; thus, heterogeneity is not easily accommodated. For this reason, the LBNL inverse-modeling approach assumes that all parameters are homogeneous within each layer. It appears that each physical layer is modeled with at most two computational layers, which may tend to mask processes occurring on a sub-layer scale such as lateral diversion in the PTn unit (Wilson, 1996). Further, the LBNL inverse-modeling does not use an approach that estimates all properties simultaneously, and inconsistently estimates some properties using the assumption of 1D vertical flow despite the lateral flow exhibited in subsequent 2D and 3D simulations using the parameters. The NRC staff considers that the LBNL 3D site-scale model may be too coarse to provide more than a general indication of subsurface processes at YM but notes that significant model refinement may be computationally infeasible. Despite these reservations, NRC staff endorse the LBNL philosophy of using all available sources of information to calibrate the site-scale model, and agree that, for many purposes, homogeneous effective properties for each layer obtained through inverse modeling may be adequate.

Another way to reconcile the disparity in scales is through upscaling. Schenker, et al. (1995), attempting to estimate layer-wide hydraulic properties from core-sample data, recognized that bulk variability is usually less than the core-sample variability and, therefore, reduced the coefficient of variation for hydraulic properties according to the vertical correlation length and layer thickness.

The sophisticated approach adopted by Rautman and McKenna (1997), building upon a series of previous SNL efforts, generates heterogeneous parameter fields based on cross-correlation of hydraulic conductivity, bulk density, and thermal conductivity. A significant advantage of this approach, relative to the inverse-modeling approach, is that heterogeneity readily can be accommodated into modeling efforts. Porosity, K_{sat}, and thermal conductivity (in the TSw unit) are considered by Rautman and McKenna (1997), although the methodology could be extended to include retention parameters. The Rautman and McKenna (1997) methodology minimizes statistical artifacts potentially introduced by faults by using the depositional environment (before faulting occurred) to perform statistical analyses, although this procedure may add statistical anomalies when considering alteration (which occurred after faulting).

Despite the attractive characteristics of the Rautman and McKenna (1997) procedure, it appears that the procedure projects core-scale properties to the grid-block scale (100 m × 100 m × 2 m) rather than projecting averaged or upscaled properties. Rautman and McKenna (1997) note that the procedure does not address the issue of upscaling. However, the procedure could be adapted to generate a fine-scale set of hydraulic properties on a subgrid within each grid block; the fine-scale properties could then be formally upscaled to arrive at effective properties. Formal upscaling that accounts for flow characteristics may generate effective properties that are different from averaged properties, as noted by Rautman and McKenna (1997), who further note that advective processes (e.g., percolation) are more likely to be affected by upscaling issues than diffusive processes (e.g., heat conduction).

If one upscales using the many-tubes approximation, which assumes that the porous medium is composed of many tubes (at the scale of core samples) in parallel, all with vertical gravity flow and all at the same suction (essentially assuming that local lateral flow is not restricted), staff analysis determined that a small percentage of the tubes (local fast pathways) carry the bulk of the flow when the cores are as heterogeneous as those reported by Flint (1997) for the PTn subunits. The assumption of locally unrestricted lateral flow may be appropriate for bedding planes in bedded units such as the PTn. If, in fact, local fast pathways carry the bulk of the percolating water, most observations from the PTn used for calibration would be representative of the bypassed portion of the matrix. Further, flow along these fast pathways may penetrate the PTn rapidly enough to account for bomb-pulse observations, even accounting for potentially tortuous lateral paths. Unfortunately, hydraulic parameters that are upscaled, accounting for the local flow paths during ambient conditions, may not be appropriate during the repository thermal pulse, during which all of the matrix would presumably participate in flow redistribution.

Modeling efforts rely heavily on these laboratory-determined rock properties, upscaling, or inverse modeling. As a check on consistency, Winterle and Stothoff (1997) modeled imbibition, using METRA (Seth and Lichtner, 1996) to verify that the hydraulic parameters used by Bodvarsson, et al. (1997a) would reproduce sorptivity measurements by Flint (1997). If reported rock properties are accurate, and the underlying physics of the UZ flow models are

correct, then models should be able to predict rock matrix sorptivity that is very close to the observed sorptivity. However, comparison of model-predicted sorptivity and observed sorptivity yielded an interesting result: numerically determined sorptivity was consistently greater than the observed sorptivity. Furthermore, the ratio of modeled to observed sorptivity varied in proportion to K_{sat}. This relationship was interpreted by Winterle and Stothoff (1997) to be suggestive of hysteretic behavior in rock moisture retention characteristics. That is, at a given saturation, capillary suction is less in a rock that is undergoing a wetting cycle that it would be in the same rock undergoing a drying cycle. Moisture retention characteristics reported by Flint, et al. (1996b) were measured in the laboratory by incrementally oven drying rock samples and measuring capillary suction; however, imbibition is a wetting process. Thus, laboratory-reported values of van Genuchten's α parameter may be too low for use in models where the flow of infiltration pulses in fractures is of interest. Implications are that infiltration at YM may travel farther in fractures than would be predicted by models using moisture-retention characteristics based on drying curves. Interestingly, calibration of the YM site-scale UZ flow model (Bandurraga and Bodvarsson, 1997) required an increase in the α values relative to mean values reported by Flint (1997).

The NRC staff considers that approaches used by DOE to estimate parameters for flow and transport simulations generally use sound methods, particularly in the most recent work. The NRC staff notes, however, that subgrid heterogeneity is not explicitly and transparently addressed in the approaches and caution that failure to consider subgrid heterogeneity may lead to qualitatively incorrect results. Small-scale modeling of heterogeneous zones is one approach that may be used to support use of uniform properties in hydrostratigraphic units of the site-scale UZ flow model.

- **Hydraulic Properties of the Fracture System**

A general understanding of fracture geometry, surface characteristics (e.g. roughness), size distributions, and spatial variation is important for modeling UZ flow in the fracture bedrock of YM. These characteristics will affect hydraulic conductivity, hydraulic connectivity, matrix imbibition, chemical diffusion, and flow channeling in the fracture system. This section includes a discussion of fracture characteristics in relation to hydraulic properties. An analysis of the fracture system characterization at YM is included in the SDS IRSR (NRC, 1998a).

Fracture characteristics are used both to estimate hydrologic properties of the fracture system and to constrain conceptual models of UZ flow at YM. Fracture geometries, orientations, and distributions, combined with permeability measured by air injection testing and modeling of pneumatic response to atmospheric pressure changes, have been the source of data used to estimate physical and hydrologic properties for the fracture system for numerical modeling of the UZ at YM. There are no direct measurements of hydrologic properties of fractures or fracture systems in the UZ, only indirect calculation of hydrologic properties based on gas permeability data and constraints by thermal and geochemical evidence. Air injection and gas permeability data are used to estimate apertures and aperture distributions that are then used to estimate hydraulic properties of the fracture systems. Since air-injection testing is a critical component of estimating hydraulic properties of fracture system, and there was some controversy about methods and interpretation of previous air-injection testing at the site, a peer review was performed by an independent, three-member panel. Recommendations of the peer

review are summarized in attachments to a U.S. Geological Survey letter (USGS, 1995). The estimates of hydraulic fracture property values are used to constrain the range of possible values in the LBNL site-scale UZ inverse modeling; as such, the fracture parameters of saturated hydraulic conductivity and van Genuchten alpha are calibrated values.

Hydrogeologic parameters for fractures are difficult to characterize through direct measurement at YM because fractures vary widely in length, connectivity, orientation, aperture, and coating type and amount. These parameters depend on the scale of observation. For example, scale dependency in conductivity of a fractured rock is attributed to three properties: (1) the variation of length or consistency of the fractures; (2) the distribution of the fractures as related to the connectivity of the fracture system; and (3) the variation in conductivity or transport capacity. Sonnenthal, et al. (1997a) provide the best available summary and analysis of data on hydrologic properties of fractures and faults in the UZ, based on data from the detailed line surveying (DLS), borehole measurements, and the air injection tests (for permeability) (Ahlers, et al., 1996; Anna, 1996; Sweetkind and Williams-Stroud, 1996; LeCain, 1997; LeCain and Patterson, 1997; Sweetkind, et al., 1997). The summary provides estimates about fracture frequencies, orientations, and connectivities in the Topopah Spring Tuff, fracture frequencies from borehole measurements, permeabilities from air-injection tests, fracture apertures, van Genuchten parameters, fracture porosity, and heterogeneity of fracture distributions. The summary also includes pneumatic responses of faults and provided estimates of fault hydrologic properties, such as pneumatic permeability and porosity of the fracture continuum. The data are organized into a consistent set to be used with the UZ hydrostratigraphic model Table 7.7 of Sonnenthal, et al. (1997a)), including mean values for fracture spacing, frequency, trace length, intensity, and the proportion longer than 1 m for 16 zones in the upper 12 sublayers of the UZ model. These are 12 hydrostratigraphic sublayers from the ground surface to the repository horizon.

A brief discussion of fracture properties as related to hydrologic properties by hydrostratigraphic unit is included below. A detailed discussion of the fracture properties can be found in the SDS IRSR (NRC, 1998a). The nonwelded PTn sublayers generally have larger fracture spacing (i.e., lower density), lower frequency, and larger trace lengths than the overlying and underlying welded tuffs of TCw and TSw, although on a sublayer basis, there is considerable overlap between the units. There are as yet few data for the CHn nonwelded unit. However, the Busted Butte test facility should provide the needed information.

In the TCw, fracture spacing is significantly smaller than the fracture length thus implying the likelihood of connectivity of fractures. Geometric connectivity is an important criterion for fracture flow capability. Air injection tests performed on the drift-scale in the ESF demonstrated the connectivity and showed that the fracture network generally behaves as a continuum, with the mean fracture permeability generally increasing as the scale of the system increases (Sonnenthal, et al., 1997a). Pneumatic responses supported by gas chemistry data led Thorstenson, et al. (1998) to conclude that vertical permeability to air of the PTn was 1 to 3 orders of magnitude less than in the TCw or TSw. Thorstenson, et al. (1998) correctly noted that the gravity force acting on water percolating through the PTn is orders of magnitude greater than the buoyant forces acting on air, hence, the "gas permeability contrast does not preclude a high rate of water percolation through the PTn."

Because the repository will be in the TSw, a more detailed reporting of fractures in the TSw was organized by Sonnenthal, et al. (1997a). In looking at all of the fractures in the TSw (down to a length of 0.3 m) and over a 100-m scale, the middle nonlithophysal unit has higher fracture densities than the other layers. The vertical air permeabilities of the other TSw units measured from boreholes in the ESF are about 2 to 3.5 times the horizontal air permeabilities, while the ratio for the nonlithophysal layer is only about 1.3 (uniform over a distance of over 1,200 m in the ESF). However, the water permeability could be underestimated if it is based directly on air permeability, especially for horizontal water permeability where blockage by water could impact air permeability testing. Also for the TSw, the number of fractures was found to be inversely proportional to fracture size, and over half of the fractures are found in the 0.3- to 1.0-m range. This would indicate that the earlier cutoff length of 1.0 m used for the average values in the different zones of the UZ model probably skewed the data input to the model (Sonnenthal, et al., 1997a).

Two important features of the model layer properties in Sonnenthal, et al. (1997a) are worth underscoring here. One, for most of the sixteen zones (in the upper 12 hydrostratigraphic sublayers), the standard deviations for fracture spacing and fracture intensity are greater than the mean values. Therefore, use of mean values in flow models will underestimate the lateral and vertical variability of permeability in the UZ. Two, more than a third of all the fractures are eliminated from the analysis due to use of a 1 m fracture-length cutoff (fractures shorter than 1 m were not measured and counted). Elimination of short fractures from nonwelded, lithophysal, or densely fractured units could lead to an underestimation of hydrologic properties, such as porosity, permeability, and fracture connectivity. Elimination of fractures less than 1 m also may modify fracture intensity interpretations near faults such as for the GDF in the ESF where the 1 m cutoff for trace length leads to extremely different fracture intensity estimates over a wide zone (Sweetkind, et al., 1997).

Major faults in the vicinity of the repository include the north-south trending GDF, SCF, Bow Ridge, and Dune Wash Faults, which are normal faults, and the northwest trending Sundance, Drill Hole, and Tea Cup Faults, which are strike-slip faults. Hydraulic properties of fault zones are impacted by the degree of associated fracturing, the geometric character of the fracturing, and the nature of the fault gouge, all of which can vary vertically and laterally. The limited pneumatic monitoring and air-injection testing on fault zones at YM is summarized in Sonnenthal, et al. (1997a). The geologic characterization of faults at YM is analyzed in detail in the SDS IRSR (NRC, 1998a).

Sonnenthal, et al. (1997a) made several recommendations for additional data collection that are worth restating here. First, that fracture mapping data should be obtained from the east-west drift to compare and combine with data from the ESF. The proposed emplacement zones all lie west of the ESF loop. Second, additional borehole testing data are needed for units below the proposed repository horizon to better constrain the fracture distribution and permeability structure of zeolitic units. And finally, if faults are expected to play a large role in formulating UZ waste isolation strategy, then additional investigations are needed to better define fault widths, frequencies, interconnectedness, and gouge properties.

It should be noted that the current NRC/CNWRA modeling approach emphasizes relatively rapid fracture flow in the UZ. Our approach places little emphasis on retardation of radionuclides in the UZ, with repository performance being much more affected by properties of

the SZ. Under this approach, bounding values are probably acceptable for hydraulic properties of fractures, reducing the need for extensive characterization of UZ fracture networks. One exception to this would be the need for ESF data on fractures within the TSw. A reasonable understanding of general fracture patterns in the ESF is needed to refine conceptualizations of conditions under which water may enter emplacement drifts and drip onto waste packages. Data from the ESF and the east-west drift should provide an acceptable reference base.

- **Model Formulations**

There are two main approaches to modeling flow in unsaturated fractured tuffs: continuum methods and discrete-fracture methods (Evans and Nicholson, 1987). Continuum methods treat the matrix and fracture systems with various levels of interaction [e.g., methods using an equivalent continuum model (ECM), a dual-porosity model, a dual-permeability model (DKM), and a multiple interacting continua (MINC) model]. Discrete-fracture models may either account for or ignore interactions with the matrix. The models are discussed by Altman, et al. (1996). The continuum models are evaluated to investigate prediction differences by Doughty and Bodvarsson (1996, 1997). The observations of fast-path bomb-pulse ^{36}Cl detected in the ESF, coupled with newer estimates of MAI that exceed matrix permeabilities, have required a shift from matrix-dominated flow models (such as the ECM approach) toward fracture-dominated methods (such as the DKM approach), to enable some portion of percolation fluxes to occur in fast pathways.

Model dimensionality is another factor that may have a large impact on transport times. One dimension simulations cannot find fast pathways through lateral flow, thereby, magnifying the impact of low-permeability zones, while 2D and 3D simulations provide increasingly greater latitude for lateral flow.

The ECM formulation, developed by Klavetter and Peters (1986), merges matrix and fracture continua into a single equivalent continuum by assuming that the pressure in the matrix and fracture continua are in hydraulic equilibrium at each spatial location, resulting in considerable computational efficiency. In general, the fracture system only carries flow when the matrix system is essentially saturated. Early versions of the 3D UZ site-scale model developed by LBNL used the ECM formulation (Bodvarsson and Bandurraga, 1996), but subsequent analyses have largely abandoned the approach in favor of the DKM approach (Bodvarsson, et al., 1997a). The GWTT-94 analyses performed by SNL used the ECM approach, but the GWTT-95 analyses used the DKM approach. A modified ECM approach was used in TSPA-95 (Andrews, et al., 1994), with a heuristic disequilibrium assumed between matrix and fractures, but DOE intends to use a DKM approach for TSPA-VA (S. Sevougian, presentation at DOE/NRC Technical Exchange on Total System Performance Assessment, March 17, 1998). The NRC staff supports the use of the DKM approach relative to the ECM approach for site-scale flow modeling as long as DOE demonstrates that the results bound the effect of episodic pulses.

Doughty and Bodvarsson (1997) conclude that the ECM is most appropriate for steady state conditions and gas-flow problems at YM, as the assumption of matrix/fracture pressure equilibrium is best met under these conditions. Doughty and Bodvarsson (1997) and Tsang (1997) find that the DKM predictions significantly differ from the ECM predictions under transient conditions, with transport times significantly slower in the ECM. The DKM provides

prediction more consistent with simulations of a ponded-infiltration experiment examining flow processes in TSw bedrock at Fran Ridge (Eaton, et al., 1996) than the ECM predictions. Doughty and Bodvarsson (1997) further conclude that the additional complexity of the MINC approach is most necessary near faults.

Discrete-fracture approaches have not been used frequently at YM but have not been ignored completely. The WEEPS model (Gauthier, et al., 1992; Sandia National Laboratories, 1994), used to assess fluxes onto a WP for TSPA, assumes that all percolation is within fractures and is gravity-driven. The model uses geometric arguments to map the intersection between flowing fractures and WPs in order to arrive at total flux onto WPs. The model apportions the available flux into flowing fractures, with a primary uncertainty being the aperture distribution of the flowing fractures.

Individual fracture segments within a fracture network are explicitly represented in a discrete-fracture formulation, with each segment having individual hydraulic and pneumatic properties. The explicit-fracture method is attractive at scales where continuum behavior is not observed (i.e., at scales small relative to fracture density) but becomes intractable once many fractures are considered. Discrete-fracture methods are not practical for use at a YM-site scale as there are an estimated 10^9 significant fractures at YM (Doughty and Bodvarsson, 1997). Anna (1996) attempted to model a portion of the North Ramp using a discrete-fracture formulation with limited success. The generated network of fractures was based on ESF observations and had generally low connectivity, but pneumatic testing suggested that fracture connectivity should have been much larger. The discrepancy between simulated and inferred connectivities may be due to those fractures not considered in the discrete-fracture model (i.e., fractures less than 1 m in trace) or to the partial pneumatic connection through the matrix not included in the formulation.

The most appropriate application at YM for discrete-fracture methods may be drift-scale modeling, as there are few enough fractures that discrete-fracture discretization requirements may be tractable, and continuum approaches may be invalid. Nevertheless, DOE drift-scale studies for isothermal flow have invariably used continuum approaches: (1) matrix continuum, with fractures included as heterogeneous pathways (Wang, presentation to Site-Scale Unsaturated Zone Expert Elicitation Panel, 1997); (2) fracture continuum, with no consideration of matrix interaction (Birkholzer, et al., 1997a); (3) equivalent continuum (Nitao, 1997); and (4) DKM (Tsang, 1997). The DOE conceptual model for seepage into drifts is not well enough defined, nor is the uncertainty reasonably enough constrained to determine, a single appropriate model at this time (TRW Environmental Safety Systems, Inc., 1997a). However, seepage and moisture studies are ongoing at YM to better evaluate the drift seepage processes, percolation fluxes, and the capillary barrier system. These investigations are titled "Percolation in the Unsaturated Zone - Exploratory Studies Facility." The objective is to conduct *in-situ* ambient cross-hole pneumatic and liquid-release niche seepage studies and alcove surface infiltration studies.

Wang, et al. (1998) presented the Phase 1 preliminary test results and numerical model analysis of seepage into drifts. This included test results of the first seepage tests at Niche 3650 and sensitivity analysis of drift seepage with two and three-dimensional numerical models. The numerical models were then tested to predict the wetting-front arrival time of the planned

infiltration test for Alcove 1. This report is the third technical report for the drift seepage testing and moisture analysis.

According to the Master Scientific Notebook YMP-LBNL-JSW-6.0, ongoing field studies include: (1) the Phase 2 drift scale seepage test; (2) field tests of flow propagation through the heterogeneous and fractured Paintbrush nonwelded tuff (PTn); (3) investigation of fracture flow and storage effects in the PTn; (4) horizontal diversion of flow along interfaces between different subunits, (5) fracture flow, fracture-matrix interaction, and matrix imbibition tests of the middle nonlithophysal unit of Topopah Springs welded unit; and (6) Alcoves 1 and 7 testing. The results of these field investigations will feed the site-scale and drift-scale models calibrated against on-going field test results in support of the TSPA for YM.

4.4.2.7 Past Evidence and Impact of Future Climate Changes on Deep Percolation

The primary sources of information for future predictions of climatic change are the paleo records. Local data include the isotopic record from Devils Hole, pack rat middens, paleospring deposits, and water table fluctuations recorded by isotopic data, while the global data include information such as the integrated marine record (see Attachment E, NRC, 1997a; Forester, et al., 1996).

The single most important data set for predicting deep percolation under pluvial conditions is net shallow infiltration. According to Forester, et al. (1996), shallow infiltration may increase by a factor of 2 to 3 as a consequence of 5 to 10 °C drops in temperature, so that significant changes in vegetation may occur (NRC, 1997b). The factor for the increase in infiltration due to climatic change (pluvial) may be larger due to the nonlinear response of infiltration to increased precipitation and cooler temperatures. The staff is currently evaluating climate analog sites to incorporate in infiltration estimates the effects of soil characteristics, vegetation, and surface water runoff phenomena.

For deep percolation, the effect of climatic changes would be expected to impact the magnitude and pattern of percolation rates, including seepage into the drifts and flow below the repository. Increased percolation through the TSw is expected to be through the fracture system as the low matrix permeabilities will not take a significantly larger magnitude of the flow. The seepage-to-percolation ratio for seepage into drifts increases (Birkholzer, et al., 1997a) due to the fractures taking up a higher fraction of the flow as percolation increases. The spatial pattern of percolation might be expected to change as different portions of the fracture system begin to carry more flow as percolation increases. Below the repository, both the perched water and water table levels might be expected to change.

Site-scale modeling of potential future climatic impacts by Ritcey, et al. (1997b) using the ECM formulation suggests increased fluxes over the northwestern portion of the repository, though there is little significant change in pattern for other areas at the repository horizon or below the repository. Ritcey, et al. (1997b) noted that modest increases, less than 10 m, in the elevation of perched water tables resulted from doubling the shallow infiltration rates.

The question of how much to increase percolation rate to account for possible climatic changes requires a linkage of paleoclimatic conditions to the shallow infiltration. Linkage of the top

boundary condition of shallow infiltration to both general and local paleoclimate information led Gauthier (1998) to use precipitation multipliers of 1 for the current dry conditions, 2 for the long-term average conditions, and 3 for the super pluvial conditions. Over the past four hundred thousand years, the long-term average conditions occurred about 80 percent of the time (Forester, et al., 1996). A constraint on the conditions is the paleo position of the maximum 100-m rise of the water table as indicated by the strontium data from calcite fracture filling and paleosprings deposits in Crater Flats (Forester, et al., 1996).

4.4.2.8 Pneumatic Responses at YM

A major topic of study at YM has been the movement of unsaturated zone gases, mainly water vapor, in response to barometric pressure changes. There have also been concerns about the possible interference of exploratory shafts and tunnels on testing in the UZ. The NRC staff developed an open item on pneumatic issues during our review of the Site Characterization Plan (see SCA, 1989, p. 4-92). Our comment (no. 123) stated that:

> The effects of ventilation of the exploratory shafts and the underground testing rooms may have been underestimated in the evaluation of the potential interference with testing and the potential for irreversible changes to baseline site conditions; also, there is not an adequate analysis of the effects of ventilation in the ESF on the ability of the site to isolate waste.

DOE (1990) responded that the exploratory shaft would be lined with poured concrete that would isolate the rock from the ventilation air. The staff did not close the open item at that time because it was not clear whether the shaft would be lined, and secondary effects of ventilation on baseline conditions were not addressed. Since that time, DOE has chosen to construct the underground exploratory facility and the east-west drift using a tunnel boring machine (TBM) rather than build vertical access shafts.

Another open item had been raised by the staff regarding possible interference by the ESF on gas chemistry sampling. This item was closed in a 1994 letter from NRC to DOE (NRC, 1994). The staff's remaining concern was with pneumatic pathways.

Early in 1993, the State of Nevada wrote to NRC questioning whether DOE could adequately characterize pneumatic pathways before the UZ was disturbed by construction of the ESF. The State felt that the potential loss of data could prevent the NRC from making a licensing finding on the issue of the fastest pathway for radionuclide release. The State's letter was forwarded to DOE by NRC staff along with a reminder that the staff also had related concerns. The topic was discussed at a meeting of the NWTRB on October 19, 1993. Then, during January 26-27, 1994 a forum was convened by the YM Affected Units of Local Government (AULG). Proceedings of this roundtable have been published (AULG, 1994).

The concern that characterization of pneumatic pathways could be precluded by penetrating the PTn with a TBM was a valid one. It was thought that if the PTn was an effective pneumatic barrier, distinction between the pneumatic system above, in, and below the PTn could be determined by responses to changes in barometric pressure. If, however, the PTn were breached by the large diameter ESF, the distinction might have been masked. Knowledge of

the effectiveness of a pneumatic barrier above a hot nuclear waste repository could be important to performance assessment.

DOE, in its Accelerated Surface-Based Testing Program, committed to collect data on ambient pneumatic conditions and perturbations caused by ESF excavation. DOE installed pressure monitoring systems in boreholes NRG-6 and NRG-7a in October and November, 1994. These holes were located along the north ramp portion of the planned ESF. Data were collected from these holes for over two years, ending in December 1996. The staff had no objections to DOE's decision to discontinue monitoring in these holes because, by that time, the TBM was almost two miles away constructing the south ramp of the ESF. The TBM was no longer within the repository horizon and, therefore, NRG-6 and NRG-7a were no longer yielding new information.

Pneumatic information was also obtained from boreholes UZ-4, UZ-5, UZ-7a, NRG-4, NRG-5, SD-7, SD-9, SD-12, and ONC-1. NRG-4 and ONC-1 were instrumented by the Nye County cooperative study program. Locations of pneumatic testing and monitoring boreholes had been sited based on the ESF layout, allowing large-scale seasonal barometric responses to be monitored along with responses to ESF construction. To give a time perspective to progress of the TBM, the front of the TBM passed closest to NRG-4 on June 16, 1995 and penetrated through the PTn into the Topopah Spring unit on June 20, 1995. The TBM passed closest to UZ-4 and UZ-5 on September 2, 1995, and closest to SD-9 on November 16, 1995. It passed SD-12 on April 4, 1996, and SD-7 on June 5, 1996 (Ahlers, et al., 1996).

Summaries of the pneumatic response data are provided by Ahlers, et al. (1996; 1997). They reported that the ESF can affect pneumatic pressures from a large distance where faults are involved. They recommended that any new pneumatic monitoring boreholes be located far enough from the ESF that the data would not be affected by the tunnel. If additional drifts are planned (such as the east-west drift), boreholes along the drift alignments should be considered. Faults were identified as fast pneumatic pathways in the PTn and the TSw. Ahlers, et al. (1997, p. 10-28) concluded that:

> Overall, simulation of pneumatic conditions at Yucca Mountain using the three-dimensional site-scale UZ model has been successful. Though some minor modifications to the model are warranted by the simulation results, the technique for pneumatic calibration produces reasonable pneumatic parameter sets. These parameter sets should be acceptable for simulation of future scenarios and predictions at Yucca Mountain.

As noted in Section 5, and based on the above discussion, the staff now considers SCP open item Comment 123 to be resolved. Sufficient data on baseline conditions have been obtained and data were collected during the construction of the ESF. Pneumatic monitoring and testing is continuing at various locations in the ESF. As of June 1998, recording of pneumatic data continues at boreholes UZ-4, UZ-5, UZ-7a, SD-12, NRG-7a, and SD-7. Nye County, Nevada, continues to record pneumatic data in NRG-4 and ONC-1.

4.4.2.9 Evidence for Fast Pathways

Early conceptualizations of flow processes at YM discounted the possibility of significant fast-pathway flows below the TCw unit, based on low infiltration rates and the large capacity of the PTn to dampen wetting pulses. The associated concept, that the TSw matrix conducted all percolation fluxes at a steady state with little or no fracture flow, was strongly challenged by observations of bomb-pulse ^{36}Cl and other radionuclides far below the PTn. It is difficult to provide strong limits on fluxes using bomb-pulse evidence, as mixing of waters distorts interpretations, so that bomb-pulse observations are only evidence of fast pathways and not necessarily focused-flow pathways. However, additional evidence that significant flux occurs in fast pathways at YM has been mounting steadily, forcing revision of conceptual models for both infiltration and subsurface flow processes.

Isotopes arising from nuclear testing worldwide in the 1950s provide the strongest evidence that fast-flow pathways exist in the subsurface of YM. Although ^{36}Cl is the bomb-pulse isotope providing the most unambiguous indication of fast water flow paths, since ^{36}Cl moves only with liquid-phase water, ^{3}H and ^{14}C (despite moving both in the air and the liquid phases) also provide supporting evidence for fast flow (Yang, et al., 1996a; Fabryka-Martin, et al., 1997). Elevated isotope levels are found in the fracture systems in the ESF and in perched water bodies. Elevated isotope levels are also found in the boreholes in the TCw (fracture-dominated flow) and at the top of the PTn. The absence of elevated ^{36}Cl in the lower portions of the PTn in most boreholes, but its presence in TSw fractures and in perched water above the CHn, is indicative of fast pathways bypassing the PTn.

Geochemical data from UZ matrix waters, perched waters, and the saturated zone suggest that fast pathways, having little interaction with the matrix, exist through the UZ. Ca^{2+}, Mg^{2+}, and Cl^- are up to 10 times more concentrated in the matrix pore water than either the perched water or the saturated zone water (Yang, et al., 1996b). The Cl^- concentrations are indicative of percolating water bypassing pore water in units above the perched water. Chloride concentrations in some portions of the CHn range from 4 to 8 mg/L (Yang et al., 1996b), which is closer to the near-surface estimate of 0.6 mg/L than to the matrix concentrations of 60 to 228 mg/L in the PTn (Fabryka-Martin, et al., 1997). Indicative of little mixing in the UZ, dissolved SiO_2 levels are consistently 50 percent higher in the matrix pore water than in perched or SZ waters.

Hydrogen and oxygen isotope ratios in perched waters are similar to the current winter-precipitation meteoric ratios, indicating that there is little evaporative loss before recharge (Wu, et al., 1996). Lateral flow from Solitario Canyon or vertical fast-pathway percolation may explain the isotope-ratio data. The similarity to current meteoric water and dissimilarity to waters north of the repository is evidence that perched water is not formed from fluids migrating from the north. Preliminary ^{14}C dates show a trend of younger water to the south (Wu, et al., 1996), providing further evidence that perched water near the repository may not be related to the high gradient zone to the north.

Carbon-14 isotopic dating provides apparent ages of 5,000 to 10,000 yr for perched waters, while apparent ages of the PTn pore waters are about 1,000 yr (Rousseau, et al., 1996; Patterson, et al., 1996). However, ^{14}C measurements in deeper portions of the CHn have indicated ages similar to or younger than 1,000 yr (Rousseau, et al., 1996). The ^{14}C data for the CHn water not only suggests fast preferential flow but also a more complex mechanism for

formation of the perched zones. Lateral flow from Solitario Canyon or vertical fast-pathway percolation may explain a portion of the water in perched zones of the CHn.

In a study of transport and water-rock interaction by Johnson and DePaolo (1994), strontium isotope data in water, whole rock, and calcite fracture fillings in the TSw were found to be consistent with fast pathway movement of water.

Studies at Rainier Mesa support the possibility of fast-pathway flow through fractured nonwelded tuffs. A sequence of lithologies similar to YM is present at Rainier Mesa, including alternating welded and nonwelded tuffs capped by a moderate-to-densely-welded tuff. However, the sequence at Rainier Mesa is primarily nonwelded with a thick sequence of zeolite-altered tuffs (Wang, et al., 1993). Percolation estimates from seepage into the tunnels, based on discharge at the portal and vapor flow, are approximately 24 mm/yr with a mean annual precipitation of 320 mm (Russell, et al., 1987; Wang, et al., 1993), or about 8 percent of the precipitation. Suggestive of fracture or fault flow, there is a distinct difference between the geochemistry of the matrix pore water and the water in the seeps (Murphy and Pabalan, 1994). The saturated zone water geochemistry is similar to that of the seeps. Residence times estimated from tritium data suggest travel times less than 6 yr from ground surface to the observation tunnels at a depth of 350 m (Wang, et al., 1993). Bomb-pulse ^{36}Cl observations in the seeps provide additional evidence for fast-path movement of water. Using the precipitation record, seep discharge rates, gross water chemistry, stable isotope composition, and two tracer tests, Russell, et al. (1987) concluded that: (1) the seep water was meteoric in origin with winter as the principal period of recharge based on hydrogen and oxygen isotope ratios; (2) the period of hydrologic response was at least 4 months; and (3) the travel time from surface to tunnel was at least 1 yr and less than 6 yr (Wang, et al., 1993). The period of hydrologic response is the time it takes for a given recharge event to cause a corresponding increase in discharge at the seeps in the tunnels. In spite of the large matrix permeabilities of the nonwelded tuffs, fault systems intercepted by the tunnels within the zeolitic horizons provide the bulk of the discharge. An estimate of 10 percent of the total percolation is from 2 seeps in the U12n tunnel while 50 to 60 percent of the 112 mapped faults in the U12e tunnel supplied most of the total discharge from the tunnel system (aqueous discharge through the portal and vapor discharge through the air ventilation system). The analogy to YM is weakened by the observation that nuclear testing probably altered the flow system, but the extent of alteration is unknown.

Observations at the Apache Leap Test Site (ALTS) featuring a sequence of fractured tuffs also suggest fast pathway flow along fractures, although the fracture system at ALTS has far wider apertures than exist at YM; mean aperture is 760 μm at ALTS (Bassett, et al., 1994) and the range of mean apertures is 131 to 497 μm for all units at YM (Sonnenthal, et al., 1997a). At ALTS, intermittent recharge from a stream penetrates to a tunnel 150 m below the ground within days to weeks (National Research Council, 1996). Infiltration tests by Rasmussen and Evans (1993) demonstrated the possibility of high water intake rates on exposed fractured rock surfaces at the Apache Leap site.

The portion of flow that occurs through fast pathways is an important consideration for repository performance. Seepage into the repository is dependent on the partitioning of percolation flux into matrix, dispersed fractures, and fast-pathway fractures or faults. Transmission capacity for matrix flow in the welded units is about 1 mm/yr assuming, that

percolation is gravity-dominated, based on effective conductivities and typical water saturations provided by Flint (1997). Any additional percolation flux is carried in discrete pathways, typically in small-aperture (capillary-dominated) fractures appropriate for continuum approaches or large-aperture (gravity-dominated) fractures or faults that may not be appropriate for continuum approaches. Partitioning between the two fast-pathway alternatives, in part, is related to the physics of flow through small-aperture fractures versus large-aperture fractures, but it is also controlled by focusing mechanisms at the ground surface and at depth. Despite the evidence presented in this section demonstrating that fast pathways occur at YM, it is difficult, however, to estimate the portion of the repository that might be contacted by fast pathways.

The discussion of mass balance of ^{36}Cl in Section 4.4.3.1 looked at the fraction of the perched water having the bomb pulse signature, with roughly 1 to 50 percent ascribable to water infiltrating in the past 50 yr. Murphy (1998) estimated that the bomb-pulse ^{36}Cl signature was primarily evident in three ESF zones, comprising 23 percent of the tunnel, which implies that roughly a quarter of the repository may experience fracture flow if the ESF is representative of the remainder of the repository footprint. Note that Murphy (1998) used a lower threshold to identify bomb pulse ^{36}Cl than was used by Fabryka-Martin, et al. (1997) in order to account for bomb-pulse dilution through mixing.

4.4.2.10 Calculated Distribution of Percolation at the Repository Horizon

A map of estimated spatial distribution of shallow infiltration, on a mean annual basis, was presented in NRC (1997b). The distribution was in qualitative agreement with the map of Flint, et al. (1996a). Using the presumption that flow above the repository is predominantly vertical, the magnitude and distribution of percolation flux at the repository horizon is equal to that of the shallow infiltration. The assumption of vertical flow means that no lateral flow at the PTn is recognized. Current efforts by the NRC staff are focused on further refining percolation estimates by adding the impact of plants and lateral flow at the bedrock interface with the alluvium, colluvium, or atmosphere.

4.4.3 Summary of Deep Percolation Topics That Warrant Further Analysis

Significant variability of flow and transport pathways and travel times is expected to occur at YM due to the natural heterogeneity, stratification, alteration, fracturing, and other characteristics of the site. The extent to which such heterogeneities of the flow system should be incorporated into the DOE site-scale UZ flow model depends on their importance for estimating seepage into the repository and flow below the repository. Conceptualizations of flow in the UZ at YM have ranged from single-continuum models, to equivalent continuum models, to dual- and multiple-continuum models, to discrete-fracture models, as the importance of particular components of the flow system was examined. Given the matrix permeability values (Flint, 1997) and assuming a unit hydraulic gradient, groundwater flowing only in the matrix would move sufficiently slowly that it would take many tens of thousands of years for shallow infiltration to go through the repository horizon and arrive at the SZ. In contrast, both geochemical evidence and transient-flow modeling have suggested that a significant amount of groundwater flux occurs in the fracture system, and that these fluxes can travel at much faster rates than in the matrix. Fluxes in the fracture systems may move sufficiently fast that some component of shallow infiltration reaches the water table in tens to hundreds of years. Differing conceptualizations of the link between the matrix and fracture systems and flow processes in

the fractures cause important differences between alternative conceptual models. The differences in the conceptualizations can have a strong impact on PA modeling and, as such, are the focus of the discussion in this section.

The development of both the repository-scale and drift-scale conceptual models at YM may be partitioned into:

- Percolation processes above the repository, which affect the spatial and temporal distribution of water moving through the repository horizon
- Percolation processes at the drift scale, which affect the release of radionuclides from the repository
- Percolation processes below the repository, which affect the transport of radionuclides from the repository to the SZ

An assessment of current understanding of these three parts of the conceptual model is summarized below for flow above, at, and below the repository.

4.4.3.1 Percolation Processes Above the Repository

Percolation processes above the repository have a direct impact on flow processes at the drifts, by affecting the amount of water that arrives at the repository horizon and the partitioning of that water between matrix and fractures. As discussed in the IRSR related to shallow infiltration (NRC, 1997b), water infiltrates into the subsurface in pulses following precipitation events. Some portion of this infiltrating water (net infiltration) eventually escapes downward from the root zone to become deep percolation. Both within wash channels above the repository and where bedrock cover is shallow (i.e., less than 0.5 m), the magnitude of the infiltration pulse can be much larger than the permeability of underlying moderately to densely welded tuff. As there is typically a plentitude of fractures within the Tiva Canyon bedrock, it is anticipated that infiltration pulses below the root zone primarily enter the bedrock fracture system and move under the dominant influence of gravity. There may be some fracture/matrix transfer within the TCw unit, but the percolating water should generally move vertically downward until a zone is reached with increased matrix permeability or reduced fracture permeability. If the fracture system exhibits numerous subhorizontal cooling joints, significant lateral flow may occur within the fractures leading to either a spreading or a coalescing of flow.

Available evidence supports the interpretation of rapid penetration of infiltration pulses into the TCw unit where bedrock alluvial or colluvial cover is shallow (i.e., less than 2 m, which corresponds to all of the repository footprint except for some wash bottoms). Neutron-probe data have been obtained for a network of 99 boreholes, with records extending nearly 10 yr for some boreholes (Flint and Flint, 1995). As discussed by Flint and Flint (1995), the average wetting-pulse penetration depth in the years 1990 through 1993 that was detected by the neutron-probe apparatus was at least 5 m for 12 of the 14 ridgetop and sideslope boreholes considered, with average wetting pulses penetration greater than 10 m in 8 of the boreholes. The neutron-probe methodology is relatively insensitive to fracture flow, so that deeper wetting pulses may have occurred without having been detected.

Further corroboration of rapid penetration of infiltration pulses is indicated by bomb-pulse ^{36}Cl found within borehole ream-bit cuttings. As discussed by Fabryka-Martin, et al. (1997), bomb-pulse ^{36}Cl has been transmitted well into the fractured bedrock (e.g., 20 to 80 m) at all but one of the shallow boreholes examined that has alluvial cover less than 2 m (most have less than 1 m of cover). Bomb-pulse ^{36}Cl was found within the PTn unit in several of the boreholes, penetrating to the TSw unit in one borehole. Bomb-pulse ^{36}Cl evidence (Fabryka-Martin, et al., 1996b) suggests that lateral flow may occur in the TCw and PTn units, based on the existence of multiple peaks in several of the boreholes.

Aside from the lower portion of the west flank of YM, which exhibits outcrops of the TSw unit, the bedded tuffs within the PTn unit form the first barrier to fracture-dominated flow within the repository footprint. These bedded tuffs have relatively large primary permeability and relatively few fractures, and the fracture system tends to be strata-bound (i.e., fractures within the PTn unit are poorly connected to those within the overlying TCw unit and the underlying TSw unit). Montazer and Wilson (1984) hypothesized that the PTn has the potential to significantly attenuate infiltration pulses due to these factors. Simulations (Buscheck, et al., 1991; Nitao, et al., 1992) suggest that an infiltration pulse penetrating to the PTn unit, either in the matrix or in fractures, should end up entirely within the PTn matrix by the time the pulse reaches the bottom of the PTn unless the fracture and the flow rates are quite large, due to strong capillary uptake from the fractures to the matrix. Furthermore, the large storage capacity of the PTn is thought to provide a strong buffer, almost completely damping out the pulse by the time it reaches the bottom of the PTn. If the PTn does damp out infiltration pulses both spatially and temporally, fluxes in the underlying TSw unit may be nearly steady state and total fracture flux would be significantly smaller than in the TCw unit, although the flow in the fractures may still be widespread. However, if the PTn causes lateral diversion and, thereby, focuses flow, fracture flow may be spatially infrequent, but those areas with fracture flow may have large fluxes. As the PTn unit thins from north (roughly 80 m) to south (roughly 20 m) within the repository block (Moyer, et al., 1996), the effects of the PTn unit should diminish from north to south.

The perched water at the base of the TSw unit does not carry a strong geochemical signature of having passed through the PTn matrix, suggesting that the bulk of the perched water may have bypassed the PTn matrix (Bodvarsson and Bandurraga, 1997; Striffler, et al., 1996; Yang, et al., 1996a,b). In particular, the chloride concentration is far larger in the PTn unit than in the perched water. The perched water may be largely the result of lateral flow from Solitario Canyon directly entering the TSw, thereby bypassing the PTn, or from lateral flow from the area of the large hydraulic gradient to the north of the repository footprint. If the perched water primarily results from net infiltration occurring above the repository, the discrepancy between the signatures of the PTn matrix and the perched water suggests that a large component of deep percolation does not pass through the PTn matrix. Flow starting above the PTn unit may bypass the PTn matrix in several ways:

- Connected fracture pathways with fracture coatings that reduce matrix/fracture interaction
- Fine-scale matrix pathways formed by heterogeneity and/or fingering
- Systematic down-dip movement within the fractures above the PTn until a fast pathway, such as a fault, is encountered that focuses flow

The different mechanisms for water moving through the PTn have different influences on flux distributions at the repository horizon within the underlying TSw unit. The TSw unit is similar to the TCw unit: densely welded, with low permeability and extensive fracturing. Matrix fluxes within the PTn unit would tend to preferentially move into the more fine-pored TSw matrix through capillarity, to the extent possible, with the excess perhaps moving downdip until sufficient pressure builds up to overcome the matrix/fracture capillary barrier. Flux pulses bypassing the PTn matrix via fractures may tend to remain within fractures in the TSw if the fracture sets are connected. As bypass fluxes become large, it becomes increasingly unlikely that the TSw matrix can conduct all percolation flux and more likely that fracture flow is initiated where the bypass fluxes contact the TSw unit.

The chloride mass balance technique, as applied by Fabryka-Martin, et al. (1996b), assumes that average chloride concentration multiplied by total flux is conserved, and flows are approximately steady state. To roughly estimate the relative components of PTn matrix flux and bypass flux, assume that:

- $C_m Q_m + C_b Q_b = C_p (Q_m + Q_b)$, where C represents concentration, Q represents flux, and the m, b, and p subscripts represent matrix, bypass, and perched components, respectively.
- Bypass fluxes arrive at the perched water body with the chloride concentration of rainfall (0.62 mg/L) that was used by Fabryka-Martin, et al. (1996b)
- PTn fluxes arrive with an average chloride concentration of 62 mg/L [a number near the middle of the range of observed PTn values reported by Fabryka-Martin, et al. (1996b)]
- Chloride concentration in perched waters is 6.2 mg/L [a typical value from Yang, et al. (1996a)]

Using these chloride concentrations in a simple mass-balance calculation, which requires that chloride from both matrix and bypass fluxes fully mix in the perched waters, suggests that bypass fluxes are roughly ten times as great as PTn matrix fluxes. As the chloride concentration in the bypass fluxes increases (indicating evaporation within the subsurface), the ratio of bypass flux to matrix flux also increases.

Using a similar mass balance technique for ^{36}Cl, the ^{36}Cl signatures from both perched water and pore waters can be used to roughly estimate flux rates for the bomb-pulse portion of the perched waters. Based on Table 4-16 by Fabryka-Martin, et al. (1997), the ratio of ^{36}Cl to chloride in perched waters obtained from boreholes NRG-7a, SD-7, SD-9, UZ-1, and UZ-14 ranges from 449×10^{-15} to 999×10^{-15}, with a mean of 590×10^{-15}. Comparable ratios from 5 samples from the TSw unit [SD-12 and ONC boreholes in Table 4-11 of Fabryka-Martin, et al. (1997)] are 235×10^{-15}, while the deepest non-bombpulse sample obtained from the PTn unit in boreholes N37, N53, N54, UZ-14, and UZ-16 average 345×10^{-15} [Table 4-10 of Fabryka-Martin, et al. (1997)]. Seven borehole observations within the PTn unit were greater than $10{,}000 \times 10^{-15}$, with a peak value of $32{,}400 \times 10^{-15}$. Within the ESF, 21 of the 141 samples obtained from formations in or below the upper lithophysal zone of the TSw unit

(station 18+00 to 69+00) were above 1,250 × 10^{-15}, with a maximum of 4,100 × 10^{-15}. Several calculations can be made:

- Assuming that the perched-water ratio is 590 × 10^{-15}, pore waters have the TSw ratio (235 × 10^{-15}), and fast-path ratio is 4,100 × 10^{-15}, about 10 percent of perched water has a bomb-pulse signature.

- Assuming that pore waters have the PTn ratio (345 × 10^{-15}), and the fast-path ratio is the largest observed at YM (32,400 × 10^{-15}), about 0.8 percent of perched water has a bomb-pulse signature.

- Assuming that pore waters have the TSw ratio (235 × 10^{-15}), and the mean fast-path ratio is 1,250 × 10^{-15}, more than 50 percent of perched water has a bomb-pulse signature.

- Assuming that fast-path fluxes are 10 times greater than matrix fluxes, and pore waters have the PTn or the TSw ratio, the fast-path ratio is 626 × 10^{-15} and 615 × 10^{-15}, respectively.

From these considerations, it is likely that at least one percent, and perhaps more than half, of the perched water infiltrated in the past 50 yr. However, flux information derived from the chloride calculations yields an estimated ratio so low that it is unlikely that all of the bypass fluxes are younger than 50 yr unless a significant portion of the perched waters come from post-bomb-pulse waters. The magnitude and spatial distribution of fracture fluxes within the TSw are likely to have a profound impact on repository performance. As discussed in Section 4.4.2.4, capillary effects tend to preclude entry of liquid into open cavities in unsaturated porous media, particularly when the medium is as fine-grained as is the TSw matrix, so that flows in the matrix will tend to divert around the drifts rather than entering the drifts. Capillary-exclusion effects are less important for fractures, especially larger fractures, so that flows in fractures are less likely to divert around drifts. The larger the flow in a fracture, the less important capillary forces are relative to gravity and the less likely that diversion will occur around a drift intercepted by the fracture. If the fracture supports film flow, only viscous and gravity forces significantly affect the flow (Kapoor, 1994) so that capillary forces are unlikely to prevent entry into the drift.

As with the TCw unit, matrix/fracture interactions are likely to be relatively limited within the densely welded TSw unit, and flows are likely to be predominantly vertical. Hence, the distribution of fracture flows initiated in the TSw at the bottom of the PTn is likely to be propagated vertically downward to the repository horizon with some spreading or coalescing of flow paths possibly occurring.

- **Modification of Percolation Due to the Paintbrush Nonwelded Unit**

The possibility that the PTn unit may cause lateral diversion due to capillary effects (at the TCw/PTn interface) or permeability effects (at the PTn/TSw interface) has long been recognized (Montazer and Wilson, 1984). The effectiveness of the PTn unit in attenuating pulses or causing lateral diversion has been examined by numerous researchers (Prindle and Hopkins, 1989; Ross, 1990; Buscheck, et al., 1991; Nitao, et al., 1992; Brown, et al., 1993; Altman, et al.,

1996; Bodvarsson and Bandurraga, 1996; Fabryka-Martin, et al., 1996a, b, 1997; Moyer, et al., 1996; Robinson, et al., 1996, 1997; Rousseau, et al., 1996; Wilson, 1996; Wolfsberg, et al., 1996; Fairley and Wu, 1997; Wu, et al., 1997; Ofoegbu, et al., 1997). In general, the PTn matrix is considered to have the potential to strongly attenuate pulses, due to large storage capacity, high matrix permeability, and capillary effects that strongly imbibe fracture waters into the matrix. The strong attenuation potential within the PTn, which would tend to reduce fluxes below the PTn to nearly steady, is often used to justify the modeling assumption that fluxes are at a steady state throughout YM. Depending on model assumptions and model parameters, however, disparate results for lateral diversion are obtained. For example, Prindle and Hopkins (1989) and Ross (1990) suggest lateral diversion increases as net infiltration increases while modeling studies reported by Bodvarsson and Bandurraga (1996) suggest that the capillary barrier effect decreases with increasing net infiltration.

Several factors appear to play a major role in determining the role of the PTn unit in attenuating and diverting infiltration pulses:

- Fracture/fault interaction with the PTn matrix
- Infiltration model
- Hydraulic properties
- Stratigraphy

Early models generally assumed that infiltration was quite small (less than 1 mm/yr) and at steady state; the PTn unit did not have significant fractures or fractures were included using the ECM conceptual model; hydraulic properties were based on early measurements reported by Peters, et al. (1984) and Klavetter and Peters (1986); hydraulic properties within layers were homogeneous; and microstratigraphy was usually not considered (e.g., several bedded-tuff layers were consolidated into the PTn unit). With such small and steady infiltration rates, the (assumed-homogeneous) matrix is sufficiently permeable to carry all percolation fluxes and fracture flow is inhibited due to capillary effects. These early models tend to indicate that significant lateral flow may occur. Significant lateral flow may be generated in the PTn in the absence of vertical discontinuities even when detailed microstratigraphy and updated hydraulic properties are considered (Moyer, et al., 1996).

Sampling from within the ESF and in deep boreholes has revealed bomb-pulse ^{36}Cl and ^{3}H in numerous locations (Fabryka-Martin, et al., 1996a, 1997; Yang, et al., 1996b), which requires that for at least some flow paths travel times are less than 50 yr to the repository horizon and the base of the TSw unit. In addition, calcite and opal fillings (their origins may be associated with fracture-flow paths) have been observed in numerous fractures within the ESF, and the portions of the PTn penetrated by the ESF exhibit numerous small-offset (slump) faults. Spurred by these observations, conceptual models have been modified to emphasize the role of fractures and faults and to consider the role of transient infiltration pulses. Recent models tend to exhibit predominantly vertical flow, less lateral diversion, and a small component of the flow bypassing the PTn matrix in fast pathways. However, significant systematic lateral flow (e.g., 500 m) is still produced with some calibration parameter sets (Bodvarsson, et al., 1997a).

Sweetkind, et al. (1995) conclude that observations of fractures in the PTn unit at 22 outcrop locations do not support interpretations of significant fracture flow within the PTn unit, due to the generally stratabound nature of the observed fractures and lack of alteration products within the fractures (although calcite fillings were observed in some of the fractures). If correct, this conclusion implies that fast pathways within the PTn, if they exist, are fault-derived or due to heterogeneity-derived channels in the matrix.

Field evidence for lateral flow within the PTn unit is derived primarily from geochemical data, such as inversions in concentration as depth increases. Kwicklis (1996) suggests that at least limited lateral redistribution may be indicated by inversions of aqueous ^{14}C data with depth in borehole UZ-14, although these inversions may also be due to fracture flow. Fabryka-Martin, et al. (1997) suggest that a model postulated by Paces, et al. (1997), in which percolating waters with two distinct strontium isotopes (resulting from areas with ridge crests and sideslopes without thick calcretes, and areas with thick calcite- and Sr-rich soils) requires mixing through lateral flow in the PTn unit to explain observed profiles within borehole SD-7.

The UZ expert elicitation panel had based its conclusions on available evidence for infiltration and deep percolation as of the end of 1996. The panel noted that lateral diversion might be expected at the TCw/PTn and PTn/TSw interfaces, and perhaps within the PTn itself, if textural differences alone were considered (Geomatrix, 1997). However, the panel generally agreed that the series of small slump faults observed in the ESF within the PTn would serve to capture flow moving laterally, diverting the flow vertically down the faults. Thus, the expert panel concluded that lateral diversion might occur over a few meters to tens of meters, but lateral diversion would not be expected to occur over a much larger scale. Most of the experts, accordingly, expected that the spatial distribution of percolation flux at the repository level is similar to the spatial distribution of net infiltration, although perhaps smoothed. One expert believed that there may be focusing processes as well as smoothing process, perhaps funneling flow into locally high-flux zones.

Two mechanisms that promote bypassing of the PTn matrix apparently have not been quantified to date: (1) potential lateral fluxes, in response to large infiltration pulses, in a TCw fracture system that is strata-bound (i.e., that terminates above the PTn); and (2) vertical fluxes in localized pathways within the PTn matrix. In the first case, large pulses of water may proceed rapidly down to the base of the fracture system. If the fractures are strata-bound or are filled with alteration products that drastically reduce fracture permeabilities, the infiltration pulse may tend to rapidly redistribute downdip until a fast pathway is encountered. If faults are not ubiquitous or if the moist conditions at the bottom of the TCw have caused widespread alteration, lateral redistribution within the TCw fracture system may be significant. In the second case, heterogeneity within the PTn matrix may cause local fast pathways within the matrix, which may not be captured by current estimates of grid-block-scale parameters. Potential causes and effects of misrepresenting heterogeneity are discussed in Section 4.4.2.3.

The NRC staff concludes that systematic lateral flow within the PTn may not occur in the vicinity of the ESF observations and would be similarly unlikely if the PTn is generally faulted over the repository block. The PTn unit is observed only in a relatively small portion of the ESF east of the GDF, and it is possible that the observed faulting is not typical of the relatively less distorted areas west of the GDF. If small-scale PTn faulting is much less frequent over the repository block, lateral flow diverting into faults may serve to localize flow rather than to prevent localized

flow. In the absence of evidence to the contrary, however, the NRC staff endorses use, in PA, of the assumption that general lateral diversion does not occur above the repository, as this conservatively passes all net infiltration generated within the repository footprint to the repository horizon.

- **Focusing of Flow Due to Faults**

There is solid evidence that faults have large permeabilities, based on observations of barometric attenuation and phase lag during the excavation of the ESF (Ahlers, et al., 1996; Nilson, et al., 1991; Patterson, et al., 1996). The character of barometric response was altered kilometers from the ESF (e.g., in borehole ONC-1), apparently due to the interaction of faults with the ESF. Faults therefore represent potential fast pathways providing water to the deep subsurface. If water is diverted laterally into the fault, these potential fast pathways may carry substantial quantities of flow. However, if no waste is emplaced close to the faults, then this water is not intercepted by those waste packages. Fault-permeability estimates presented by Sonnenthal, et al. (1997a) (their figure 7.7) range from 3×10^{-13} to 6×10^{-10} m^2. Sonnenthal, et al. (1997a) further categorize faults into normal faults (large- and small-displacement) and strike-slip faults, all with different deformation features (fracturing gouge) resulting from different formation processes.

Observations of bomb-pulse ^{36}Cl in the ESF have prompted LANL and USGS researchers to hypothesize that three conditions are required for observations of flowing water to occur within the ESF (Fabryka-Martin, et al., 1997):

- A continuous fracture path must extend from the surface to the sampled depth (implying that a fault must cut through the PTn)
- Values of MAI at the surface must be at least 1 mm/yr (in order to initiate and sustain fracture flow)
- The residence time of water in alluvium must be less than 50 yr (alluvial thickness must be less than 3 m)

As noted by Fabryka-Martin, et al. (1997), predictions based on these conditions appear to be reasonably consistent with observations in the northern half of the ESF but are inconsistent with the paucity of bomb-pulse ^{36}Cl observations in moist fractures in the southern half of the ESF. Fabryka-Martin et al. (1997) suggest that, if the conceptual model for observations of bomb-pulse ^{36}Cl in the ESF is correct, requiring that the PTn be cut by a fault, then there may be significant connection between the fault and fractures in the welded unit. This suggestion is based on observations of bomb-pulse ^{36}Cl spread laterally downdip from the Sundance Fault (SDF) in a swath 300 m wide within the ESF (Levy, et al., 1997), which appears to travel laterally as much as 200 m within subhorizontal cooling joints in the middle nonlithophysal zone. An important implication of these observations is that significant downdip redistribution may occur within the fractures of at least some densely welded units, although fracture permeabilities are inferred to be as much as ten times greater in the vertical than the horizontal direction (Sonnenthal, et al., 1997a). Nicholl and Glass (1995) offer further evidence that considerable spreading can occur within the TSw fracture system, demonstrated with a ponded infiltration experiment at Fran Ridge where the TSw unit crops out. Thus, even if systematic

lateral redistribution in and above the PTn unit does focus flow into faults, these locally concentrated fluxes may be significantly smoothed through lateral spreading before reaching the repository horizon.

Water will not enter a fault in the UZ unless the matrix is sufficiently saturated to overcome the capillary barrier represented by the fault. Other barriers, such as low permeability fracture coatings, may also be present. In order to focus flow within a fault possessing a significant capillary or other barrier, it is necessary for water to collect updip of the fault. This collected water will tend to make the updip side of the fault, where water is entering the fault, wetter than areas further updip from the fault, and thereby may cause enhanced vertical flows below the wetter region. As the main drift of the ESF parallels the GDF on the updip side, inferences drawn from observations within the ESF may be unrepresentatively wetter than the repository block as a whole if vertical fluxes are enhanced through significant collected water above the ESF. Note that waters within the GDF are likely to exit through gravity, so that the matrix in the immediate vicinity of the west-dipping fault is likely to increase in wetness as the fault is traversed from west to east at the ESF elevation.

The impact of a fault is likely to be most significant when the fault is perpendicular to the stratigraphic dip. From geometric arguments (all else being equal), north-trending faults at YM (e.g., the GDF) may tend to have a greater impact on UZ flow than north-west-trending faults (e.g., the SDF) as flows can divert around north-west-trending faults, to some extent. On the other hand, different fault-forming mechanisms may yield significantly different hydraulic properties, which may override the geometric arguments.

The focusing or spreading of flow, and the flow pathways in general, under current conditions does not necessarily reflect that under future conditions. A change in the amount and distribution of infiltration may lead to a change in the predominant flow pathways, or at least change the proportions of flow in various pathways. Also, active tectonic stresses on the YM block may alter the flow pathways by modifying the hydrologic properties along the fault or by creating new pathways. It is likely that reductions in fault and fracture apertures in one area may be accompanied by the dilation of other discontinuities. The NRC staff review of DOE methods may need to consider the potential impact of structural changes to the fault system. One approach would be to analyze the sensitivity of repository performance to altered patterns of percolation.

- **Influx on the West Flank**

Solitario Canyon may provide sources of infiltrating water with potential for impacting repository performance. These sources include infiltration from numerous small channels incised into the bedrock of the west flank of YM, distributed infiltration from the shallow colluvial cover and bedrock exposures on the west flank of YM, and percolation along the SCF. The potential for these sources to impact repository performance has not been quantitatively evaluated to date.

Portions of the west flank of YM lie above the repository footprint but below the PTn outcrop, so that infiltration in these areas may reach the western edge of the repository with none of the PTn buffering discussed in Section 4.4.2.3. Although the west flank of YM is steep, fractured bedrock has minimal surface cover in many locations, which may enable significant infiltration. Any waters infiltrating below the PTn outcrop may flow directly to the repository or may continue

to the TSw/CHn interface and flow laterally to form part of the perched water bodies observed at this interface. The possibility of direct recharge within the TSw outcrop was noted by the State of Nevada (Lehman, 1992; L. Lehman, letter to E. Smistad and A. Van Luik, November 14, 1994).

The main Solitario Canyon channel is west of the SCF and does not lie above the footprint. Based on geometric arguments and the predominance of vertical flow, it does not appear likely that flow from the main channel during large runoff events will move laterally towards the repository. However, the SCF offsets sufficiently near the repository block to juxtapose the PTn unit, to the west of the fault, with the TSw unit, to the east of the fault. Under these conditions, it is plausible to expect that any lateral diversion occurring in Solitario Canyon will intercept the SCF (Lehman, 1992). Since there is no evidence for or against flow moving across the fault zone in the UZ, and there is little evidence for lateral flow in the PTn above the repository footprint, it is considered unlikely that groundwater flow from beneath the channel during runoff events will laterally move towards the repository along stratigraphic boundaries.

However, any laterally diverted percolation fluxes from Solitario Canyon may pass across the steeply west-dipping SCF and proceed vertically to the CHn unit. The diverted waters from Solitario Canyon may then form a significant portion of the perched water bodies observed at the TSw/CHn interface. This scenario has implications for the formation of the perched water beneath the repository as well as implications for dilution of radionuclides below the repository.

The potential for influx from Solitario Canyon was considered briefly and dismissed by two expert panels (Unsaturated Zone Hydrology Peer Review Team, 1991; Geomatrix, 1997) without quantitative justification. Nevertheless, there is potential for significant inflow arising from along the west flank of YM in Solitario Canyon to pass through the repository footprint. The SCF impacts repository design in terms of standoff distance from fault zones and flow in along the fault may contribute to the perched water bodies.

4.4.3.2 Percolation Processes at the Drift Scale

An understanding of the nature of water flow into drifts is important for two reasons: first, water in the vicinity of WP may elevate relative humidity, thereby, accelerating corrosion and WP failure; second, almost all radionuclides are expected to have a dominant release pathway of water traveling through drifts, contacting waste, and transporting dissolved or colloidal waste through the geologic setting.

- **Nature of Flow into Drifts (Drift Seepage)**

The conceptual model developed for unsaturated flow through repository drifts depends, to a large extent, on whether drifts will be backfilled after waste emplacement and, if so, on the type of backfill material used. If backfill is to be used, it is necessary to take into consideration the moisture retention and permeability properties of the backfill before an effective assessment of the effects on flow can be considered. For example, a coarse, well-sorted backfill would allow water to pass easily through the drift; it would have a very low residual water content; and it would not produce enough capillary suction to imbibe water from drift walls. Conversely, a fine or poorly-sorted backfill would have a lower permeability, a higher residual water content than the well-sorted backfill, and could imbibe water out of drift walls toward the WP, depending on

the saturation of the ESF wallrock. Although the higher capillary suction of a fine, poorly-sorted backfill can result in more uniform contact of water with the WP surface, the same capillary suction could prevent water from entering the WP. Shotcrete coatings on walls of tunnels or emplacement drifts, if applied, would have an effect on dripping patterns. This would have to be independently evaluated by the staff. The USGS (1998) has submitted to DOE a level 4 milestone report, SPH261M4, regarding the hydraulic properties of backfill materials. The staff have not yet evaluated this report.

In the absence of backfill, water dripping from the drift crown is the only mechanism for water to directly contact the WP. In this case, there are several factors that should be considered in estimating the amount of water that could potentially drip onto a WP. For example, the angle that a fracture intersects a drift will affect the potential for fracture flow to divert laterally around the drift. The dip angle will also affect the amount of water required to overcome any capillary barrier to dripping. The hydraulic properties of a fracture affect the fluxes within the fracture and the degree to which a capillary barrier between fractures and the open drift will act to divert flow around the drift. Several other factors, such as fracture frequency, fracture intersections, fracture coatings, and degree of heterogeneity, should also be considered. Long-term dripping from fractures is also likely to result in stalactite formation—especially in the high-evaporation environment that could result from WP heating. Formation of stalactites tends to focus fracture dripping on constant locations.

The case of partial filling of the drifts with backfill will exhibit features of both the full backfill and no backfill scenarios. Diversion of matrix flow and dripping from fractures may occur at the crown of the drift. The dripping water plus water imbibed from sidewalls of the drift will be somewhat distributed around the WP, although vertical flow through the backfill from a dripping crown would concentrate some of the moisture.

A conservative approach to incorporating drift seepage into PA models is to assume that 100 percent of the percolation flux that intersects a drift will enter the drift opening and contact a WP. Only a fraction of percolating waters is likely to enter drifts based on geometric arguments, i.e., the relatively small percentage of repository area that will contain waste packages. Also, because of the capillary barrier imposed by the drift opening, some percolation flux is expected to be diverted around the drift. Presumably, there is a percolation threshold, below which no seepage into the drift will occur. The DOE PA model currently takes credit for diversion of flow around drifts; their characterization of drift seepage is based on both modeling and field studies. A more conservative approach than 100 percent of the percolation flux intersecting the drift may be envisioned if focusing or funneling of flow incorporates flow from a larger area than the repository into the repository. Given the intensity of fracturing in the TSw, NRC staff believe that, on the average, the amount of flow funneled to the repository will be the same as the amount funneled away from the repository. New information on the fracture system in the TSw may change the NRC staff views on seepage into drifts.

Wang, et al. (1997) reported preliminary results of field seepage tests conducted in two niches in the ESF. Of the five tests conducted, one did not result in flow into the niche; another induced flow to reach the ceiling and migrate along the mined surface as film flow, but water did not drip into the niche; and dripping from fractures into the niches was observed in the remaining three tests. Of the three tests where dripping was observed, the mass of water collected in the fluid collection system ranged from 9.5 to 27 percent of injected mass. The

NRC believes that the niche and alcove tests are extremely useful for corroborating drift-scale numerical model and that measurements and experiments in the east-west drift will similarly provide useful information.

Birkholzer, et al. (1997a,b) used a 3D fracture continuum model to simulate seepage into drifts under both isotropic conditions and anisotropic permeability conditions. Heterogeneity was applied to the permeability field with no consideration of possible correlation between permeability and fracture α values. The modeled steady-state percolation fluxes ranged from 5 mm/yr to 1,000 mm/yr. Seepage into drifts was found to start when steady-state percolation fluxes were on the order of tens of millimeters per year, with heterogeneity in the fracture continuum being a key factor controlling the rate of seepage. The same fracture continuum model was used to simulate the niche studies, with generally good agreement between the model and observations, reportedly occurring with no calibration or fitting (Birkholzer, 1998).

A similar modeling effort was conducted using 2D and 3D dual-permeability models with a fracture-matrix interface factor to allow for a reduced wetted contact area between fractures and matrix. Results of this effort, reported by Tsang (1997), indicate that the inclusion of fracture-matrix interaction is only important when percolation flux occurs as transient pulses.

A continuum model requires definition of a representative elementary volume (REV). This requires that any heterogeneities should be incorporated at a scale either much smaller than the grid scale (i.e., subgrid heterogeneity) or much larger than the grid scale (i.e., parameter variability within the model). Accordingly, the assumption of a fracture continuum requires that the fractures either be numerous relative to the grid scale (subgrid) or be explicitly accounted for (parameter variability within the model). Sonnenthal, et al. (1997a) report that measured fracture frequencies in the TSw unit (counting only fractures at least 1 m in length) range from 0.48 to 4.45 m^{-1}. If the continuum approximation requires numerous fractures, a continuum approximation for fractures of this size and larger may require tens of meters to achieve a representative elementary volume, which is larger than the drift diameter. Using an *ad hoc* criterion of 5 fractures per grid block length to enable the fracture-continuum assumption, drift-scale simulations with 0.5-m grid blocks (fairly coarse) would require fracture frequencies of roughly 10 m^{-1}, implying that the assumption of a fracture continuum may be violated at the drift scale and models assuming a fracture continuum may misrepresent important fracture/drift interactions.

The assumption of uniform, steady-state infiltration in the fracture continuum model does not take into account potential episodic fracture flow. Modeling results that indicate that the PTn unit has a large capacity to attenuate large infiltration pulses, together with the presence of the PTn over almost all of the repository footprint, support the assumption of steady-state conditions at the repository horizon. However, given the existence of perched water at the base of the TSw that shows geochemical evidence of having partially bypassed the PTn (e.g., Striffler, et al., 1996; Yang, et al., 1996a,b), the potential for episodic infiltration pulses should not be discounted entirely.

In a fracture continuum model, diversion of percolation flux around the drift is possible at all spatial locations, due to the continuum assumption, and diversion is controlled by random heterogeneities. In reality, the diversion path of fracture flow around a drift is controlled by geometric factors, particularly, fracture orientation: fractures that intersect the drift at highly

oblique angles require a longer flow path for diversion and, thus, are more likely to result in dripping. NRC staff believe that correlation structures used in the DOE fracture continuum model do not appear to capture this effect of increased diversion path length caused by oblique fractures. Moreover, continuum models do not account for fracture intersections, which may form highly permeable linear pathways that can focus flow toward drifts. Furthermore, it is assumed in the fracture continuum model that all water in fractures is influenced by capillarity; the possibility of sheet-type flow in large-aperture fractures is not considered. Because sheet flow along surfaces of large-aperture fractures is not held by capillary forces, it is more likely to result in dripping where such flows intersect drifts. The predominance of sheet-type flow in fractures at the ESF horizon may be supported by the predominance of fracture coatings (Paces, et al., 1998b) occurring on only one side of the fractures.

Fracture permeability distributions used in the DOE fracture continuum model are based on drift-scale air permeability measurements, analysis of cores, and ESF fracture mapping. Estimations of fracture α values are based on calibration of the Site-Scale UZ Model (Bodvarsson and Bandurraga, 1997a). In general, narrow-aperture fractures are expected to have lower permeability and more capillary suction (lower α values), with the opposite being true for wide-aperture fractures. Inclusion of such a correlation in seepage models would cause low-permeability fractures to have higher saturations than high-permeability fractures, which may affect both seepage into, and diversion around, drifts. Correlation between fracture permeability and fracture α value is not considered in the DOE model, although it is recognized that both fracture frequency and fracture aperture affect fracture permeability, while only fracture aperture affects fracture α. Dual-permeability drift scale-model results, reported by Tsang (1997), predict a reduction in drift seepage, when fracture α values are correlated to fracture permeability. Based on this result, a lack of correlation between these parameters in a seepage model can be considered a conservative assumption.

An additional caution regards the use of air-permeability testing to infer fracture hydraulic permeability. There is a possibility that water-bearing fractures could exhibit low air permeability because of water filling the fracture voids. This would be especially true for narrow-aperture horizontal fractures with high capillary suction, which can wick away significant quantities of water. In areas where the horizontal fractures have smaller apertures than the vertical apertures, capillary suction may generate a moisture-dependent anisotropy for water that is primarily horizontal rather than vertical at low saturations.

- **Distribution of Drifts with Potential for Seepage**

The quantity and distribution of water that seeps into drifts depends on the amount and spatial variability of deep percolation that reaches the repository horizon, and on the variability in hydraulic properties of fractures that intersect drifts. Two quantities are used to parameterize seepage into drifts for the DOE model: the seepage fraction and the seep flow rate. The seepage fraction is defined as the fraction of WP contacted by seeps while the seep flow rate is the flow rate onto those packages that are contacted by seeps. Ranges for these parameters are estimated stochastically, using the 3D heterogenous fracture continuum model described in the previous section; they are based on weighted distributions of fracture permeabilities and α values, and a broad range of percolation fluxes are used in this estimation method. It is assumed that there is no correlation between these model input parameters. Based on the distribution of fracture properties, a distribution of seepage threshold fluxes is calculated, and

the seepage fraction is the fraction of drifts that receive percolation flux above their respective seepage thresholds while the seep flow rate is the portion of percolation flux in excess of the seepage threshold. In the DOE PA model, seepage is calculated for six repository regions under present climate conditions, long-term average climate, and a super-pluvial climate. It is presently assumed by DOE that all seepage that enters the upper half of a drift will contact a WP.

The NRC approach to incorporating seeping drifts into a PA model is currently based on the approach used in TSPA-95 (TRW Environmental Safety Systems, Inc., 1995), assuming that the matrix will carry all fluxes up to the matrix K_{sat} with any excess flows occurring in the fractures. Matrix fluxes are assumed to divert around the drift, while fracture flows enter the drift, with both the matrix K_{sat} and the percolation fluxes assumed to be independent and lognormally distributed.

An option under consideration by DOE for emplacement of canisters is to create a stand-off distance from fault systems that have been recently active on a geologic time scale. An active fault is one that has indications of movement over the last 2 million yrs (Elater and Nolting, 1996). Stand-off of 60 m is limited to the active faults, such as the SCF, the Drill Hole Fault, and the Abandoned Wash Fault. However, for the GDF, the distance that canisters should be shifted away from the fault is 120 m due to the large air permeability values and large fracture zone width (Elater and Nolting, 1996). The NRC staff review of methods used for determination of stand-off distance should consider variability along fault systems, both the dip of the fault and the strike of the fault relative to the drift, and the geochemical evidence suggestive of spreading laterally away from faults. In the ESF, ^{36}Cl appears to have spread laterally away from the main fault trace of the SDF over 200 m along the cooling joint system (Levy, et al., 1997).

4.4.3.3 Percolation Processes Below the Repository

The nature of percolation below the repository horizon affects the formation of perched water, the spatial distribution of flux to the water table, groundwater velocities, and radionuclide advection, dispersion, sorption, and decay. If percolation is dominated by matrix flow through the CHn rather than fast pathways, slow travel times, increased adsorption (with resulting augmentation of retardation and decay), and mixing with the relatively large volume of water in the matrix pores are expected to occur. The potential for adsorption is particularly great in zeolitic horizons.

Flow paths from the repository horizon to the base of the TSw unit are expected to be predominantly vertical within the TSw fracture system. At the base of the TSw unit and below, flow paths are more uncertain. In nonwelded vitric units, flows are expected to be predominantly vertical within the matrix, but fracture flow may occur as well. In areas with significant zeolitization, there may be complex combinations of matrix and fracture flows, with strong possibilities of lateral flow. The nature of flow through the CHn is the primary source of uncertainty in flow paths and travel times from the repository to the water table.

- **Flow Through Non-Welded Vitric and Zeolitic Horizons**

Percolation in the TSw unit is expected to occur primarily in the fracture system. The highly fractured TSw basal vitrophyre overlies the porous nonwelded CHn, leading to the possibility of

lateral flow and perched water in areas where the vertical transmission rate of the CHn is exceeded. The presence of perched water above altered units in the CHn signifies slow vertical percolation within the altered units, providing the potential for lateral flow to bypass the altered zones and enter faults or unaltered zones. The absence of perched water above the vitric portions of the CHn suggests that percolation is rapid enough to conduct fluxes under current climatic conditions.

The vitric zones are sufficiently permeable that percolation may be primarily within the matrix. Zeolitic alteration of glassy tuffaceous material has been shown to drastically reduce permeability without significantly affecting porosity (Loeven, 1993). Measured permeabilities in the vitrified and de-vitrified horizons are generally 1 to 2 orders of magnitude higher than in the altered zones. Hydraulic conductivity measurements of 5 vitric samples from the CHn range from about 1×10^{-5} to 5×10^{-6} m/s, whereas, zeolite-altered core measurements ranged from about 3×10^{-7} to less than 1×10^{-12} m/s [the lower limit of the measurement technique (Flint, 1997)]. The saturations in vitric units are generally lower than those in altered units, indicating greater drainage properties for the vitric versus the altered (zeolitic).

Flow in the vitric portions of the CHn may also be through fractures. The characteristics of fractures and fast pathways in the vitric portion of the CHn are not well known. However, there are indications that water moved quickly into the vitric zones. Major element chemistry and ^{14}C data suggest that matrix water below the perched water is distinct from the perched water (Fabryka-Martin, et al., 1997; Rousseau, et al., 1996). The underlying matrix water appears to be younger, and to have bypassed the perched water in the CHn layers. This could be explained either by fracture flow through the vitric or matrix flow through a small thickness of the vitric layers followed by lateral flow beneath the perched zone. Where the vitric overlies the zeolitic alteration, the transitional contact in the north is less than 20 m below the basal TSw vitrophyre in the north and 460 m below in the southwest (Rousseau, et al., 1996).

The impact of large structural features on travel times could be significant. According to Ritcey, et al. (1997a), the fastest travel times are expected for paths in the center of the repository block where a greater amount of fracture flow would occur or where flow might be along stratigraphic contacts to structural features such as the GDF and Dune Wash Fault. The hydraulic properties of the faults dictate whether perching or drainage down the fault to the saturated zone will occur. Wu, et al. (1996) hypothesized that travel paths south of Dune Wash divert to the east, and, if the GDF is neither a barrier nor a conduit, continue eastward in the fractured TSw to meet the water table near the Bow Ridge Fault. However, the perched water noted in boreholes SD-7, SD-12, SD-9, NRG-7, UZ-1, UZ-14, G-2, and WT-6 is an indication that the GDF is likely (at least locally) to be a barrier with relatively low permeability, and possibly altered near the perched water. There are insufficient data on the lateral characteristics of the GDF to determine the continuity of perched zones at YM.

The CHn mineralogy is highly variable, with both lateral and vertical gradational variations, due to nonuniform alteration of parent tuffs. The general distribution of zeolitic alteration in the repository block is described by Moyer and Geslin (1995) and Carey, et al. (1997). Based on the interpretations of Moyer and Geslin (1995) and Hinds, et al. (1997), there is a gap in the zeolite alteration in the southwestern portion of the repository area (Figure 3). The LBNL model (Hinds, et al. 1997) is based on four layers in the geologic stratigraphy from the basal TSw,

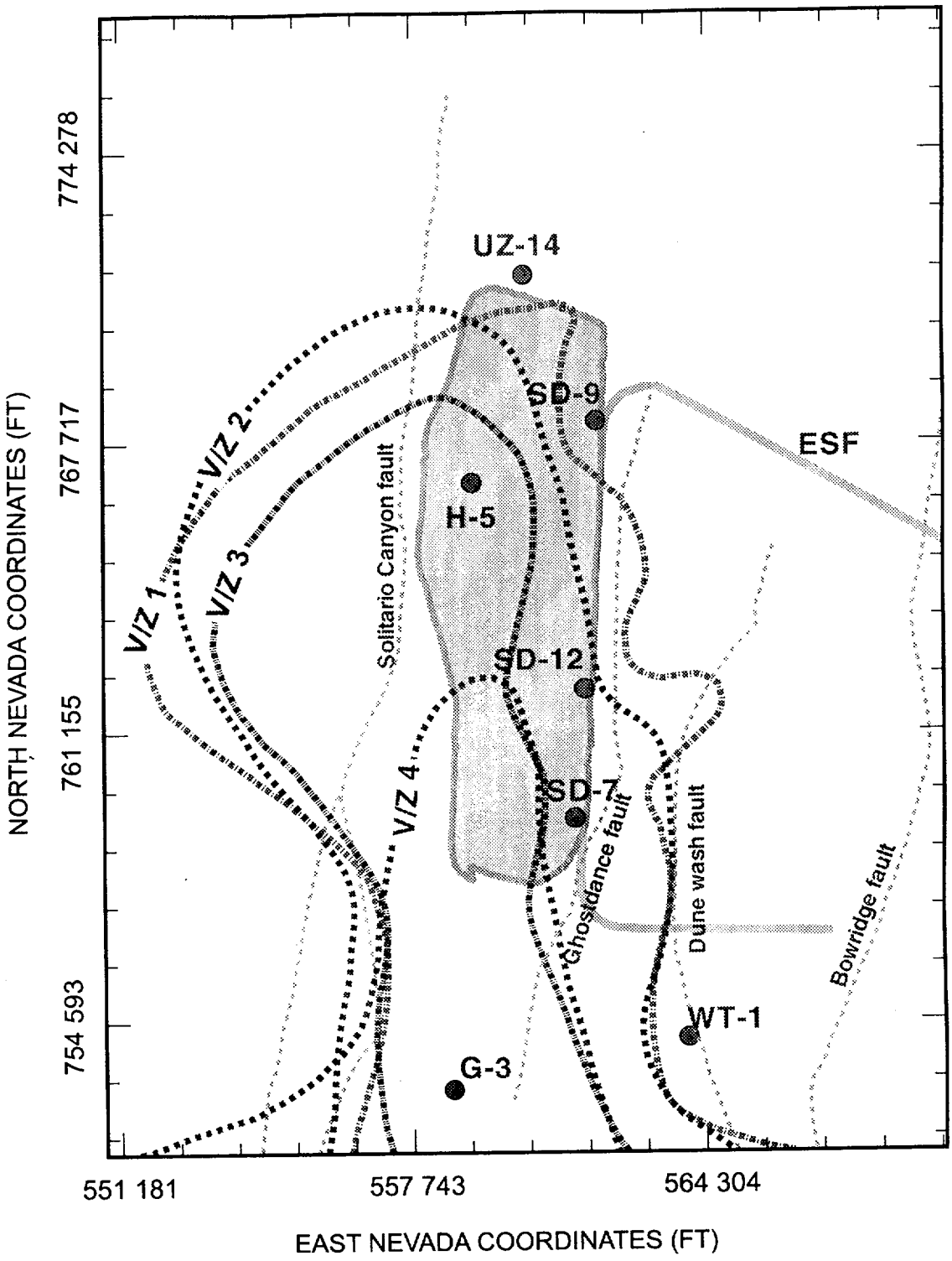

Figure 3. Transitions from zeolitic to vitric zones in the basal vitrophyre of the Topopah Springs Tuff, the Calico Hills Unit, and upper Prow Pass Tuff used by Lawrence Berkeley National Laboratory in the site-scale unsaturated zone model. The model accounts for four layers, all of which include a transition (V/Z) from vitric to zeolitic. This figure is a modified version of Figure 4-8 (page 4-12) of Bodvarsson, et al. (1997a).

through the CHn, to the upper Prow Pass unit. Each sublayer is divided into a homogeneous layer of vitric or zeolitic portions as delineated by a threshold of ten weight percent zeolite alteration. In the LBNL model, appropriate hydrologic properties for each zone are assigned, but are kept uniform throughout each zone. However, given the limited data available to support this generalized description of the zeolite distribution, new information may significantly change the interpretation.

In contrast to the LBNL interpretation, the LANL site-scale flow and transport modeling (Robinson, et al., 1997) used the ISM2.0 geologic framework and adds a mineralogic module that modifies the CHn sublayer properties based on the amount of zeolite alteration; hence, heterogeneous properties are incorporated into the numerical model for flow and transport. The mineralogic model is based on the work of Chipera, et al. (1997) and Carey, et al. (1997), where the x-ray data from boreholes were interpolated onto the geologic section using a program called STRATAMODEL. In their conceptual model, Robinson, et al. (1997) assumed that flow would more readily occur in the vitric and the slightly altered zones. Zones of heavy zeolite alteration would have low permeability, thus, promoting lateral flow around, rather than vertical flow through, the zeolites. However, a small amount of zeolites may not impact the permeability of the vitric zone. Hence, the predominance of sorption of radionuclides would be postulated to occur in the slightly altered zones rather than the heavily altered zones. The wide range, from 10 to 10,000 yr, in the particle tracking results of Robinson, et al. (1997) captures the uncertainty in flow paths through the CHn unit, with short times reflective of fast pathways through faults and long times reflective of flow through zeolitic matrix. Thus, understanding the detailed distribution of the mineralogy in the Calico Hills Unit is of utmost importance for flow and transport below the repository.

A total of 1503 records from 20 boreholes in the YM block extend into or cross the CHn; 18 of the boreholes fall in the area outlined in Figure 3. Typically, there are 10 to 35 analyses in the zone from the basal TSw unit to the upper Prow Pass units. The area below the western portion of the repository is poorly constrained (Carey, et al., 1997) due to data available in only three boreholes of which only one is considered reliable (G-3, one mile south of repository). Chipera, et al. (1997) report thinly intercalated layering of the vitric and zeolitic zones that would have been easily missed by the previous sampling intervals of 15 to 40 m. They also contend that there are no data to support the "misconception" of holes in the zeolite layers, indicating instead, that there are intercalated vitric and zeolitic layers at each borehole.

Figures 4 and 5 represent the interpolated data from the LANL STRATAMODEL program conformally mapped onto the GFM3.0 geologic section (Geologic Framework Model; documentation not yet released). The geologic portion of ISM2.0 and the GFM3.0 models do not differ in the region around the zeolites. In the figures, the zeolite weight percent is conformally mapped to the Tac and the Tacbt (basal part of Thtbt) units using 0.1 as a vertical factor to support the lateral continuity of the altered zones. Figure 3 represents the distribution in the vicinity of the contact between the Tac and the Tacbt. Figure 5 represents the distribution on a plane that is a slice at the elevation of 826 m msl. Figures 4 and 5 would be expected to illustrate the V/Z 4 transition in Figure 3. These figures are presented not as a more accurate representation of the zeolite distribution but rather indicative of the lack of data to constrain the distribution of zeolites in the CHn and the representative hydrologic properties for those zones. The purported hole in the zeolite alteration in the southwestern portion of the

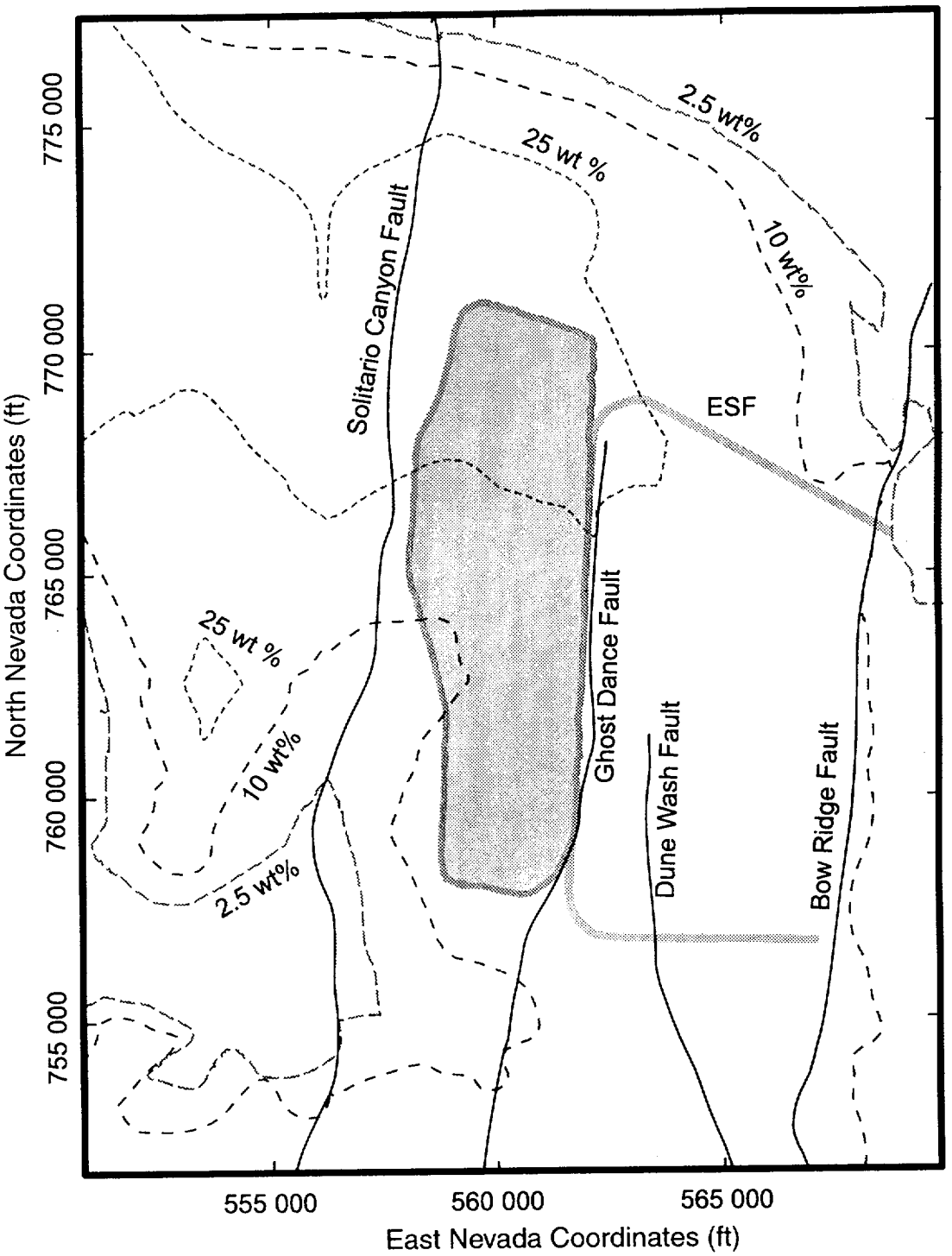

Figure 4. Zeolite weight percent contours over the same area as Figure 3 using interpolated data referenced in Carey, et al. (1997) in the lower portion of the Calico Hills Formation.

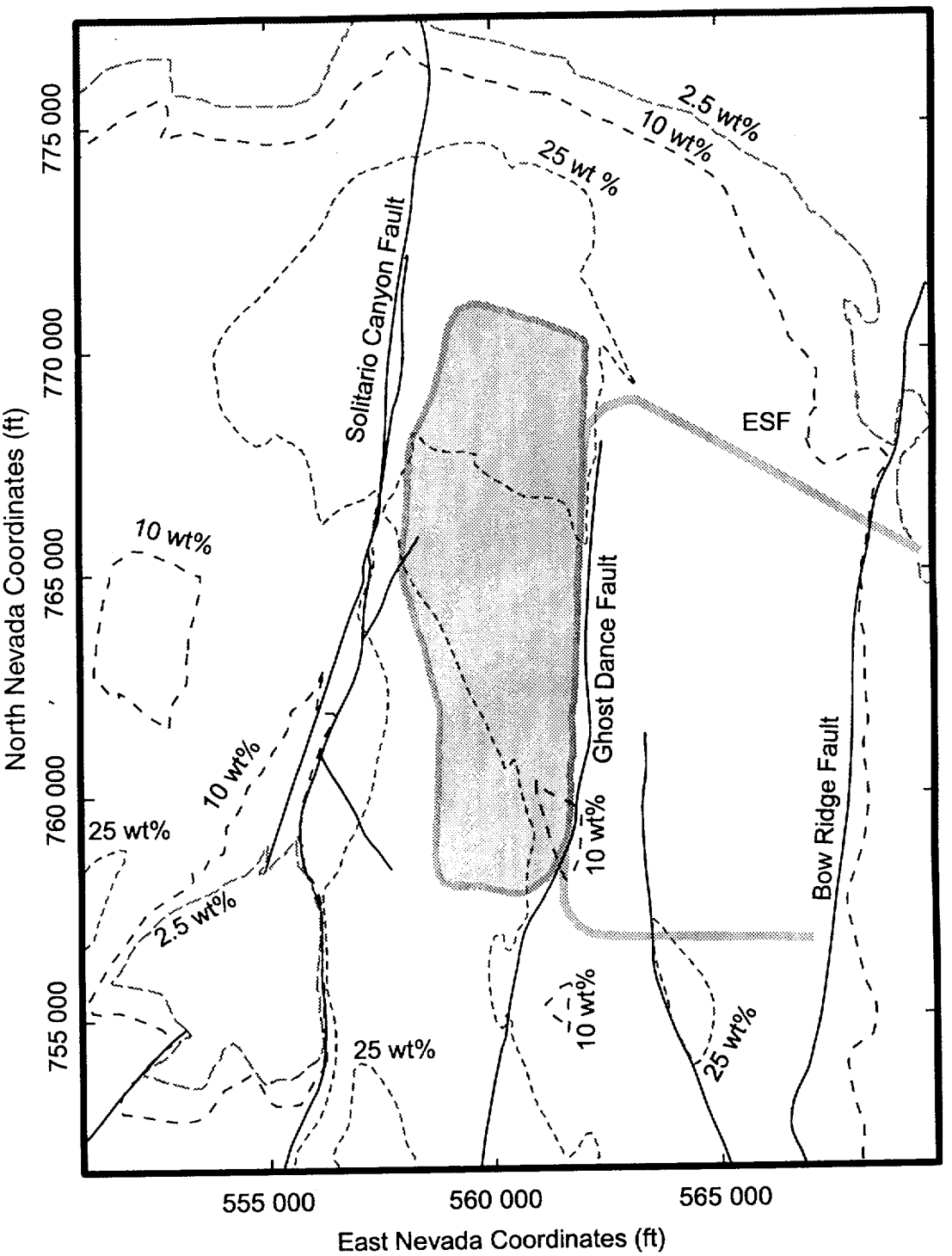

Figure 5. Zeolite weight percent contours over the same area as Figure 3 using the interpolated data referenced in Carey, et al. (1997) at the 2709 foot elevation (above mean sea level).

ATTACHMENT B

INITIAL ASSESSMENT OF DILUTION EFFECTS INDUCED BY WATER WELL PUMPING IN THE AMARGOSA FARMS AREA

INITIAL ASSESSMENT OF DILUTION EFFECTS INDUCED BY WATER WELL PUMPING IN THE AMARGOSA FARMS AREA

Prepared for

Nuclear Regulatory Commission
Contract NRC-02-97-009

Prepared by

R.W. Fedors
G.W. Wittmeyer

Center for Nuclear Waste Regulatory Analyses
San Antonio, Texas

Revised
January 1998

ABSTRACT

A preliminary study was undertaken to gain insights into the factors controlling borehole dilution effects in the Amargosa Farms area from a potential release at the proposed Yucca Mountain repository. Dilution in individual boreholes depends on the fractions of water drawn from contaminated and uncontaminated production zones, which in turn depend on the depth of the well, screened intervals, aquifer hydraulic parameters, pumping rates, and distribution of radionuclides across a plume. Dilution arising from infiltration or groundwater mixing underneath the repository was not included in this analysis.

The fundamental question addressed by this study includes how variations in well construction practices, hydraulic parameters of the basin-fill aquifer, and pumping rates affect capture of radionuclide plumes of specified shapes. Detailed statistical analysis of magnitude and spatial distributions of water usage and well bore construction practices was conducted for the Amargosa Farms area. A sensitivity analysis for borehole dilution was performed to assess the effects of reasonable variations in aquifer hydraulic parameters, well depths, screening practices, and variations in pumping rates of irrigation and domestic supply wells for various radionuclide plume configurations. A distinction is made between dilution factors based on volumetric fluxes of the capture and plume areas and those based on dispersion during transport. In general, the volumetric flux-based dilution due to wellbore mixing reduced radionuclide concentrations by less then an order of magnitude. The range of dilution was primarily affected by pumping rates and plume thickness. The choice of modeling the plume with significant vertical dispersion (thick plume) versus little or no vertical dispersion (thin plume) had a significant impact on the borehole dilution factors. The dispersion (transport)-based dilution factors ranged from one to two orders of magnitude with the conservative lower bound delineated by the ratio of the source concentration and the centerline concentration of a plume.

CONTENTS

FIGURES

FIGURES (Cont'd)

TABLES

ACKNOWLEDGMENTS

This report was prepared to document work performed by the Center for Nuclear Waste Regulatory Analyses (CNWRA) for the Nuclear Regulatory Commission (NRC) under Contract No. NRC-02-97-009. The activities reported here were performed on behalf of the NRC Office of Nuclear Material Safety and Safeguards (NMSS), Division of Waste Management (DWM). The authors thank Chad Glenn (NRC) for his assistance in obtaining data from the Nevada Division of Waster Resources, Ron Martin for his assistance with geographic information (GIS) data; J. Winterle, A. Armstrong, and R. Baca for their technical reviews; and B. Sagar for his programmatic review. The authors would also like to thank C. Gray for his editorial review and C. Garcia for secretarial support. The report is an independent product of the CNWRA and does not necessarily reflect the views or regulatory position of the NRC.

QUALITY OF DATA, ANALYSES, AND CODE DEVELOPMENT

DATA: CNWRA-generated original data contained in this report meet quality assurance requirements described in the CNWRA Quality Assurance Manual. Sources for other data should be consulted for determining the level of quality for those data.

ANALYSES AND CODES: The GFLOW Version 1.1, PATCHI Version 1.1, and STRIPI Version 1.1 computer codes were used for analyses contained in this report. These computer codes are controlled under the CNWRA Software Configuration Procedures.

1 INTRODUCTION

Yucca Mountain (YM), Nevada, was originally proposed as a deep geologic repository for high-level radioactive waste due in part to its favorable hydrogeologic regime. Moisture fluxes within the 700 m thick unsaturated zone at YM were presumed to be small (< 0.1 mm/yr) due to the region's arid climate and the low permeability of the tuff units comprising the mountain (U.S. Department of Energy, 1988). Low moisture fluxes should reduce the rate of waste canister corrosion, subsequent dissolution of the exposed waste form, and transport of radionuclides to the accessible environments. However, recent studies (Stothoff, 1997; Flint and Flint, 1994) suggest that mean annual infiltration at YM may be as high as 15 mm and provide convincing evidence that there are fast pathways, albeit probably spatially focused, from the surface of YM to at least the depth of the repository (Fabryka-Martin et al., 1996). Radionuclides not sorbed by the zeolitized bedded tuffs that underlie the repository (e.g., technetium, iodine, neptunium), or diffused from fluid-conducting fractures into the rock matrix within welded tuff units, will enter the water table, which, based on current engineering designs, lies 250 to 300 m below the repository. Current hydrogeologic studies (Czarnecki and Waddell, 1984; TRW Environmental Safety Systems, Inc., 1995) indicate that radionuclides that enter the saturated zone beneath YM would generally flow to the south-southeast into western Jackass Flat within the welded tuff aquifer and then south-southwest into the Amargosa Desert where the water table lies within an alluvial aquifer. In order to demonstrate compliance with a risk- or dose-based standard, mixing that occurs due to saturated zone transport and active pumping of wells may play a major role in reducing radionuclide concentrations.

Saturated zone dilution of radionuclide concentrations depends on the bulk flow rate of water beneath YM at locations where radionuclides enter the water table, the degree of mixing caused by large-scale variations in the groundwater velocity field in the welded tuff and alluvial aquifers, and mixing in boreholes where water may be pumped for domestic or agricultural use. Clearly, the amount of dilution depends on the duration and degree of mixing along the radionuclide transport path, while the estimated risk or dose depends on the ultimate use of water pumped from the aquifer. Estimating dose or risk requires definition of a potentially exposed population and the potential biosphere pathway by which an individual would be exposed to released radionuclides (TRW Environmental Safety Systems, Inc., 1995). In the TSPA-95 (TRW Environmental Safety Systems, Inc., 1995), it was assumed that the peak dose to the maximally exposed individual is received by a person drinking 2 L of water per day pumped from the welded tuff aquifer at a location just outside the boundary of the controlled area (5 km outside the repository footprint). However, National Academy of Sciences recommendations may require determining the peak dose to the average member of a critical group, based on current water and land use practices in the YM area. Therefore, it is prudent to consider populations currently residing downgradient from YM, such as the Amargosa Farms area (figure 1-1), that produce at least a portion of the food they consume using local groundwater to irrigate their crops. However, one should consider variations in individual expected dose within the critical group due to differences in well locations, well construction, and pumping rates.

As noted in Kessler and McGuire (1996), dispersive transport processes are relatively ineffective at reducing contaminant concentrations in a steady-state groundwater flow regime. If there are large temporal variations in the magnitude and direction of the groundwater velocity field, then mixing and attendant dilution during transport may be significant. Current conceptual models of the YM saturated groundwater system would suggest that the flow regime is relatively unperturbed by fluctuations in the magnitude and location of recharge and discharge. However, increased pumping for irrigated agriculture in the Amargosa Farms area over the past 30 yr may have had some effect on the groundwater flow

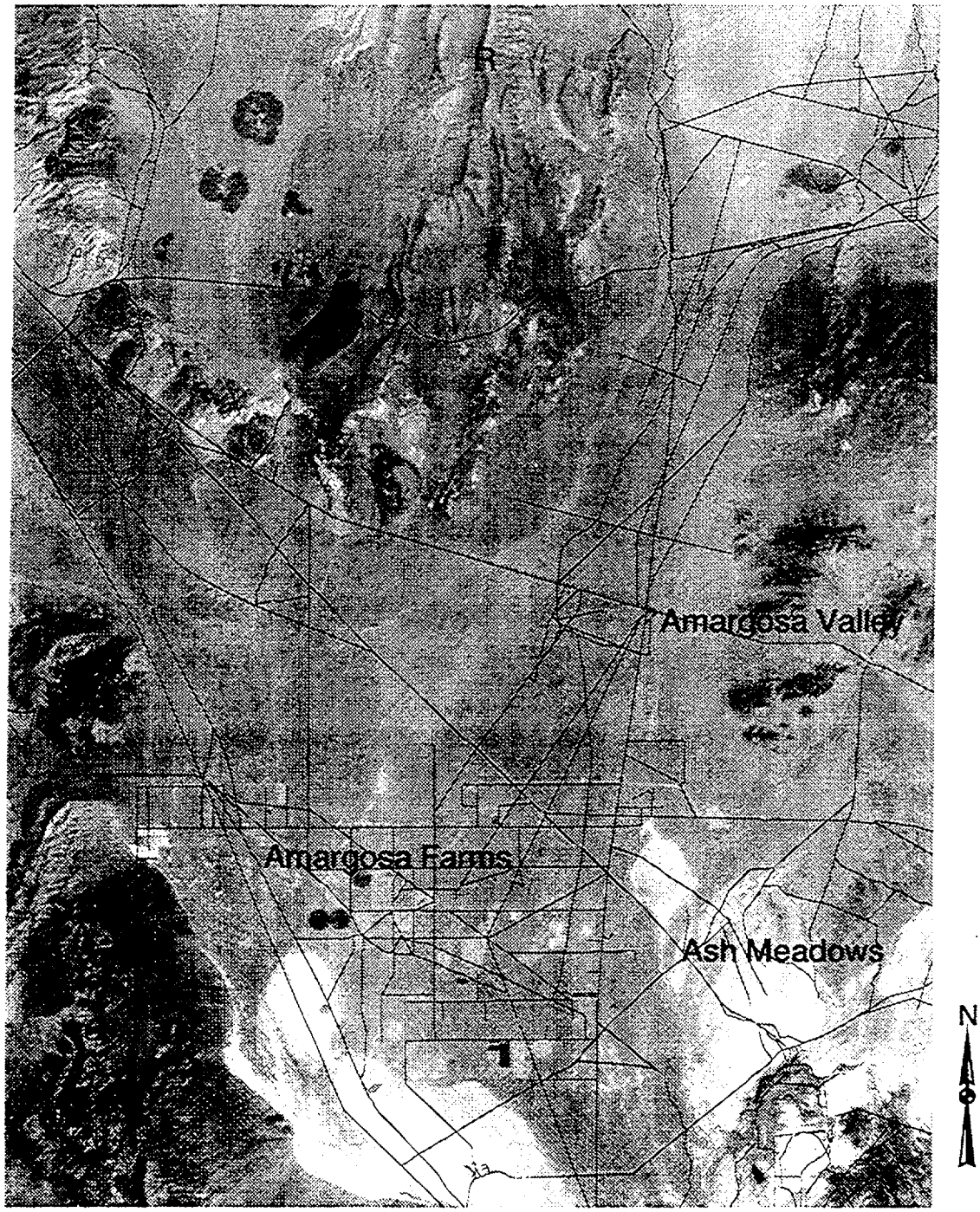

Figure 1-1. Lower Amargosa Desert region south of proposed Yucca Mountain repository site (R) including Amargosa Valley and Amargosa Farms

regime. Nonetheless, in the present study it is assumed that pumping has no effect on the groundwater flow regime between YM and receptor locations. If the primary effect of pumping on the flow regime is enhanced mixing or more rapid transport, the assumption of steady state flow conditions, if not realistic, is at least conservative from the standpoint of radionuclide dose.

Dilution factors can be defined in a number of ways. Each of the three definitions mentioned in this report are based on a particular approach to addressing dilution. The first approach addresses dilution that results from dispersion of a solute during transport; the dilution factor is calculated as the ratio of concentration at the source area to that at the receptor point. The second approach addresses dilution due to mixing and is calculated as the mass release rate divided by the largest flux of water into which the solute may be mixed and used by a critical group. The third approach addresses dilution due to the intersection of the capture zone of a pumping well with the plume configuration at the withdrawal location. In this case, the dilution factor is calculated as the ratio of the plume area intercepted by the capture area and the entire capture area. The third approach is used in this report to describe borehole dilution from the geometric standpoint and it may be linearly combined with the first approach for a total borehole dilution factor. Usage of the first two approaches is described further below.

Baca et al. (1997) and Kessler and McGuire (1996) used the first approach to calculate point dilution factors (P-DF) where point refers to concentration at a single point. Under assumptions of steady state flow, estimated dilution factors due to dispersive mixing along the saturated zone transport pathway from the proposed YM repository to locations 20 to 30 km to the south have ranged from 5 to 50 (Baca et al., 1997) and from 4 to 44 (Kessler and McGuire, 1996). In both analyses, the reported dilution factors were determined by solving the advection-dispersion equation. Baca et al. (1997) contoured the P-DF while Kessler and McGuire (1996) tabulated P-DFs based on centerline concentration. In TSPA-93 (Wilson et al., 1994), TSPA-95 (TRW Environmental Safety Systems, Inc., 1995), and Iterative Performance Assessment Phase 2 (Nuclear Regulatory Commission, 1995) it was assumed that additional dilution occurs at the receptor location due to mixing of clean and contaminated water in the borehole and, in the case of TSPA-95, due to mixing of waters from groundwater basins influent to the central region of the Amargosa Desert.

In the ongoing NRC Iterative Performance Assessment (IPA) Phase 3, the borehole dilution factor corresponds to a single well that is pumped at a rate sufficient to supply all water needs for the critical group in question. For example, if there are assumed to be 12 quarter-section, center pivot irrigation plots under cultivation with alfalfa at Amargosa Farms, the equivalent annual well discharge[1] is 9,300,000 m^3. If the critical group consists of a residential community of 500 persons located 5 km south of YM, the equivalent annual well discharge[2] would be 103,700 m^3. Borehole dilution factors can be computed directly for the critical groups if the volume of contaminated water captured by the well is known. For example, if, the volume of contaminated water captured by the well at Amargosa Farms is 930,000 m^3, the dilution factor is 10. However, in order to determine a dose, one must compute the radionuclide concentration in the borehole and, hence must also know the concentration of radionuclides in the contaminated water captured by the well. Inherent in this approach, the assumption is that the entire radionuclide plume is captured and that there is no well-to-well variation in the concentration. This report

---

[1] 12 plots × 126 acres/plot × 5 ft of water/year ÷ (8.107×10^{-4} m^3/acre-ft).

[2] 150 gal/person-day × 500 persons × 365.25 days/yr × 3.785×10^{-3} m^3/gal.

addresses the validity of this assumption considering the concept of borehole dilution as well as the distribution of pumping well locations and pump magnitudes.

1.1 GEOSPHERE RELEASE PATHWAYS CONSIDERED IN TSPA

Farming in the Amargosa Farms region is partially related to the accessibility to well water. The combination of non-arable land and large depths to the water table restrict farming-based population growth to the area immediately south of the town of Amargosa Valley. The water table gradually approaches the land surface toward the southern reaches of the Amargosa Farms area. Exposure scenarios are assumed to occur through a combination of drinking water and ingestion of locally raised produce and livestock. The lengths of the groundwater flow paths from YM to domestic and commercial wells and irrigation wells are approximately 25 and 30 km, respectively.

1.2 LITERATURE REVIEW

In groundwater hydrology, the term borehole dilution is used to describe several phenomena including: (i) contaminant sampling biases resulting from improper monitor well construction, (ii) the effectiveness of pump and treat remediation systems, and (iii) capture zone analysis. Borehole dilution is used to explain one to two order-of-magnitude differences in values between concentrations measured in sampling wells and concentrations measured in the aquifer; however, the concentration in the borehole may be greater than the *in situ* or resident concentration. Borehole dilution is also the name of a procedure used to estimate permeabilities or seepage velocity in a single well bore through analysis of the dilution rate after release of a solute in the wellbore. Borehole dilution in the present work refers to dilution of the resident contaminant concentrations in a wellbore due to pumping a well that captures both contaminated and uncontaminated portions of the aquifer.

Six factors that may significantly affect the borehole concentration are: (i) well pump rate and well distribution in the well field, (ii) regional hydraulic gradient, (iii) transmissivity, (iv) hydrostratigraphy and anisotropy, (v) well penetration depth and length of screen, and (vi) vertical and horizontal contaminant plume distribution. Analytical solutions for flow can incorporate the effects of well pump rates, well design, and regional gradients under certain restrictions for a sensitivity analysis. Complex numerical models are generally required to analyze the effects of heterogeneity in the hydraulic properties and simulate complex plume configurations, especially if three-dimensional (3D) effects are considered to be important. An increase in the spacing of the wells may increase the capture zone horizontally but may decrease the capture zone vertically and may introduce gaps in the capture zone between wells where contaminants may escape. An increase in the regional hydraulic gradient will act to decrease the capture area. An increase in the anisotropy will increase the capture zone horizontally but decrease it vertically.

Analytic solutions (Schafer, 1996; Faybishenko, et al., 1995; Grubb, 1993) and analytic element methods (Strack, 1989; Haitjema, 1995) have been published for estimating capture zones for partially penetrating wells in steady state 3D flow fields. Sensitivity analyses of effects that include vertical movement of water or solute in a heterogeneous domain require the use of numerical models. A good illustration of the factors that affect capture zone size and shape is found in Bair and Lahm (1996). Bair and Lahm (1996) used a finite difference method to determine the steady state flow field and particle tracking to delineate the size and shape of the capture zone. They determined the magnitude of changes to the capture zone area due to perturbations in the regional gradient, well penetration, pump rates, well

configuration, and degree of hydraulic conductivity anisotropy in the context of an idealized pump and treat design.

Three published articles on numerical simulation of 3D flow in and around a wellbore contain pertinent information for refined modeling in the vicinity of a single well. Chiang et al. (1995) simulated 3D flow and advective solute transport in the vicinity of a partially penetrating well in order to understand the order of magnitude difference in contaminant concentrations between well samples and point aquifer samples. The concentration profile in the aquifer was known. The well bore was modeled as separate elements with a permeability in the range of that predicted for laminar flow in a tube. They noted that their transient simulation results asymptotically approached the simple, mass balance-based result which assumes a flat water table.

Akindunni et al. (1995) simulated 3D flow near a well for various screen and plume positions. They approximated the well using a Neumann boundary condition at the edge of the domain at which the discharge was equally apportioned to the nodes along the screened length of the well. They compared vertically averaged values of concentration for both the wellbore and the aquifer. In the transient simulations, concentrations differed significantly in the well and aquifer. Concentrations in the wellbore were higher or lower than the vertically averaged aquifer value depending on the relative position of the plume depth and screened interval. However, over long times, the concentration in the wellbore asymptotically approached the vertically averaged aquifer value. In addition to screen position and plume position, they also investigated the dependence on screen length and anisotropy. Again, initial concentrations differed significantly but long time concentrations appeared to approach the vertically averaged aquifer value. As expected, simulations with large anisotropy ratios for hydraulic conductivity exhibited less vertical mixing than the isotropic case.

Reilly et al. (1989) also modeled the wellbore as a column of hydraulically connected cells; however, their focus was on wellbore flow in a monitoring well with implications for sampling bias and cross-contamination. In a monitoring well, cross-contamination will act to dilute the plume. Of note was their conclusion that greater than half the aquifer-to-wellbore flow occurred in the top ten percent of the screened length while greater than half the wellbore-to-aquifer flow occurred in the bottom ten percent of the screened length. Hence, solute plumes approaching the top of the screened portion will enter the wellbore while plumes approaching the bottom will tend to flow around the well. This finding may be pertinent for the Amargosa Farms area when irrigation wells are shut down, but is probably irrelevant during periods of pumping.

1.3 METHODS USED TO CONDUCT STUDY

Wellbore design and pumping practices in the Amargosa Farms region may have a significant effect both on the capture of a potential plume and, from another perspective, on the radionuclide concentration of the water pumped from the wells. Existing databases were analyzed in order to characterize the location, design, and production of wells. An important feature of the wells in the Amargosa Farms region is that they partially penetrate the alluvial aquifer thickness. The first wells encountered in a path of a simulated plume released from the proposed repository site are low pumping rate domestic, commercial, and quasi-municipal wells at a distance of approximately 25 km. Large pumping rate irrigation wells capable of lowering the water table over square kilometers of area are located at a distance of approximately 30 km.

The analytic element method is used to model 3D flow in the vicinity of a partially penetrating well. Particle tracking is used to delineate a capture area for different well designs, pumping rates, and regional flow characteristics. The capture area is determined at an upgradient point from the well location where the flow is essentially one-dimensional (1D); for example, no longer 3D. Also, the cross-sectional area of a plume entering the Amargosa Farms region is approximated by using two-dimensional (2D) and 3D solutions to the advection-dispersion equation. Geometric arguments are utilized to estimate dilution factors due to the portion of the plume captured. For dilution factors based on dispersive transport, numerical integration is used to estimate a representive concentration for the portion of the plume captured.

1.4 LIMITATIONS OF STUDY

The geometric borehole dilution factors reported here account only for borehole dilution due to pumping in the Amargosa Farms area. Dilution due to mixing with clean water, either underneath the repository or at the northern portion of Fortymile Wash, or from any interbasin transfers is not included. The dilution factors calculated using the different approach may not be linearly combined nor directly compared except under certain restrictions. A comparison of the Total-system Performance Assessment (TPA) streamtubes of Baca et al. (1997) with the geometries of the capture zone and plume configuration are not possible since they are derived from different phenomena.

Three significant assumptions are used in this study, in part due to the scarce amount of data for the groundwater in the alluvial sediments of Amargosa Farms region. Material properties are considered to be homogeneous and isotropic, the flow field is assumed to be uniform, and steady state pumping rate and contaminant transport are assumed to represent the effects of borehole dilution. The latter assumption specifically addresses that the irrigation pumping patterns can be approximated by an annual pump volume. The dilution factors calculated for steady state flow and transport provide an upper bound for those that would result from a transient analysis.

This study addresses borehole dilution induced by a single well, pumping at a rate comparable to an actual well in the Amargosa Farms area. This differs from the IPA Phase 3 approach where the entire volume of water needed by the critical group is used in determining radionuclide concentrations for dose calculations, hence all the wells are assumed equally mixed.

2 HYDROGEOLOGY OF THE AMARGOSA DESERT

The Amargosa Desert is a northwest-trending, triangular-shaped alluvial basin bounded on the north by Bare Mountain, YM, and the Specter Range, on the east by the Resting Spring Range, and on the west by the Funeral Range and Black Mountains. Elevations on the valley floor range from 975 m mean sea level (msl) at the Amargosa River narrows near Beatty and 720 m (msl) at the proximal edge of the fan formed by Fortymile Wash as it discharges from Jackass Flat to less than 610 m (msl) at Franklin Lake playa south of the Amargosa Farms region.

2.1 STRUCTURE AND DEPOSITIONAL HISTORY

The Amargosa Desert is an alluvial valley that resulted from large-scale block faulting in the Basin and Range Province (Plume, 1996; Bedinger et al., 1989). Sediments deposited in depressions created by Tertiary to Quaternary block faulting can be classified as alluvial fan, lake bed, and fluvial deposits. In general, the coarsest materials (gravels and boulders) were deposited near the mountains, and the finer materials (silts and clays) were deposited in the central part of the basin. The distribution of sediment is generally associated with distance from the mountains. Alluvial fans with steep gradients and coarse sediments flatten and coalesce basinward, interfingering with the lake bed deposits. Within the alluvial fans there is a complex interfingering and interbedding of fine and coarse sediments due to shifting of fluvial processes across the top of the fan. The finer grained, distal portions of the fans merge laterally and interlayer with the lake deposits. The lake bed deposits can include beach sand and gravel lenses, silts and clay layers, and evaporites from playa-type environments. The fluvial deposits of recent times consist of sand and gravel lenses along present or ancestral streams. These exhibit a greater degree of sorting than the alluvial fan deposits.

Repeated upheaval events led to a complex interbedding and interlayering of the proximal and distal facies of the alluvial basin sediments. The repeated upheavals, together with the lateral and down gradient transitions within the alluvial fan and grading into the lake bed or playa deposits, has strong implications for flow and transport on a basin-wide scale.

The Amargosa Farms region is in the distal portion in terms of sediment facies of an alluvial basin where lowland fans and lake beds would comprise much, but not all, of the stratigraphic section. Geologic lithologies and maps are described in Burchfiel (1966), Denny and Drewes (1965), Fischer (1992), Naff (1973), Swadley (1983), Swadley and Carr (1980), and Walker and Eakin (1963). Recent maps of the central Amargosa Desert area have followed the lithologic characterization of Hoover et al. (1981). Local features pertinent to the hydrogeology include the presence of tuffaceous beds (ash fall), limestone horizons, perched water systems (especially where the Funeral Mountain fanglomerates overlie lake sediments), common occurrence of caliche, and cementation of sand and gravel units. The high east-west hydraulic gradient, in the otherwise north-south regional gradient, between Amargosa Farms and Ash Meadows is thought to be due to low permeability lake bed sediments faulted into juxtaposition with the conductive Paleozoic carbonates of Ash Meadows.

The thickness of the alluvial sediments in the Amargosa Farms region in not well known. Bedinger et al. (1989) report the basin-fill as greater than 1,300 m, possibly as thick as 2,000 m for basins in the Death Valley Region. Oatfield and Czarnecki (1991) used geophysical data to estimate the thickness of the alluvial valley fill sediments in the range 800 to 1,100 m for the Amargosa Farms area.

Laczniak et al. (1996) infer depths up to 1,140 m on their east-west cross-section across the Amargosa Farms area.

2.2 BASIN-SCALE GROUNDWATER FLOW

Hydrographically, Amargosa Desert is part of the Death Valley groundwater flow system, which is a series of topographically closed intermontane basins connected at depth by the Paleozoic carbonate aquifer. The Death Valley groundwater system is further subdivided into three basins: (i) the Alkali Flat-Furnace Creek Ranch sub-basin; (ii) the Ash Meadows sub-basin; and (iii) the Oasis Valley sub-basin. The Amargosa Farms region is in the southern portion of the Alkali Flat-Furnace Creek sub-basin and adjacent to the Ash Meadows sub-basin (D'Agnese et al., 1996; U.S. Department of Energy, 1988). The Ash Meadows sub-basin, which drains the eastern and northeastern basins of the Death Valley regional flow system, is not believed to be influent to Alkali Flat-Furnace Creek Ranch sub-basin in the vicinity of the primary agricultural pumping area.

The diverse mix of geochemical signatures in the Amargosa Desert area suggests that the groundwater comes from a combination interbasin flow, upwelling from the deep Paleozoic carbonate aquifer, and intrabasin flow from the northwest and from the north (Winograd and Thordarson, 1975). Due to high evapotranspiration rates for the Amargosa Desert, most of the recharge occurs through the ephemeral stream channels (Osterkamp et al., 1994; Savard, 1995). Since the stream channels in the Amargosa Farms portion of the Amargosa Desert rarely have flow, the recharge estimates of Osterkamp et al. (1994) are about 0.5 percent of precipitation. Precipitation is generally between 100 and 200 mm for the Amargosa River basin (Osterkamp et al., 1994).

The groundwater contribution from the proposed YM repository area is a small portion of the southward flow along Fortymile Wash. The contribution from the Ash Meadows springs area to the Amargosa Farms area may be minimal. The Ash Meadows springs line and high gradient toward the Amargosa Farms area is a reflection of the hydraulic conductivity contrast across a gravity fault which abuts the carbonates of Ash Meadows on the east side with the confining playa deposits on the west side (Naff, 1973).

3 WELL CONSTRUCTION AND WATER USE IN THE AMARGOSA FARMS AREA

Characterization of well construction practices and water use specific to the Amargosa Farms area is presented in this section. Some aspects have been presented elsewhere (e.g., U.S. Department of Energy, 1988) but either the level of detail was not sufficient or data were included for other areas of the Amargosa Desert region.

Four sources of information were used to characterize well construction and water use in the Amargosa Farms area. The well permit database, well driller's logs, and annual water use estimates were obtained from the Nevada Division of Water Resources (Nevada Division of Water Resources, 1997a,b,c; Bauer and Cartier, 1995). A fourth source was the Ground-Water Site Inventory (GWSI) portion of the National Water Information System developed and maintained by the U.S. Geological Survey (USGS) (U.S. Geological Survey, 1989). The well permit tables, well driller's logs, and annual water use tables are recorded by location using the standard range, township, section, quarter section, and possibly quarter-quarter section coordinate system. The tables are organized by hydrographic basin with the Amargosa Desert being defined as basin 230. The Amargosa Farms area of the Amargosa Desert includes townships (T) 15, 16, and 17 south (S) and ranges (R) 48 and 49 east (E), as well as the western half of R50E.

The GWSI database uses both the township-range coordinate system as well as the longitude-latitude coordinate system. The wells in Amargosa Farms and Amargosa Valley are taken as those bounded by −116° 21' 34" to -116° 37' 15" west longitude and 36° 40' 10" to 36° 20' 53" north latitude. For graphical purposes, township-range coordinates and latitude and longitude coordinates are converted to UTM section 11 coordinates using the NAD27 datum. The former conversion is made directly to UTM by assuming a well is in the middle of the smallest reported area (e.g., quarter section). The latter conversion is made using a USGS-supplied conversion program.

3.1 NUMBER AND DISTRIBUTION OF WELLS

A division of wells into two categories based on water use is made here for the purpose of presentation of separate results for different receptor pathways. Domestic and quasi-municipal wells can be characterized as having low but continuous pump rates throughout the year. Irrigation wells and commercial and industrial wells constitute the large pump rate category. Although irrigation wells operate intermittently through the growing season, they are approximated in this study as a continuously pumping well at the annual rate estimated from the annual volume pumped.

There are no municipal wells in the Amargosa Farms area. Instead, quasi-municipal wells and domestic wells support direct human use. In addition, a portion of the irrigation wells (well driller's logs) and industrial wells (Buqo, 1996) may also supply water for direct human use. Five percent of the total irrigation wells recorded in the well driller's log also listed domestic use. Dependent on the State Engineer's concurrence, the water use category associated with a permit may be changed at a later date.

There are 508 wells recorded in the State of Nevada's well driller's logs which date back to at least 1921. Many of these wells are no longer in operation. The GWSI database contains 224 well records for approximately the same area of central Amargosa Desert. The well permit database contained 185 certificated or permitted water rights entries. The estimated water use tables from the Nevada State

Engineer tracked as many as 72 entries in one year (1996) and a combined 126 different entries over the span 1983–1996. Individual domestic wells are not recorded in the state water use tables, nor were quasi-municipal wells prior to 1996 for Hydrographic Basin 230.

The distribution of wells spatially and across water use categories is illustrated in table 3-1 by Township and figure 3-1 by Range and Township. The U.S. Department of Energy (DOE) (1988) identifies nine quasi-municipal wells, five commercial wells, and three industrial wells that were active. Changes in water use category may occur on permitted or certificated water rights. A majority (70 percent) of all wells were drilled in T16S. Figure 3-1 shows that the domestic wells are concentrated in T16S and R48-49E. Locations of sections where 14 or more (up to 40) domestic wells have been drilled according to the well drillers logs are also marked in figure 3-1.

3.2 STATISTICAL ANALYSIS OF WELL CONSTRUCTION PRACTICES

The GWSI database (U.S. Geological Survey, 1989) also contains information on well construction. Of the 227 wells from the Amargosa Farms region listed in the database, 188 records included water table depth, 113 included screen positions, and 15 records included specific discharge data. Although 18 wells had multiple screened portions, a majority of the screened portions are closely spaced. This is reflected in the fact that there is only a 1-m difference between the average of the sum of the screened portions and the average of the length of the combined screened portion. Table 3-2 is a statistical summary of relevant well characteristics. Of note are the averages of 11 and 62 m depths from the water table to the top and bottom of the screened portions, respectively.

3.3 ESTIMATION OF WATER USE

For the Amargosa Desert, designated as Hydrographic Basin 230, the state has estimated the perennial yield to be 24,000 acre-ft-yr (Buqo, 1996). Committed water use, which includes both certificated and permitted water use, is over 41,000 acre ft-yr. This situation makes it unlikely that new permits will be granted by the State Engineer. In the past few years, proceedings for water users to demonstrate beneficial use have led to thousands of acre-feet of forfeiture for well permits. These proceedings may have had an impact on the number of water users reported in the basin during the mid-1990's (Buqo, 1996).

On a volume basis, the water pumped in the Amargosa Farms region is predominantly used for irrigation and mining. The bulk of the mining related water use is in the playa area, which lies south of the farming area. The St. Joe Bullfrog Gold Mine is also a large-volume water user as reported in the tables for the Amargosa Desert but it is not located in the Amargosa Farms region. Historically, groundwater pumping for irrigation increased significantly in the late 1950's (D'Agnese, 1994; and Buqo, 1996). Irrigation use was 3,000 acre-ft by 1962, 9,300 acre-ft by 1967, and 7,300 acre-ft in 1973. Kilroy (1991) reports rapid declines in the water table during the 1970's and less severe declines in the 1980's. The declines are 20 to 30 ft in three different areas of Amargosa Farms with the largest being a northeast-trending trough near the Nevada-California border in T16S, R48E.

Since 1983, the Nevada State Engineer has tabulated water use for individual users and summarized annual use by category, although data for 1984 were not recorded. Table 3-3 is the annual summary of water use with both the Amargosa Desert total and the Amargosa Farms portion total. The

Table 3-1. Distribution of wells by water use across Townships T15,16,17S using well driller's logs. There are 34 log entries classified as other. See figure 3-1 for layout of Townships and Ranges.

Township	Domestic	Irrigation	Industrial/ Commercial	Quasi-Municipal
T15S	12	5	2	1
T16S	207	120	1	3
T17S	55	65	1	1

Table 3-2. Statistics for well construction practices and water level positions for wells recorded in GWSI database in Amargosa Valley and Amargosa Farms area.

Well Characteristic	Average	Standard Deviation	Number	Minimum	Maximum
Distance from Water Level to Top of Screen (m)	11	13.0	113	0	66.0
Distance from Water Level to Bottom of Screen (m)	62	36.7	113	1.7	219
Distance from Water Level to Screen Centerline (m)	35	23.1	113	1.2	124
Total Screen Length (m)	52	33.2	113	0.9	191
Distance from Top to Bottom of Screens (m)	53	33.1	113	0.9	191
Depth of Well (m)	83	42.6	172	0.9	229
Wellbore Diameter (m)	0.31	0.08	112	0.032	0.41
Specific Discharge (m^2/hr)	32.3	33.4	15	2.34	104

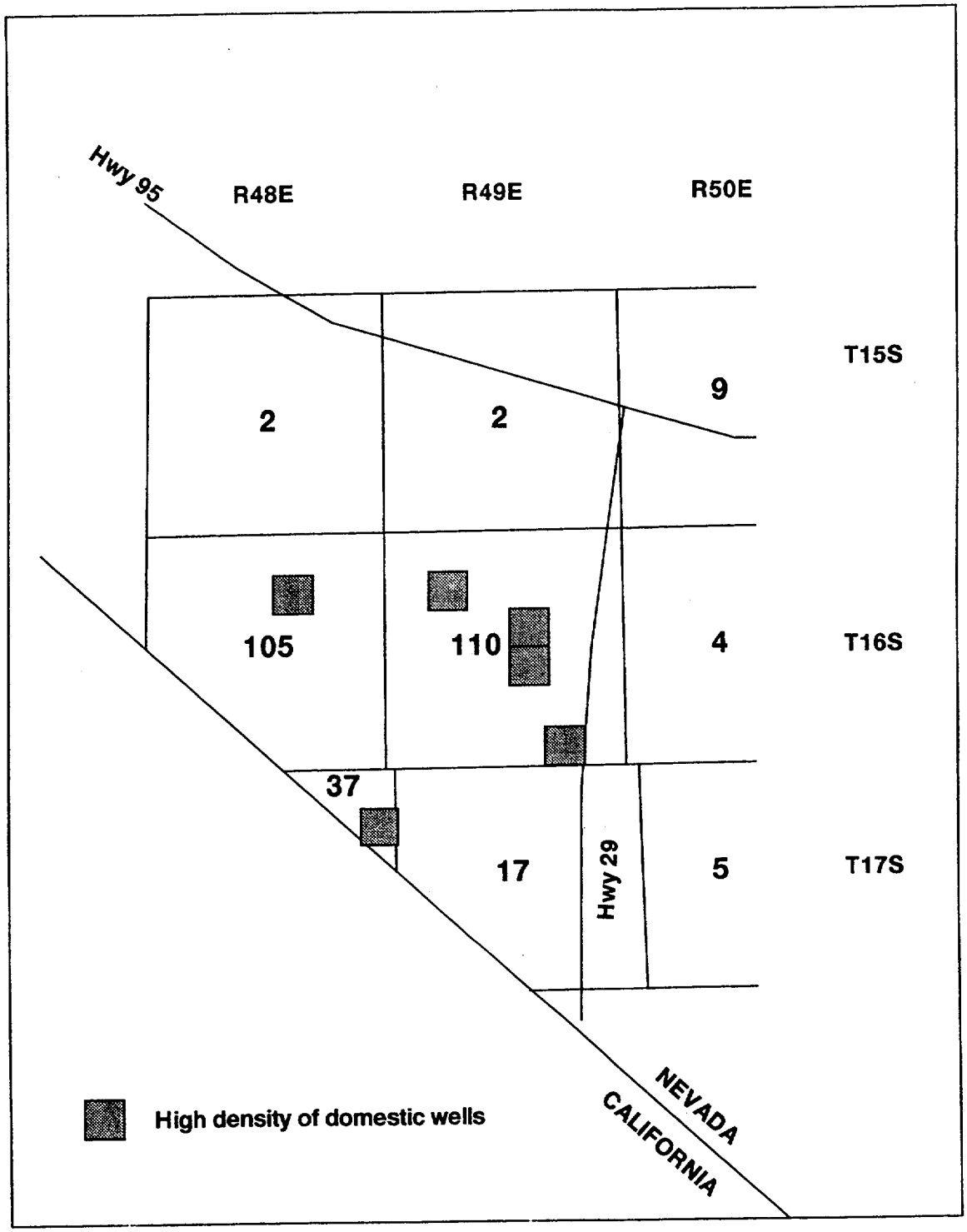

Figure 3-1. The distribution of domestic and quasi-municipal wells based on range and township from well driller's logs. The number of wells in each range and township includes those listed for dual usage, domestic, and irrigation. Locations of sections (1 square mile) with 14 or more domestic wells are highlighted.

Table 3-3. Annual estimates of water use by type; International Minerals Venture Floridan (IMV), American Borate (AB), quasi-municipal (QM), commercial (COM).

Year	Basin-230 Total Acre-ft	Irrigation Acre-ft	IVM/AB Acre-ft	QM/COM Acre-ft	Domestic Acre-ft	Amargosa Farms Total Acre-ft
1996	13,613	11,033	1,019	204	50	12,306
1995	15,035	12,354	780	10	100	13,244
1994	12,595	9,977	717	10	100	10,804
1993	11,300	8,659	1,007	10	100	9,776
1992	8,164	5,711	654	10	100	6,475
1991	6,122	4,942	450	10	100	5,502
1990	7,807	4,953	887	10	125	5,975
1989	3,921	1,566	1,413	10	125	3,114
1988	4,109	2,978	996	10	125	4,109
1987	6,137	5,700	302	10	125	6,137
1986	7,238	6,553	550	10	125	7,238
1985	9,672	8,472	950	20	230	9,672
1983	9,500	9,105	125	20	230	9,500

annual totals increased significantly from 1993 to 1996 due to large increases in irrigation use with the largest volume being 13,244 acre-ft in 1995.

Individual domestic water use is not recorded in the State Engineer's tables, and individual records for quasi-municipal water users did not start until 1996. Annual estimates were lumped together for the domestic and quasi-municipal/commercial use for each year, although there is some recategorization occurring in 1996. A 1 acre-ft annual usage is assumed for every household, although this may be an over-estimate (Buqo, 1996). However, the DOE (U.S. Department of Energy, 1988) states that the annual household usage estimate is 1,800 gpd. One acre-ft is about 895 gpd or about 3.4 m^3/d.

Individual records for each irrigation user are tabulated (appendix A) for the years 1983, 1985–1996 and pertinent summaries are included in table 3-4. For individual users, the maximum annual pump volume for any particular user in 3,960 m^3 (1,170 acre-ft). The average for all years for an individual irrigation user is 828 m^3 and the range in any particular year is 348 to 1,300 m^3. The number of irrigation users for any year ranged from 15 in 1991 to a high of 55 in 1996. Most of the groundwater

Table 3-4. Summary statistics of individual irrigation users on an annual basis.

Year	Average (m^3/d)	Number of Users	Minimum (m^3/d)	Maximum (m^3/d)
1996	772	55	3.4	2,707
1995	886	51	6.8	2,928
1994	771	44	3.4	3,960
1993	711	41	3.4	3,960
1992	645	30	3.4	3,368
1991	1116	15	67.7	3,960
1990	645	26	16.9	2,675
1989	348	16	16.9	1,354
1988	503	20	8.5	2,370
1987	900	20	8.5	2,912
1986	1300	17	8.5	2,928
1985	1134	25	76.9	2,928
1983	1083	26	16.9	2,116
Overall	828	–	–	–

pumping occurs in T16S, R48-49E, and T17S, R49E. Figure 3-2 shows the distribution of groundwater pumping for the year 1996 by township and range based on the individual records (no domestic wells are recorded). Figure 3-3 shows the distribution for 1996 relative to the streamtube model boundaries used in Baca et al. (1997). In combination, figures 3-2 and 3-3 illustrate two important points based on 1996 data. One, domestic or quasi-municipal wells are likely to be the first wells encountered by a plume migrating from the proposed YM repository. Two, large pumping rate wells capable of capturing a plume are not encountered until about 30 km from the proposed YM repository.

In summary, the typical pump rates range from 300 to 2,000 m^3/d for irrigation wells and 3 to 6.8 m^3/d for domestic wells. Although the Hydrographic Basin of Amargosa Desert is over-appropriated, actual usage has remained less than 65 percent of the estimated perennial yield. Groundwater pumpage in the Amargosa Farms portion of the Amargosa Desert has led to a decline in the water table locally up to 10 m.

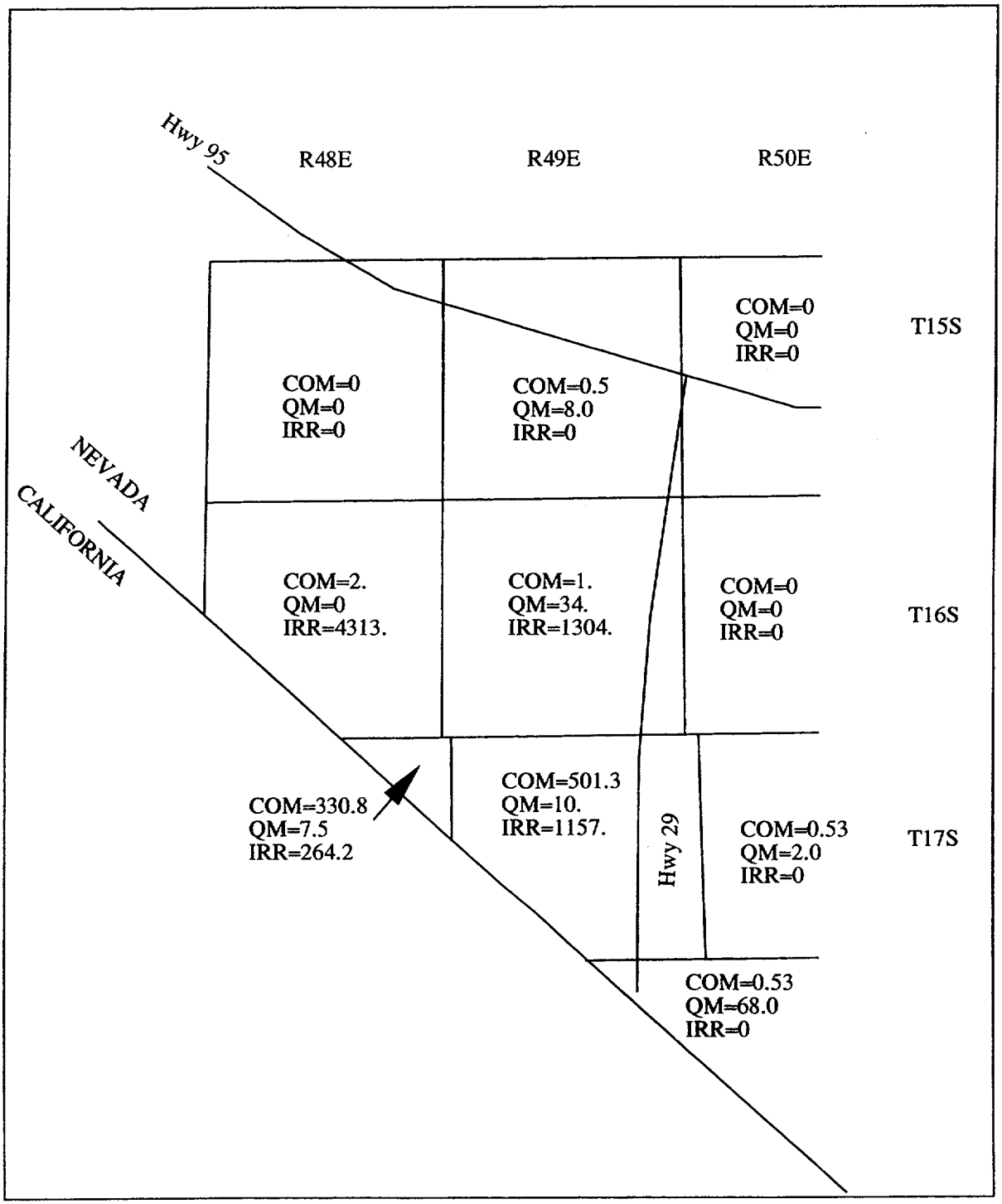

Figure 3-2. Distribution of annual water use (acre-ft) by type and by range and yownship for commercial, irrigation, quasi-municipal wells for the year 1996.

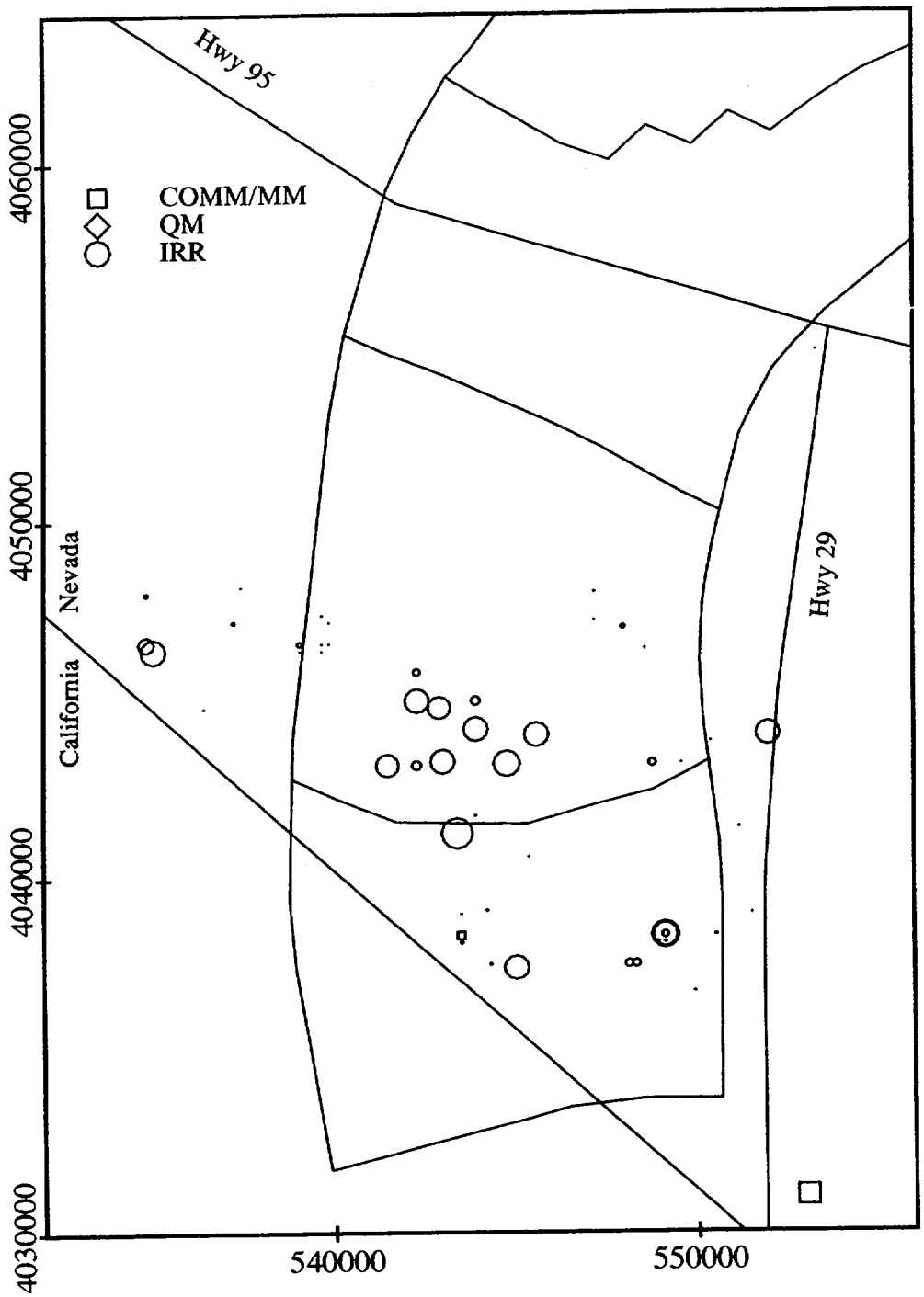

Figure 3-3. Distribution of water use by type for the year 1996. The symbol size for each category is scaled to the magnitude of groundwater pump volume. Data are from Nevada Division of Water Resources (1976b) and are converted to Universal Transverse Mercator Section II coordinates so as to correspond with the streamtube model of Baca et al. (1997).

4 THREE-DIMENSIONAL CAPTURE ZONE ANALYSIS AND PLUME DELINEATION

The approach used here to estimate borehole dilution factors in the Amargosa Farms region is to separate them into two components; one, the factor due to volumetric-flux; and two, the factor due to dispersion during transport. The factor due to volumetric flux is a comparison of the cross-sectional areas of a capture zone of a pumping well to the intercepted portion of a contaminant plume. In all cases, the areas discussed here refer to the cross-sectional area normal to the principal direction of regional flow. The second component of borehole dilution is the effect due to dispersion during transport. It is calculated as the ratio of the source concentration to the areal average concentration of the portion of the plume which is captured by a pumping well.

Other types of dilution factors include that used by Baca et al. (1997) and Kessler and McGuire (1996) based on normalized concentration variations during passive transport, and that used in IPA Phase 3 based on a mass release rate into a total volumetric flux potentially used by a critical group. The dilution factor due to dispersive transport used in this report accounts for the distribution of concentration across a plume whereas that used by Kessler and McGuire (1996) only accounts for concentration reduction along the centerline of the plume. Direct usage or comparison of the borehole dilution factor and the IPA Phase 3 dilution factor is restricted by the reference to different volumetric fluxes.

Different configurations for the intersection of the plume and the capture area are possible. For domestic wells, the capture area is generally much smaller than the cross-sectional area of a plume that has undergone transverse spreading due to macro-dispersion during transport along a 20- to 30-km pathway (figure 4-1). Hence, there would be little borehole dilution even if the well was aligned along the center of the plume, and any borehole dilution that did occur would be due to vertical gradients in the plume concentration. For a 2D plume of prescribed thickness, the location of the plume relative to the capture area affects the dilution factor. For irrigation wells, or any high discharge wells, the capture area is generally thicker than the plume. The capture area may be wider or narrower than the contaminant plume depending on the problem. In all cases, the well is assumed to be in the transverse center of the plume which is the conservative assumption.

The effects of the regional gradient, transmissivity, pumping rate, and screen position and length on the area of the capture zone can be described in qualitative terms. An increase in transmissivity or the regional gradient will decrease the width of the capture area. An increase in the pumping rate will increase the capture area. An increase in the depth of a partially penetrating well will increase the vertical capture area but decrease the horizontal capture area. The position and distribution of the plume in relation to the capture zone will control the dilution of the solute in the well bore.

At present, there are few data for the hydraulic properties, well construction, and pumpage in the Amargosa Desert or Amargosa Farms. Moreover, the size, location, and shape of a plume are uncertain and usually must be obtained from large-scale transport modeling. Because of the relative paucity of site-specific data, the focus of this study is relating dilution trends to generic well design and plume configuration.

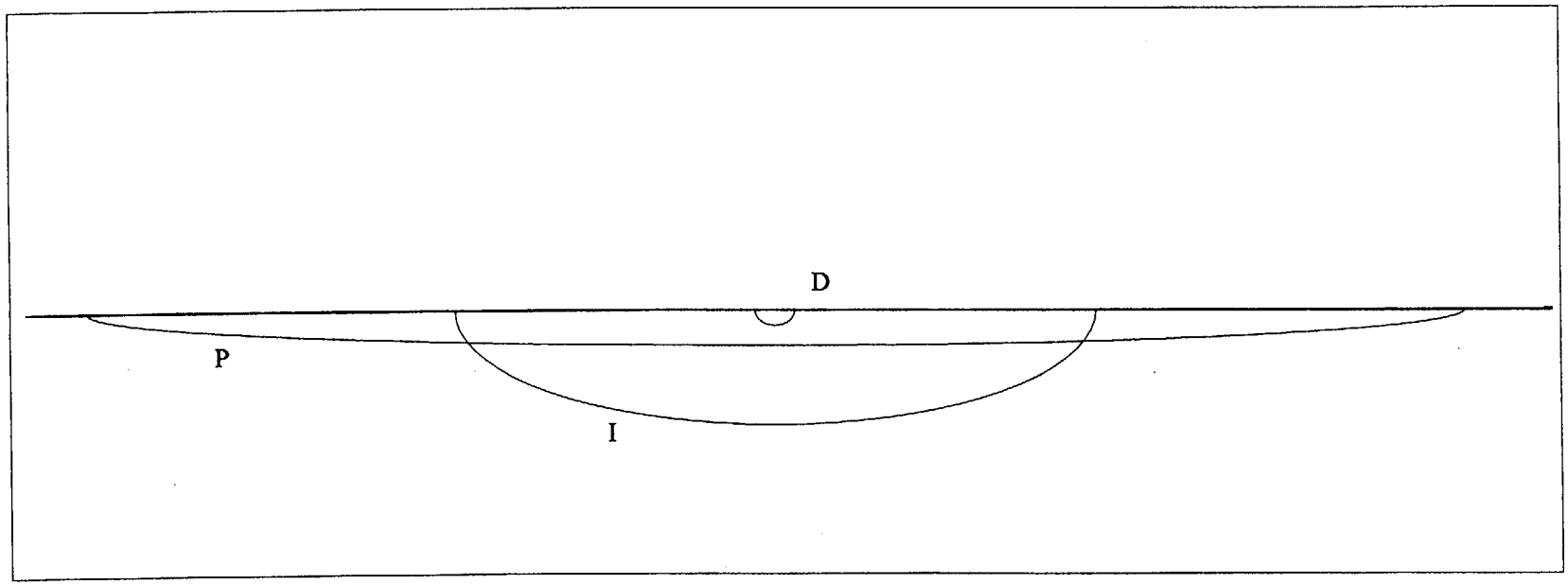

Figure 4-1. Comparison of plume cross-section (P), irrigation well capture area (I), and domestic well capture area (D).

4.1 DETERMINATION OF FLOW FIELD AND CAPTURE ZONE

The groundwater flow simulation program GFLOW Version 1.1 (Haitjema, 1995), that is based on the analytic element method, was used to estimate the size and shape of capture zones for individual wells. GFLOW is designed to simulate partially penetrating wells in a uniform regional gradient. There are other types of elements in GFLOW for modeling groundwater flow fields that were not used. The 3D effects of the partially penetrating well are superimposed on the 2D regional flow field. At some distance from the well, the vertical components due to pumping become negligible. Forward or backward particle tracking is used in GFLOW to determine a capture area at some distant, upgradient point where vertical flux components become insignificant. This capture area is a vertical plane normal to the direction of regional flow.

4.1.1 Description of the Analytic Element Method

The Analytic Element Method (AEM) provides a composite analytic solution which satisfies the differential equation in an unbounded domain. Delineation of streamlines is more precise than with standard numerical methods since both the head and the velocities are known at every point, rather than solely at computational nodes. Combined 2D and 3D modeling is accomplished by superposition of 3D effects on the general 2D solution. For example, near a partially penetrating well, a 3D solution is used. However, at a location sufficiently far from the well, the vertical flow components are negligible and a 2D approximation to the well may be superimposed on the solution. AEM is not well suited for complex flow problems in which material property heterogeneity is large.

The equations for flow in AEM are written in terms of discharge potentials instead of hydraulic head. The discharge potential is defined differently for confined, unconfined, 1D flow, 2D flow, or for any analytic element. An advantage of the AEM is that the solution to the equation for flow written in terms of the discharge potential is not dependent on whether the problem domain being solved is confined or unconfined. Once the strength of the potential is known for each analytic element, the head or groundwater discharge may be determined at any point in the flow domain. The solution for the partially penetrating well is based on work by both Muskat and Polubarinova-Kochina (Haitjema, 1995) for the representation of the strength distribution along a line sink (point sinks along a line) while constraining the discharge to a fixed value.

4.1.2 Ranges for Parameter Values

Four parameters are varied to test their effects on the capture area including: (i) pump rate, (ii) well screen position and length, (iii) regional gradient, and (iv) hydraulic conductivity or transmissivity. The pump rates range from those typical of domestic wells to those typical of irrigation wells. A reasonable range to use for the pump rates for domestic or quasi-municipal wells is 1 to 75 m^3/d. The DOE estimate (U.S. Department of Energy, 1988) for a single household is 1,800 gpd (6.8 m^3/d) while the State of Nevada uses 1 acre-ft per household (3.4 m^3/d) noting that this value is probably too high (Buqo, 1996). The high end of the domestic range corresponds to a quasi-municipal well or to multiple domestic wells modeled as a single well. For example, the first wells in a potential plume's path are multiple domestic, quasi-municipal, and small commercial wells near the junction of highways 95 and 29 at Amargosa Valley. For irrigation wells, pumping may be as high as 4,000 m^3/d; however, a more typical large irrigation pump rate is 2,116 m^3/d (625 acre-ft/yr). The average pump rate from 1983–1996 was about 800 m^3/d while the lowest was 300 m^3/d for any particular year.

The average screened length of the wells in the Amargosa Farms region (top to bottom) is 53 m while the maximum screen length is 190 m (table 3-2). The typical screen position starts 11 m below the static water level at the time of construction. Hence, the typical well modeled here will be screened from the water table to 60 m below the water table. Sensitivity analysis for the screen position, for domestic wells only, will account for the adjustment steps of about one standard deviation of the screen position.

The range of regional hydraulic gradients considered is 0.01 to 0.001. Bedinger et al. (1989) list a value of 0.003 for generic basin-fill environments in the Death Valley Region. Estimates for the Amargosa Farms area made from water table maps by Kilroy (1991), the DOE (U.S. Department of Energy, 1988), and Nichols and Akers (1985) fall within the 0.001 to 0.01 range. Most estimates are in the 0.001 to 0.005 range; the 0.01 values are from the east-west gradients immediately south and east of Amargosa Valley and may reflect the abrupt decrease in transmissivity across the northern end of the so-called Gravity fault, which has been inferred along the Ash Meadows spring line.

The range of transmissivities reported for basin-fill alluvium in the Death Valley Region is 10 to 400 m^2/d (Plume, 1996; U.S. Department of Energy, 1988; and Winograd and Thordarson, 1975). Since Amargosa Farms is in the area of sediments facies of lower fans and lowland sediments, rather than the coarser sediments of the upper and middle fan deposits, the saturated hydraulic conductivities should encompass a wide range and be highly heterogeneous relative to other basin-fill. Plume (1996) estimates a range of 0.006 to 43 m/d for saturated hydraulic conductivity while the DOE (U.S. Department of Energy, 1988) reports a range of 0.21 to 2.9 m/d. The transmissivity is a product of the saturated hydraulic conductivity and the saturated thickness of the aquifer. The aquifer thickness is assumed to be 1,000 m for all modeling scenarios.

4.1.3 Sensitivity Analysis for Capture Zone

The effects of reasonable variations in transmissivity, regional gradient, and pumping rate for all well types are presented in this section. In addition, the effects of screen position and length for domestic wells are presented. Due to their large discharge rates and small degree of well penetration relative to the aquifer thickness, the effects of screen position and length are negligible for irrigation wells. The capture area is determined at an upgradient point from the well location where the flow is essentially 1D, for example, no longer 3D. At this upgradient point, the width and thickness are at a maximum for the capture area. A table of the widths and depths of the capture area results is included in appendix B.

The effect of a partially penetrating well compared with that of a fully penetrating well is shown in figure 4-2 for a small irrigation well pumping at 300 m^3/d. The maximum screen length of 190 m is marked as maximum on the figure. The capture width of the fully penetrating well is about 44 percent of that for the typical partially penetrating well.

Figure 4-3 represents the capture zone width and thickness for combinations of regional gradients and transmissivities for a large pumping rate well of 2,116 m^3/d (625 acre-ft/yr). The combination of a regional gradient of 0.001 and transmissivity of 200 m^2/d (the lowest represented here) leads to a capture width of about 5,600 m, which captures nearly the entire width of a streamtube (Baca et al., 1997) that brackets the repository. Conversely, a larger gradient (0.005) and higher transmissivity (400 m^2/d) lead to a much smaller capture area, 1,800 m wide by 720 m deep. A similar trend also occurs for low-discharge, domestic wells (figure 4-4). Maximum capture areas are created either by the smallest regional gradient (0.001) or the lowest transmissivity (10 m^2/d) for capture thicknesses up to

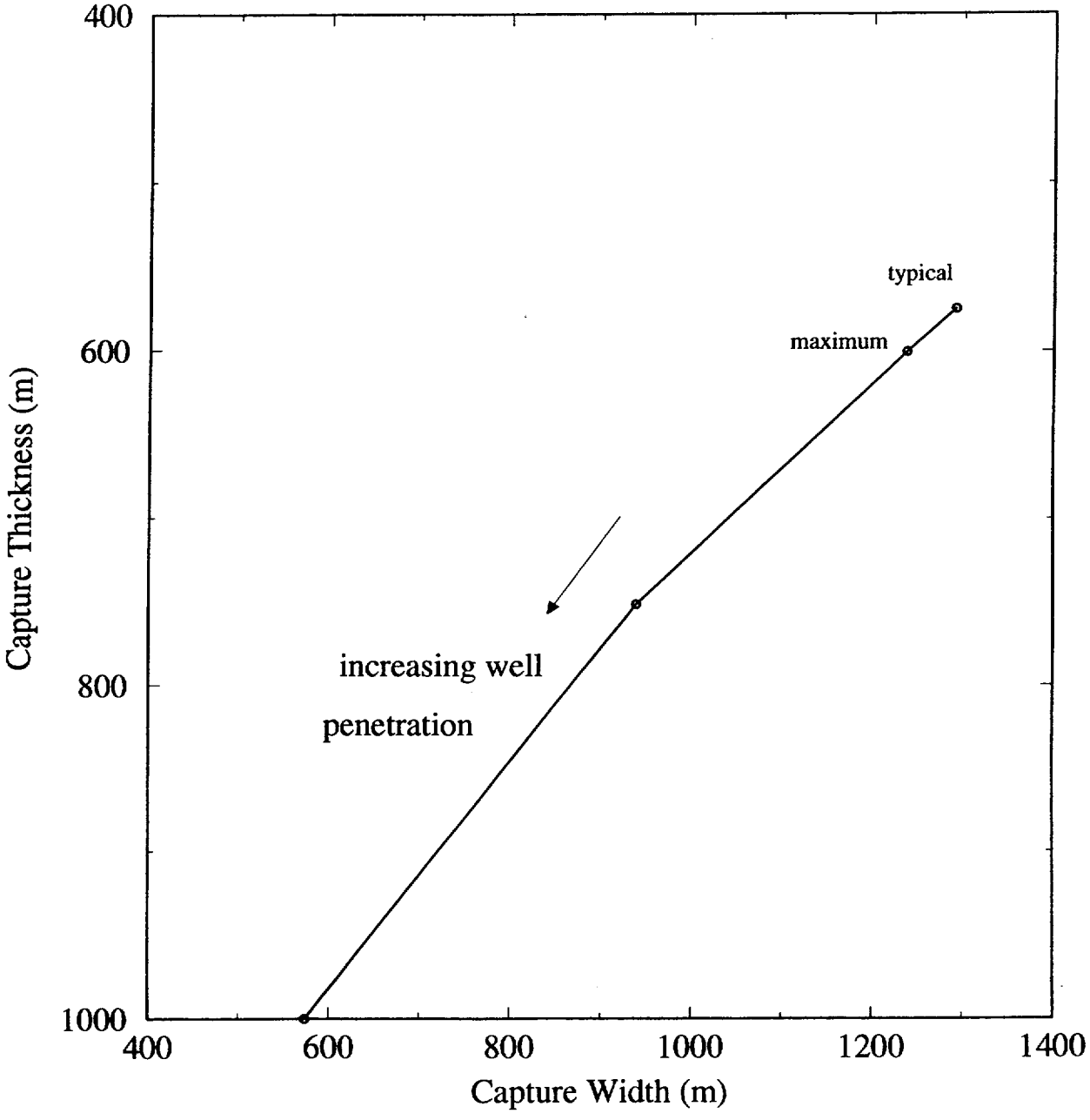

Figure 4-2. This plot illustrates the effect of well penetration depth (60, 190, 500, and 1,000 m) on a small irrigation capture zone width and thickness. A pump rate of 300 m^3/d and regional gradient of 0.005 are used. The "maximum" denotes the maximum well penetration depth and "typical" denotes the typical well penetration depth for the Amargosa Farms region.

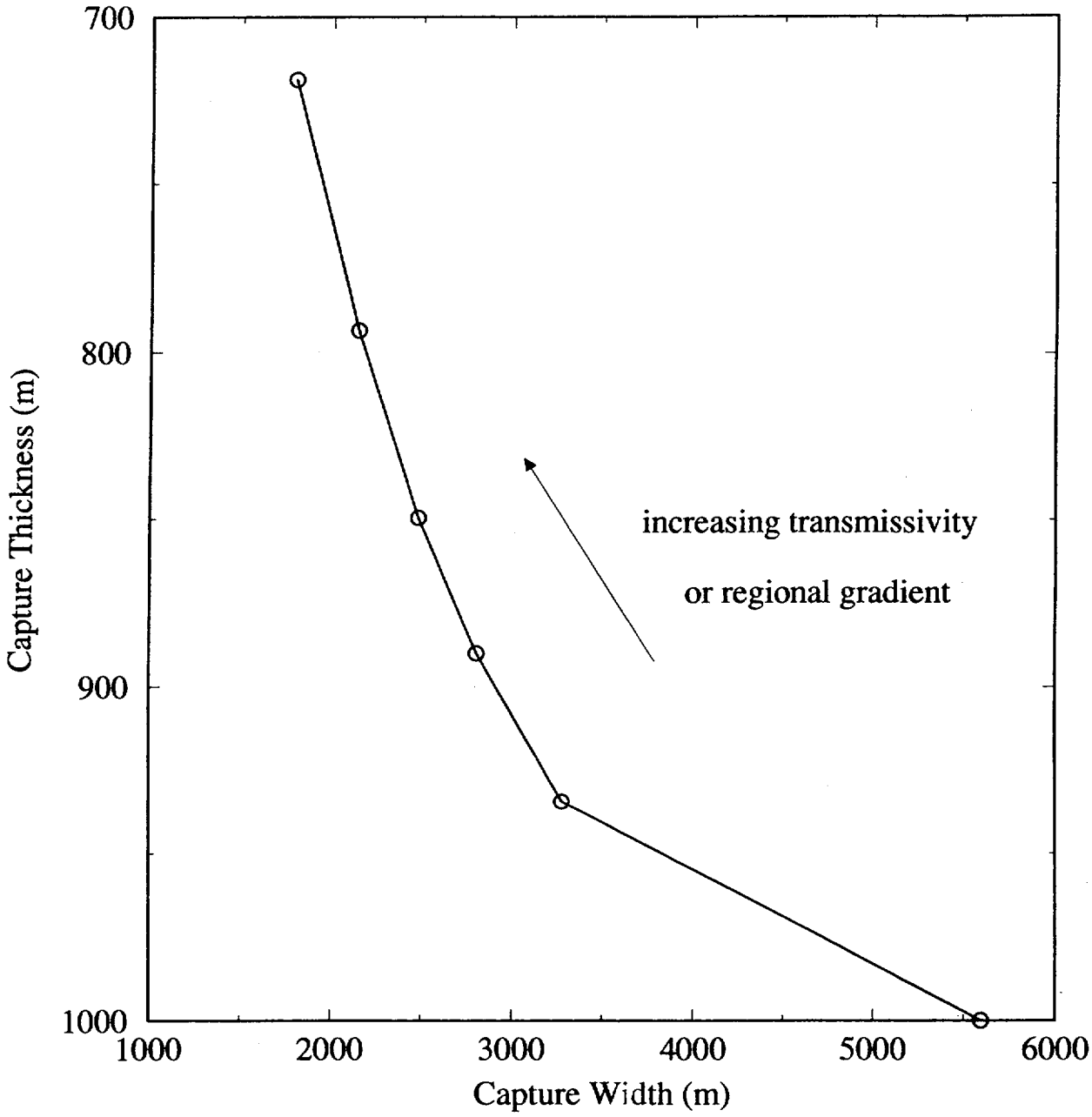

Figure 4-3. Effect of combinations of transmissivity (200, 300, 400 m^2/d) and hydraulic head gradient (0.001, 0.002, 0.003, 0.005) on a large irrigation well's capture zone width and thickness. A pump rate of 300 m^3/d is used.

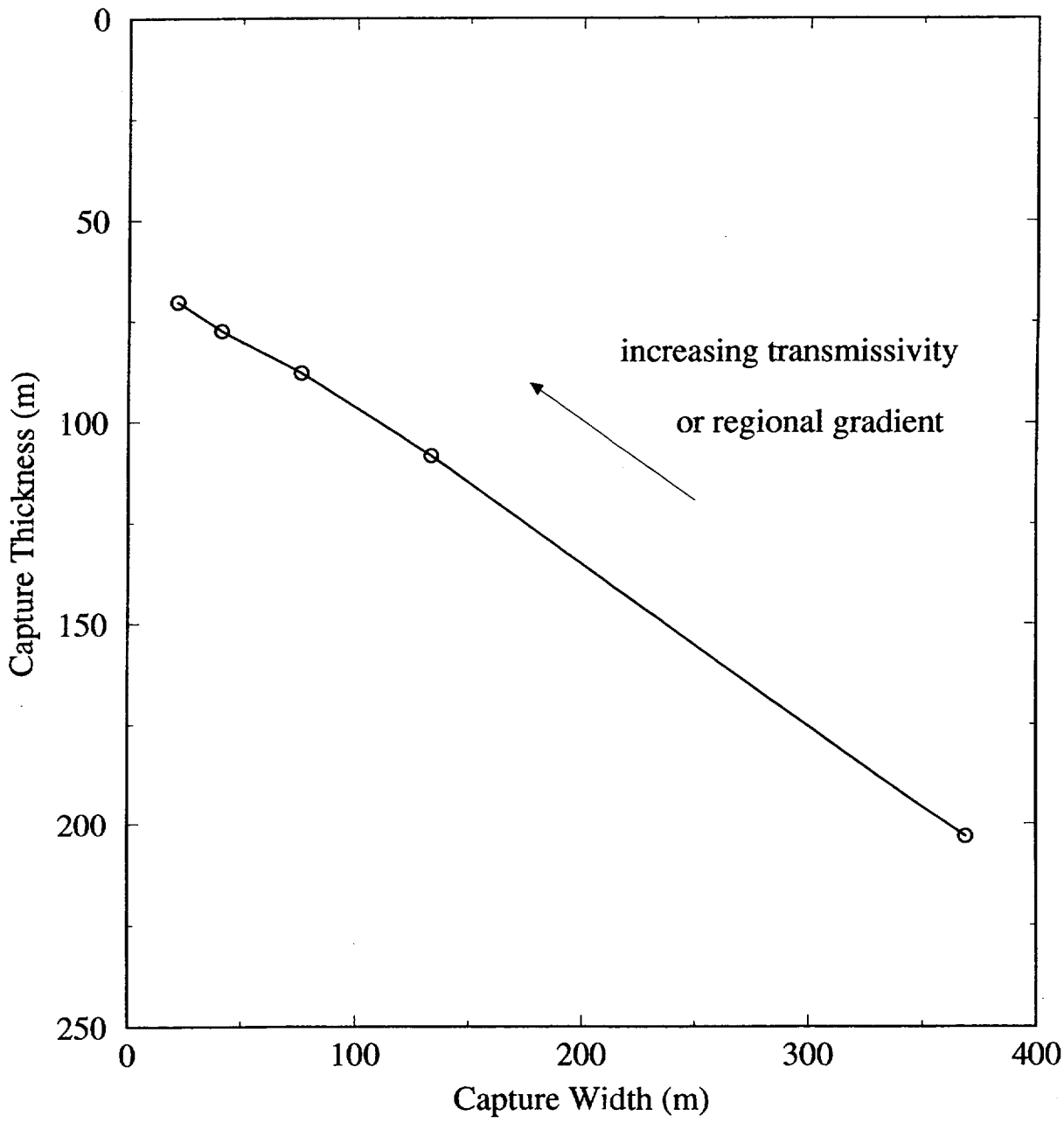

Figure 4-4. Effect of combinations of transmissivity (50, 100, 200, 300, 400 m^2/d) and hydraulic head gradient (0.001, 0.0025, 0.005, 0.01) on a domestic well's capture zone width and thickness. A pump rate of 3 m^3/d and the screened portion is 60 m long starting from the water table.

200 m. Since the Darcy velocity is a function of the hydraulic conductivity and hydraulic gradient, figures 4-3 and 4-4 also illustrate the effect of Darcy velocity on capture width and thickness.

The effect of pump rate on the capture area is presented in figure 4-5. A gradient of 0.005 and transmissivity of 100 m^2/d are used for all pump rates. Of significance for borehole dilution is that all wells in the low pump rate range (<75 m^3/d) will have capture areas that would be much less than the plume area based on 3D advection-dispersion equation modeling.

4.2 RADIONUCLIDE PLUME SHAPE AND LOCATION

The potential release and subsequent movement of radionuclides from the YM repository is likely to follow a path generally southeast to Fortymile Wash and then continue south to southwest toward the Amargosa Valley and Amargosa Farms areas. A more precise delineation of the flow path under current conditions is a point of debate due to a lack of data and the absence of any detailed hydrogeologic study in the Fortymile Wash and lower Amargosa Desert areas. The shape of the plume at a 30-km distance from the proposed repository, in particular the amount of vertical dispersion which leads to an increase in the plume thickness, is yet another unknown. Vertical dispersion may be limited by the possible presence of confining horizons (Naff, 1973) in the lake bed facies of the basin-fill sediments.

Given the uncertainty of the plume configuration, two scenarios were analyzed. The first scenario was a plume modeled for 3D dispersion. The second scenario is a plume for which no vertical dispersion is incorporated. Both scenarios are simulated to a steady state solution to assess the maximum dimensions of a plume reaching a well.

Dispersion, adsorption, and radioactive decay of the radionuclides will occur along this transport path. Adsorption and decay depend on the particular radionuclide. However, most of the radionuclides of concern in the far field (e.g., ^{237}Np, ^{129}I, ^{99}Tc) have half-lives greater than 10,000 yr. Adsorption also depends on the surface mineralogy of the porous media as well as the chemistry of the groundwater. There are no site specific data for adsorption in terms of distribution coefficients for the valley fill sediments. Considering these points, the conservative approach of neglecting both decay and adsorption is adopted.

In order to evaluate dilution due to both vertical and horizontal capture of clean water by a pumping well, an estimate of the shape of a potential plume is needed. Specifically, the configuration of the cross-sectional area perpendicular to the direction of flow is needed. Analytic solutions to the advection-dispersion equation were previously used to describe the plume shape at downgradient points from YM in TSPA-95 (TRW Environmental Safety Systems, Inc., 1995 and Kessler and McGuire, 1996). The advection-dispersion equation for 3D dispersion and 1D flow is

$$\frac{\partial C}{\partial t} = D_x \frac{\partial^2 C}{\partial x^2} + D_y \frac{\partial^2 C}{\partial y^2} + D_z \frac{\partial^2 C}{\partial z^2} - V \frac{\partial C}{\partial x} \qquad (4\text{-}1)$$

where C is the concentration, D_x, D_y and D_z are the dispersion coefficients in the coordinate directions, V is the seepage velocity in the principal direction of flow, and t is time.

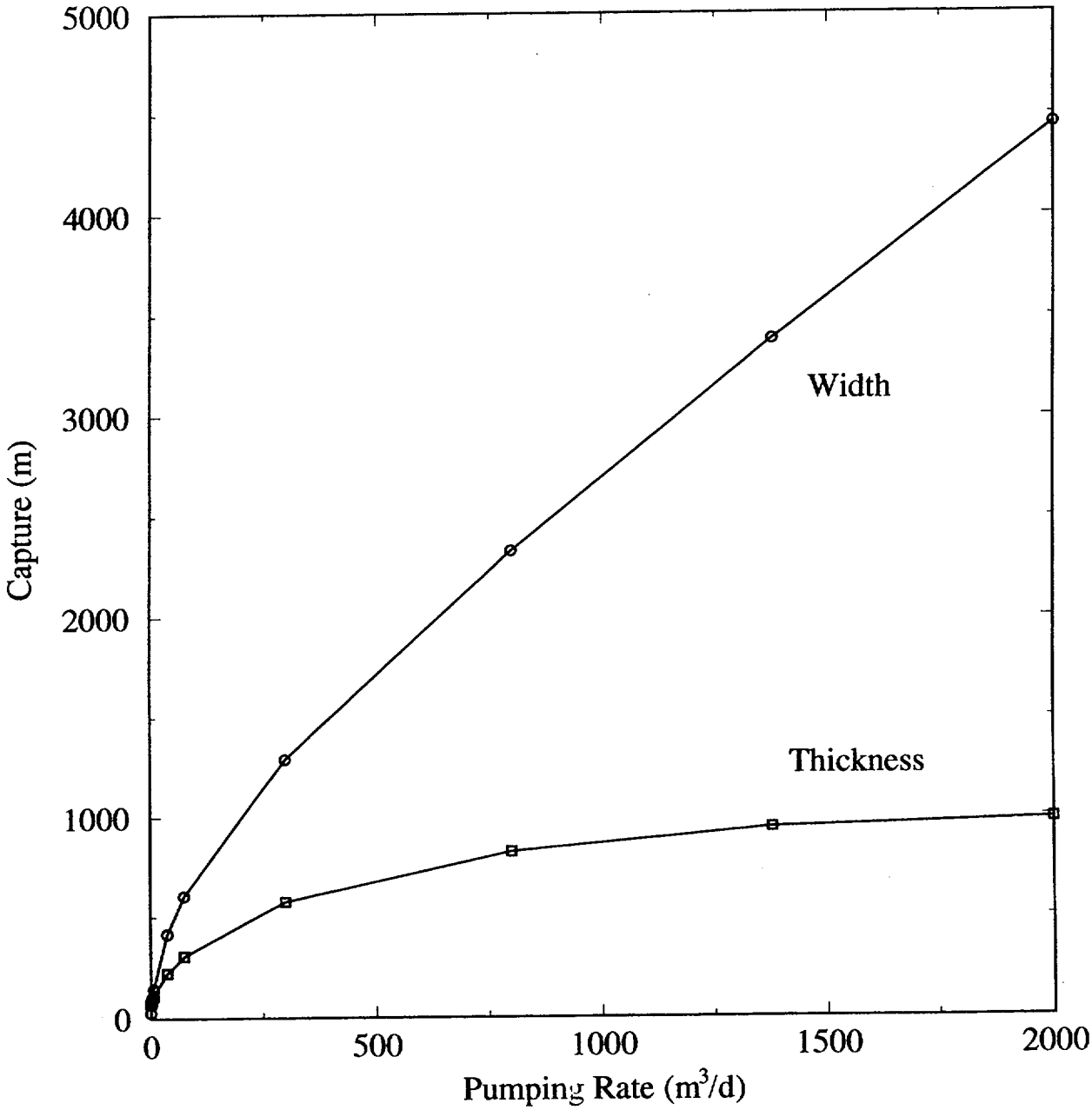

Figure 4-5. This plot illustrates the effect of pump rate (range 1 to 2000 m^3/d) on the capture zone width and thickness. A transmissivity of 100 m^2/d and regional gradient of 0.005 are used.

4.2.1 Transport Parameters

The initial source size, seepage velocity, and the dispersivities all control the plume configuration after 30 km of advective-dispersive transport. Kessler and McGuire (1996) noted the inverse relationship between source size and mean concentration reductions. They also found that a doubling of the source thickness led to an increase of 17 percent in the plume width at 25 km. Similarly, a 60-percent increase in the source width led to an increase of 6 percent in the plume width at 25 km. In this study, the source size will be held constant at 500 by 25 m for the 3D dispersion plumes and 500 m wide for the 2D dispersion plumes.

Since transport simulations were run to steady state in order to determine maximum plume dimensions, a reasonable value of the seepage velocity along the flow path from the repository, or from the accessible environment, to Amargosa Farms is needed. Seepage velocity is related to the Darcy flux by porosity. The Darcy flux for the transport analysis need not be the same as that for the capture zone analysis since the former represents the porous media and hydraulic head gradients from the repository to Amargosa Farms while the latter represents the Amargosa Farms area. Seepage velocity for transport was chosen to represent the mean pathway velocity from the tuff through the alluvium. Baca et al. (1997) report calculated ranges of Darcy flux of 0.01 to 3.7 m/yr for the saturated tuff aquifer and 0.4 to 0.7 m/yr for the alluvium. Assuming a porosity of 0.3 for the alluvium, the seepage velocity would be in the range of 1.3 to 2.3 m/yr. Kessler and McGuire (1996) used a seepage velocity of 1.76×10^{-6} m/s (55 m/yr) although it is not clear whether site-specific information (gradient, hydraulic conductivity, porosity) was used to obtain this estimate. The value of 2.4 m/yr used here for seepage velocity is closer to that approximated from the Darcy flux values reported by Baca et al. (1997).

The value of the concentration at the source is chosen to approximate a mass release rate of 10 Ci/yr, which is taken as an upper bound for mass release rates as delineated by the ^{99}Tc example in Mohanty et al. (1997). Assuming that dispersion off the constant concentration boundary is negligible, the concentration corresponding to 10 Ci/yr is 4.38E−6 Ci/l for a source size of 500 by 25 m and a Darcy velocity corresponding to a seepage velocity of 2.4 m/yr with a porosity of 0.3. The assumption of negligible dispersion off the source boundary as compared to advective flux off the boundary is reasonable at long times. However, since the plume configurations scale directly for steady state problems, the value of the concentration at the boundary conditions does not affect dilution factor estimates; as long as normalized values of concentration are reported and not absolute concentrations.

Simulation of 3D dispersion requires values for the longitudinal, horizontal transverse, and vertical transverse dispersivities. Generally, dispersivities are considered to be scale dependent (Gelhar et al., 1992). TSPA-95 (TRW Environmental Safety Systems, Inc., 1995) assumed relatively large transverse dispersivities which resulted in exceptionally large plumes (especially in the vertical direction) and large dilution factors (10^3 to 10^5). Kessler and McGuire (1996) recognized that there is a limit to the heterogeneity scale that a plume would encounter, although they nonetheless used a vertical transverse dispersivity equal to the horizontal dispersivity. This seems unlikely in light of the lithologic layering in the alluvial basin sediments. Contaminant plumes generally exhibit limited vertical spreading (Gelhar et al., 1992) Thus, small vertical transverse dispersivities values are likely. In a literature review of measured dispersivity values and ratios, Gelhar et al. (1992) note that horizontal to vertical transverse dispersivity ratios are often 1–2 orders of magnitude different. Furthermore, the measured vertical dispersivity values were all reported in Gelhar et al. (1992) to be less than 1 m; generally, in the range 0.06 to 0.3 m for scales ranging from 20 m to 10 km. In addition, the vertical transverse dispersivity

values exhibited no scale dependency. The longitudinal and horizontal transverse dispersivity are scale-dependent with their ratio equal to one order of magnitude. For the constant concentration source, the longitudinal dispersivity and the velocity do not affect the mean plume concentration in steady state transport. Plume size is controlled by the transverse dispersivities.

In this study, the location of the radionuclide source area is the same as that assumed by Kessler and McGuire (1996). A patch source area aligned perpendicular to the flow direction is located at the edge of the accessible environment or fence as described in Kessler and McGuire (1996), as opposed to locating the source area at the repository. The conceptual model consists of a release from the repository reaching the accessible environment from where it is modeled as a patch source to obtain a plume configuration 15 to 25 km further along Fortymile Wash to the Amargosa Farms area. Noting the variations in the flow path lengths, the accessible environment is approximately 5–7 km from the repository, the quasi-municipal and domestic wells first encountered at Amargosa Valley are about 15 km from the accessible environment, and the majority of irrigation wells first encountered are at about 25 km from the accessible environment.

4.2.2 Plume Dimensions for 3D Dispersion from Constant Concentration Source

The analytic solution to Eq. (4-1) for the constant concentration patch source as described in Wexler (1992) is

$$C(x,y,z,t)=\frac{C_0\ x\ \exp\left[\frac{Vx}{2D_x}\right]}{8\sqrt{\pi D_x}}\int_o^t \tau^{-\frac{3}{2}}\exp\left[-\left(\frac{V^2}{4D_x}+\lambda\right)\tau-\frac{x^2}{4D_x\tau}\right]\left[\operatorname{erfc}\left(\frac{(Y_1-y)}{2\sqrt{D_y\tau}}\right)-\operatorname{erfc}\left(\frac{(Y_2-y)}{2\sqrt{D_y\tau}}\right)\right]\left[\operatorname{erfc}\left(\frac{(Z_1-z)}{2\sqrt{D_z\tau}}\right)-\operatorname{erfc}\left(\frac{(Z_2-z)}{2\sqrt{D_z\tau}}\right)\right]d\tau \quad (4\text{-}2)$$

where C_0 is the concentration at the source, τ is a dummy variable of integration for time, λ is the decay coefficient, exp is the natural exponential, and erfc is the complementary error function. The dispersion coefficients in the x-, y-, and z-directions are defined as the products of the seepage velocity and the dispersivities in the x-, y-, and z-directions, respectively. This equation is the solution to the 3D solute transport equation for a vertical patch source aligned normal to the principal direction of flow where the patch dimensions are devined by Y_2-Y_1 and Z_2-Z_1. The solution to the advection-dispersion equation is valid for a 1D uniform flow field and 3D dispersion for a constant concentration source in an aquifer of infinite depth and lateral extent. Adsorption and radioactive decay of the solute are incorporated into the solution but were not used in this study. In the PATCH I Version 1.1 program, Wexler (1992) uses a Gauss-Legendre numerical integration technique to evaluate Eq. (4-2); however, possible round-off errors were reported for solutions at small distances and long times using this technique. For a similar problem, Domenico and Robbins (1985) simplify the integral problem by

summing over a specified number of continuous point sources in a patch. However, they too noted numerical errors at small distances and long times.

Tables 4-1 and 4-2 contrast plume width and thickness for various sets of dispersivity values at 15 and 25 km, respectively, from the source area located at the accessible environment. The longitudinal dispersivity value is reported in the tables but its magnitude is not a controlling factor for the results. The plume width and thickness are delineated at a threshold concentration of approximately $10^{-4} \times C_0$. The P-DF is also included in tables 4-1 and 4-2. These values will be used as a reference point for the dispersion-based dilution factors estimated in the following section. Where the centerline concentration can be used as a conservative estimate of the plume concentration, borehole dilution factors due to dispersion will be calculated by accounting for the distribution of concentration across a plume.

A reduction of the transverse dispersivities by 80 percent leads to a 46-percent reduction in plume width and thickness at 25 km. The ratio of the horizontal and vertical transverse dispersivities is kept at an order of magnitude. The percentages are approximately the same for the 15-km results. Similarly, a 50-percent reduction in the transverse dispersivities leads to a 24-percent reduction in plume width and thickness at 25 km.

4.2.3 Plume Dimensions Neglecting Vertical Dispersion for Constant Concentration Source

From the literature (Bedient et al., 1994), it is evident that existing plumes (caused either by accidental contamination or by deliberate injection of tracers for experimental purposes), typically show that plumes are often confined to a thin layer near the water table. Exceptions would occur in areas of high infiltration. The extreme case is to assume no vertical dispersion so the plume remains the same thickness as the source area but is dispersed laterally. This conceptual model for plume movement can be modeled using the following solution for 2D dispersion for a line source of specified width and constant concentration (Wexler, 1992):

$$C(x,y,t)=\frac{C_0 x}{4\sqrt{\pi D_x}}\exp\left(\frac{Vx}{2D_x}\right)\int_0^t \tau^{-\frac{3}{2}}\exp\left[-\left(\frac{V^2}{4D_x}+\lambda\right)\tau-\frac{x^2}{4D_x\tau}\right] \left[\operatorname{erfc}\left(\frac{(Y_1-y)}{\left(2\sqrt{D_y\tau}\right)}\right)-\operatorname{erfc}\left(\frac{(Y_2-y)}{\left(2\sqrt{D_y\tau}\right)}\right)\right] d\tau \quad . \tag{4-3}$$

The solution to Eq. (4-3) is implemented in the STRIPI Version 1.1 program of Wexler (1992). The solution for the line source can be extended to any source thickness.

In light of the arguments presented in the previous section, a reasonable selection of sets of dispersivities is 20:2, 50:5, and 100:10 for the longitudinal and transverse directions (table 4-3). These are depth-averaged dispersivity values which are not strictly comparable to the set of dispersivity values for 3D dispersion. When no vertical dispersion is included, the plume widths increase by between 16 and 29 percent for corresponding transverse dispersities.

Table 4-1. Plume configuration and point dilution factor at 15 km from the source area for a range of dispersivity values. C_c is the centerline concentration. The source area is 25 m thick by 500 m wide.

a_x:a_y:a_z (m)	Thickness (m)	Width (m)	P-DF = C_o/C_c
20:2:0.2	330	2,200	6
50:5:0.5	480	3,100	13
100:20:2	830	5,200	48
100:10:1	640	4,000	25
100:10:0.1	250	4,300	9

Table 4-2. Plume configuration and point dilution factor at 25 km from source area for a range of dispersivity values.

a_x:a_y:a_z (m)	Thickness (m)	Width (m)	P-DF = C_o/C_c
20:2:0.2	410	2,600	9
50:5:0.5	580	3,700	21
100:20:2	970	5,800	80
100:10:1	780	4,800	41
100:10:0.1	290	5,200	14

4.3 BOREHOLE DILUTION FACTORS BASED ON VOLUMETRIC FLUX

Volumetric flux-based borehole dilution factors (F-BDF) are determined by comparison of the plume and capture zone configurations (figure 4-1). The ratio of the cross-sectional area of the capture zone to the cross-sectional area of the portion of the plume which intersects the capture area in the plane perpendicular to the principal direction of flow is the dilution factor due to borehole mixing based on

Table 4-3. Plume configuration in terms of width at 15 and 25 km and point dilution factor for a source area width of 500 m and no vertical dispersion.

a_x:a_y (m)	Width (m) at 15 km	P-DF = C_o/C_c at 25 km	Width (m) at 15 km	P-DF = C_o/C_c at 25 km
20:2	2,330	1.5	2,860	1.8
50:5	3,410	2.1	4,230	2.6
100:10	4,640	2.8	5,800	3.6

volumetric flux comparisons. In other words, the F-BDF is the ratio of the capture and the intersection area. No credit is taken for the distribution of the concentration across the plume in the calculation of the F-BDF. All plumes in this section are modeled from a constant concentration source.

Generally, the plumes are wider than the capture zone but not as thick. Four plume scenarios are chosen to represent a range of conditions. The first and second scenarios are 10 m and 25 m thick plumes for which no vertical dispersion has occurred. The width of the plume depends on the horizontal transverse dispersivity that is used. For domestic wells, it does not matter what dispersivity is chosen since all plumes are wider than all domestic well capture zones. The third and fourth scenarios incorporate vertical dispersion with dispersivity ratios of 20:2:0.2 and 100:10:0.1. The F-BDF for the third and fourth scenarios are presented for the large pumpage irrigation wells.

4.3.1 Domestic Wells

The plume configuration that results from 3D dispersion from a constant concentration source will generally be larger than the capture area of a single domestic well, a closely spaced collection of domestic wells, or a quasi-municipal well for wells typical of the Amargosa Farms area. Hence, with the assumption of a uniform plume concentration, there will be no borehole dilution. Only for the smallest vertical transverse dispersivity values (less than 0.2) and for the largest pump volumes from a closely spaced collection of domestic and quasi-municipal wells will there be vertical gradients that are strong enough to capture clean water and provide borehole dilution.

The effects due to pumping rate, screen position, transmissivity, and regional gradient on the F-BDF are shown in figures 4-6 to figure 4-9. The plumes of thickness 10 and 25 m with no vertical dispersion are used for the calculation. As expected, the factors for the 10-m thick plume are greater than those for the 25-m plume. Again, the F-BDF do not include effects due to concentration differences in the plume.

For a typical domestic well that pumps 1,800 gpd, the F-BDF decreases from 10 to 4 when the plume thickness increases from 10 to 25 m at the 25-km distance (figure 4-6). The difference in the factors increases as the pumping rate increases. The F-BDF for the 10-m plume range between 7 and 26 for pumping rates in the range of domestic and quasi-municipal wells. Similarly, the F-BDF for the 25-m plume range between 3 and 10.

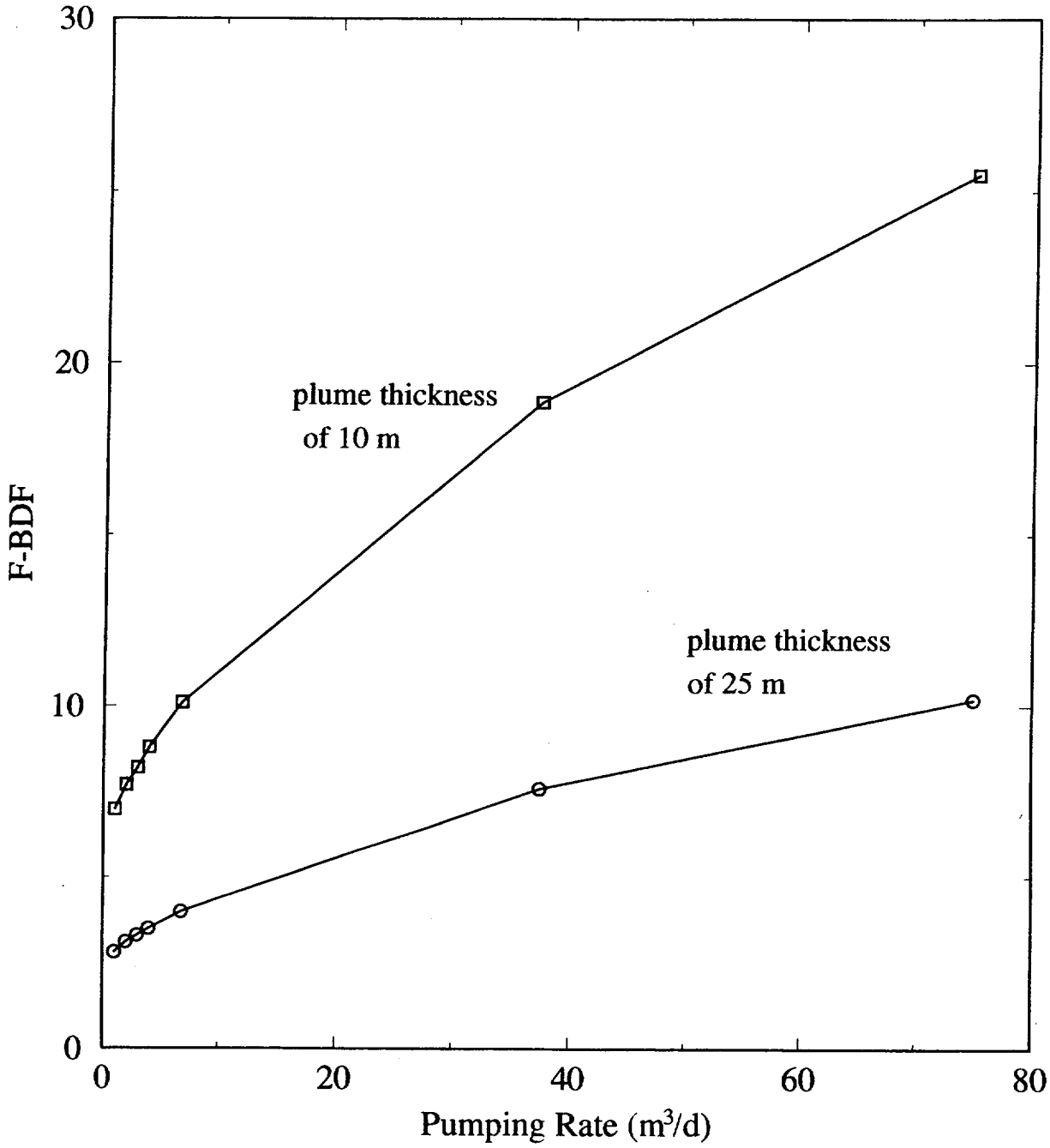

Figure 4-6. Effect of pump rate (range 1 to 75 m^3/d) on the flux-based borehole dilution factor for plumes of thickness 10 m and 25 m (no vertical dispersion). The regional gradient is 0.005 and the transmissivity is 100 m^2/d for all cases.

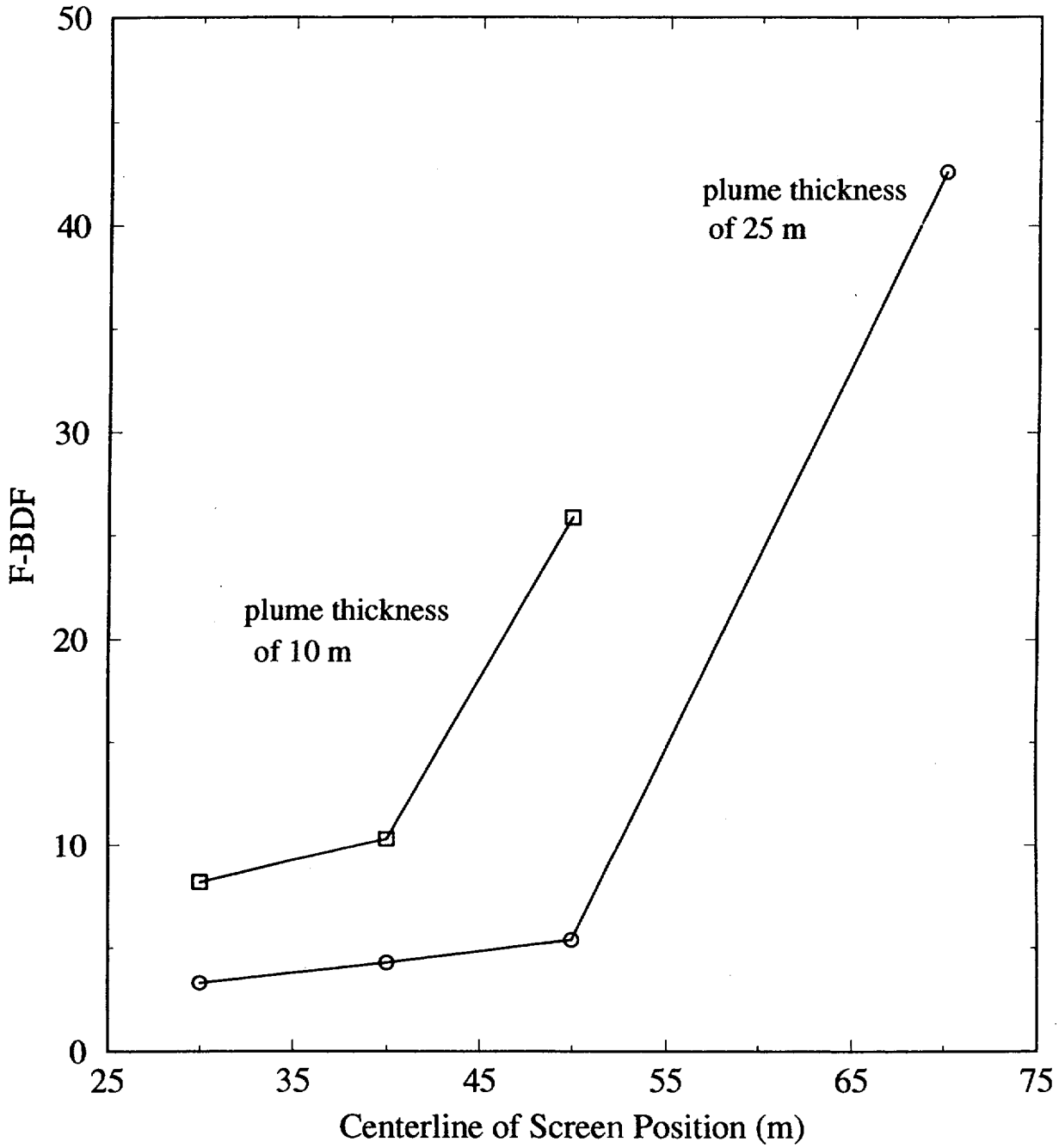

Figure 4-7. Effect of screen position for domestic-sized wells on the flux-based borehole dilution factor for plumes of thickness 10 m and 25 m (no vertical dispersion). All screen lengths are 60 m, the regional gradient is 0.005, and the transmissivity is 100 m^2/d for all cases.

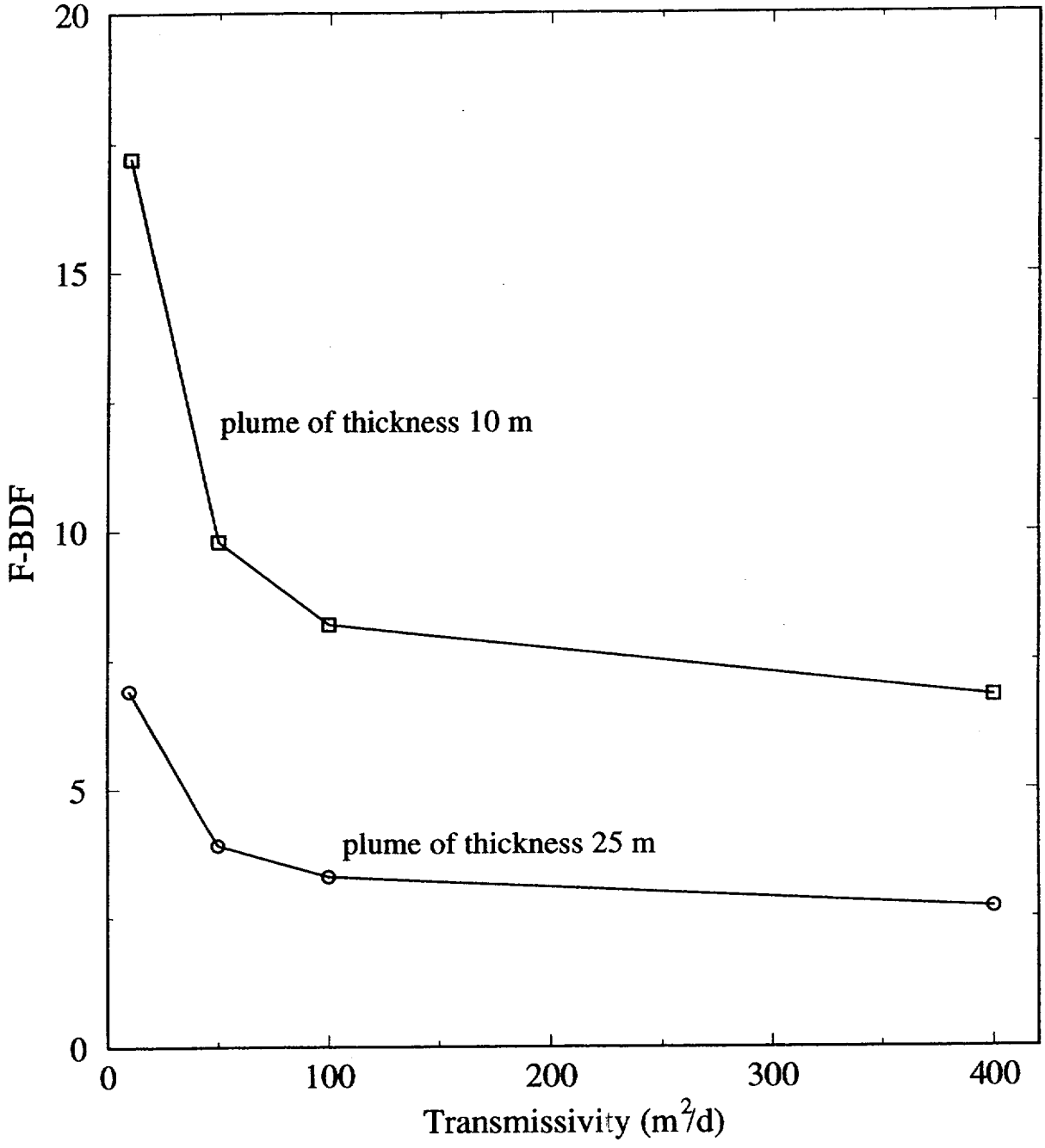

Figure 4-8. Effect of transmissivity (10, 50, 100, 400 m^2/d) on the flux-based borehole dilution factor for plumes of thickness 10 m and 25 m (no vertical dispersion). The regional gradient is 0.005 and the pump rate is 3 m^3/d for all cases.

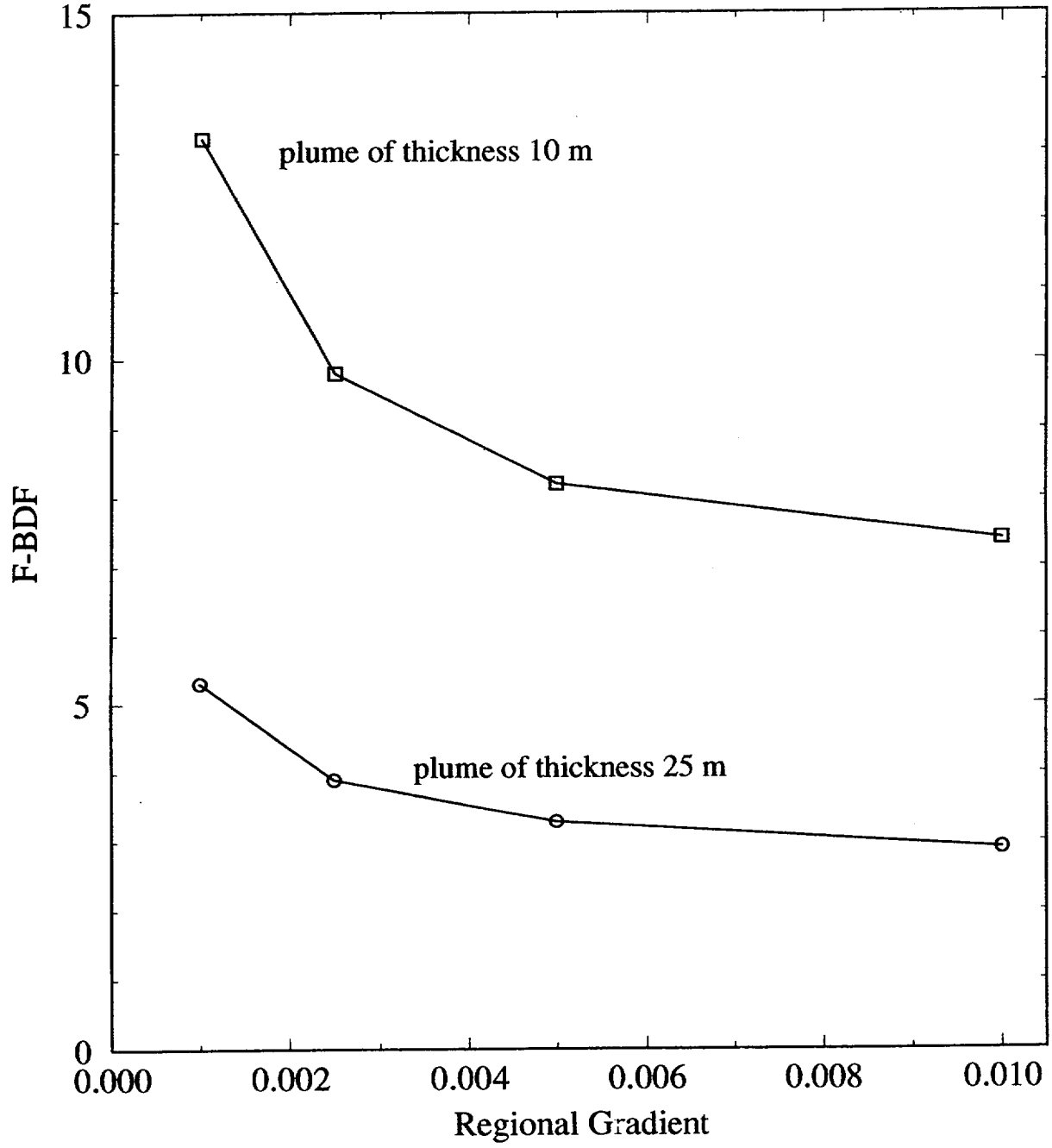

Figure 4-9. Effect of the regional gradient (0.001, 0.0025, 0.005, 0.01) on the flux-based borehole dilution factor for a domestic-sized well and plumes of thickness 10 m and 25 m (no vertical dispersion). The transmissivity is 100 m^2/d and the pump rate is 3 m^3/d for all cases.

The position of the screened portion of the well does not have a significant effect for domestic wells for the 25-m plume until screened portions are lower than three standard deviations from the average screen position (figure 4-7). The limited effect of screen position is due to a combination of the center of mass of the plume being near the water table as well as the small impact on the capture area due to different screen position and lengths. Within about two standard deviations from the average position of the screen, the F-BDF do not vary by more than a factor of 2. In all scenarios, the plume is assumed to be at the water table. The borehole dilution factors are in the 3 to 5 range and 8 to 10 range for the 25 and 10-m plumes, respectively, unless screen positions lower than three standard deviations from the average are considered.

The effect of transmissivity and regional gradient on F-BDF for the 10 and 25-m-thick plumes with no vertical dispersion are not significant until the smallest values of transmissivity and gradient are used (figures 4-8 and 4-9). For transmissivities greater than 50 m^2/d, the F-BDF is in the range of 7 to 10 for the 10-m-thick plume and 3 to 7 for the 25-m-thick plume. A regional gradient of 0.001 leads to a F-BDF of 13 for the plume thickness of 10 m while the larger gradients range from 7 to 10. The F-BDF for the 25-m-thick plume are between 3 and 5.

4.3.2 Irrigation Wells and Plumes with No Vertical Dispersion

The F-BDF were calculated for irrigation wells using the scenario of a 25-m-thick plume with no vertical dispersion. In this scenario, the large vertical gradients and deep capture for the wells lead to large amounts of clean water mixing in the borehole with the contaminated water from the plume. Depending on the capture zone width and the plume width, some horizontal mixing of clean and contaminated water may occur. The width of the plume depends on the transverse dispersivity. Figure 4-10 shows the F-BDF for a well pumping rate of 300 to 2,000 m^3/d for plumes using three different dispersivity values. Since the plume width decreases as the dispersivity decreases, the F-BDF increases as the dispersivity decreases. This effect is not present at the low pumping rates for the particular flow field parameters chosen for this comparison. The F-BDF range from 19 to 49 for all dispersivities sets. It must be re-emphasized that the F-BDF only reflects the effects of contaminant concentration reduction in the borehole and not the effects of dispersion on the resident or aquifer contaminant concentrations. This explains the otherwise counter-intuitive observation that, for high capacity wells, the F-BDF increases as the transverse dispersivity decreases.

4.3.3 Irrigation Wells and Plume with Vertical Dispersion

The F-BDF are calculated for irrigation wells using the scenario of a plume where 3D dispersion from a constant concentration source occurs. The effect of dispersion on the concentration during transport on the borehole dilution factor is not considered here; only the shape of the plume is considered in the dilution factors. Generally, the capture zones are thicker and narrower than the thin but wide plumes. Depending on the dispersivity values used for the plume and the pumping rate and hydraulic properties used for the capture zone, the capture zones may be wider than the plume. Only for low pumping rates are the plumes thicker than the capture zone; this occurrence leads to no volumetric-based borehole dilution.

Plume shapes using dispersivities of 100:10:0.1 m and 20:2:0.2 m are compared to capture areas in order to calculate F-BDF. The plume for the 100:10:0.1 scenario is wider but thinner than the plume for the 20:2:0.2 scenario. Figures 4-11 to 4-13 show the effects of pumping rate, transmissivity, and regional gradient on the F-BDF which generally range from 1 to 5 regardless of dispersivity values used. For the pumping rate (figure 4-11) and the regional gradient (figure 4-13) curves, the two

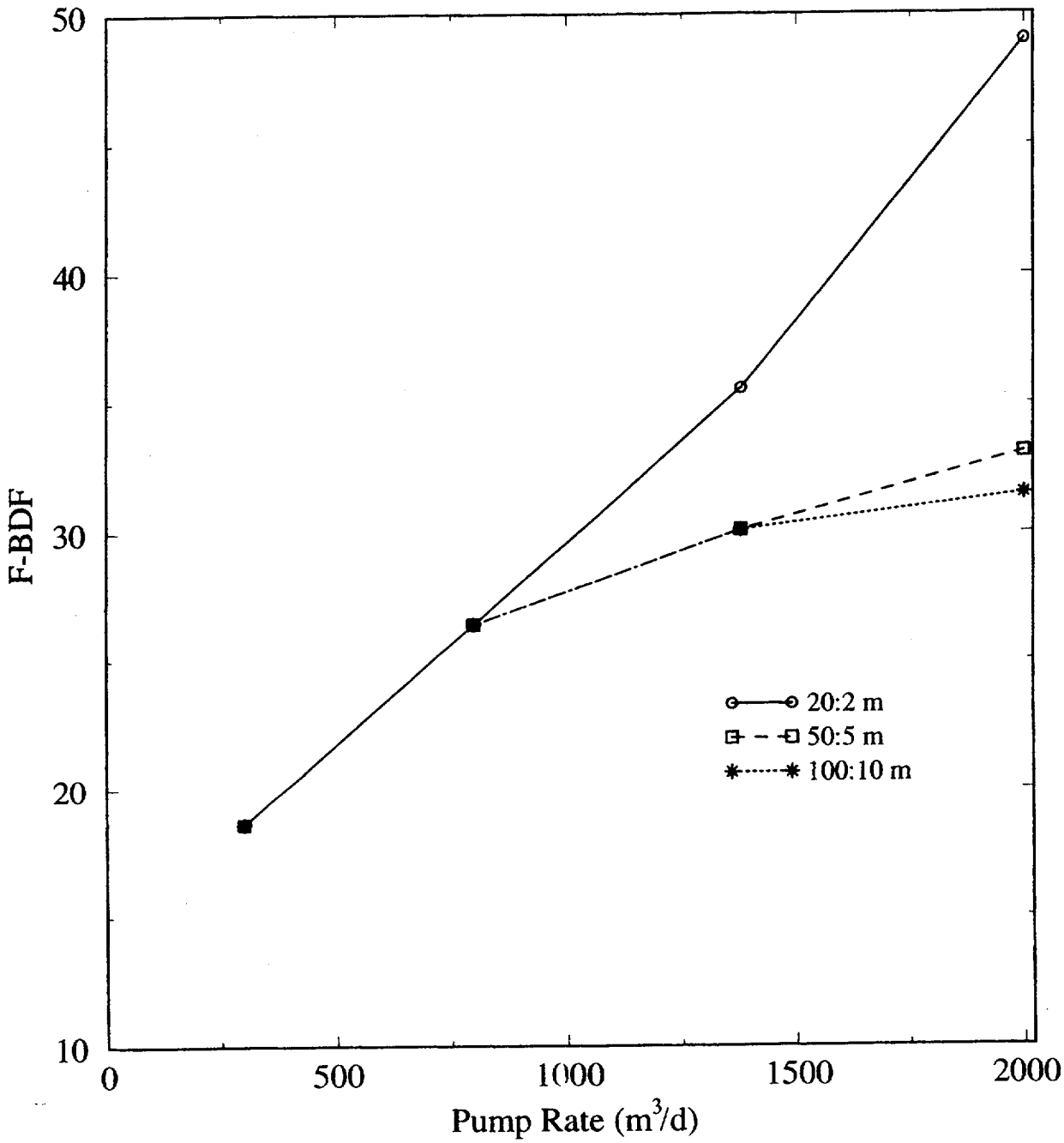

Figure 4-10. Effect of pump rate on flux-based borehole dilution factors for irrigation wells and a 25 m thick plume with no vertical dispersion. Three curves are plotted for different sets of dispersivity values.

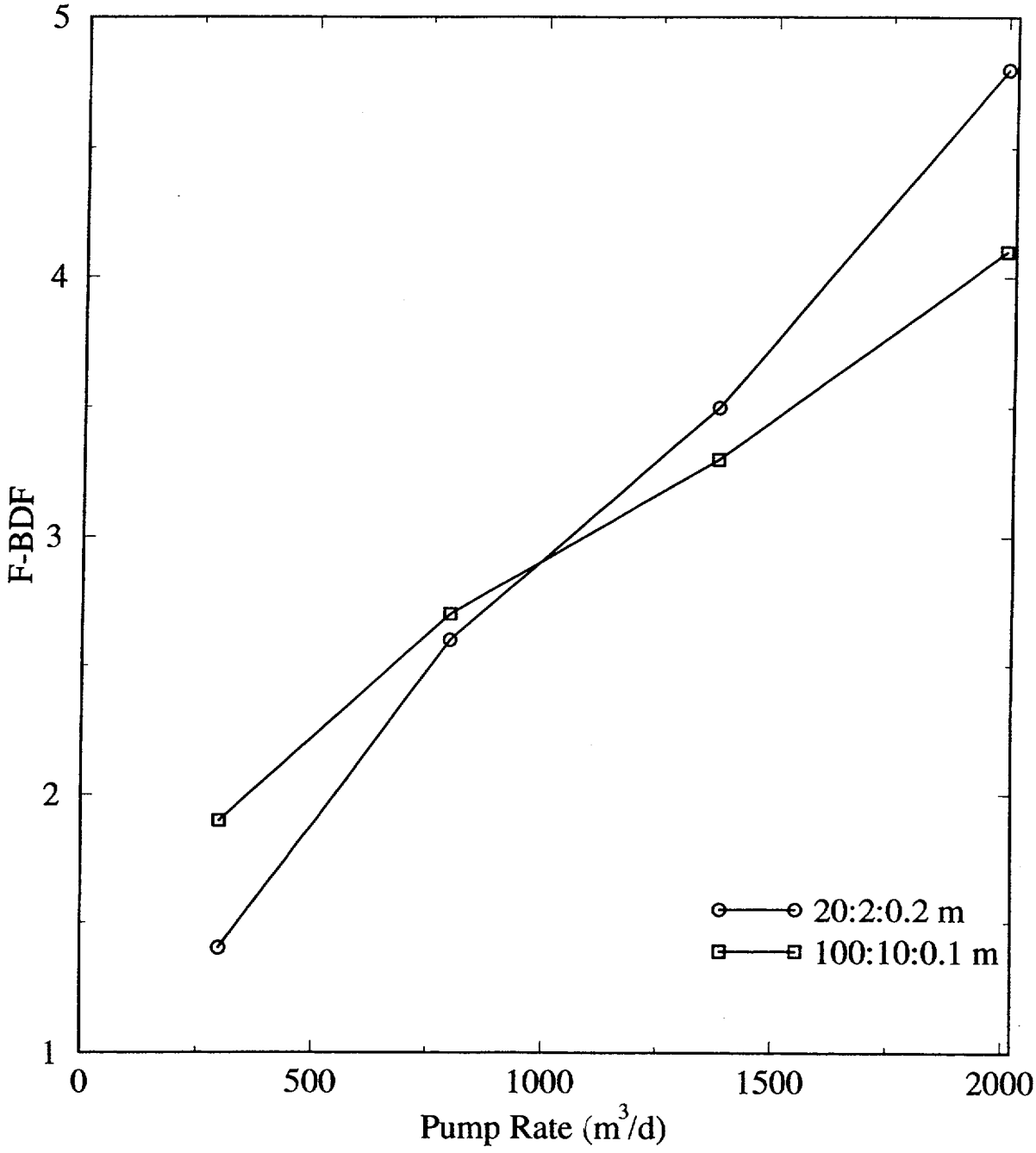

Figure 4-11. Effect of pump rate on dilution factors for irrigation sized wells and a plume with 3D dispersion. Curves are plotted for two sets of dispersivity values.

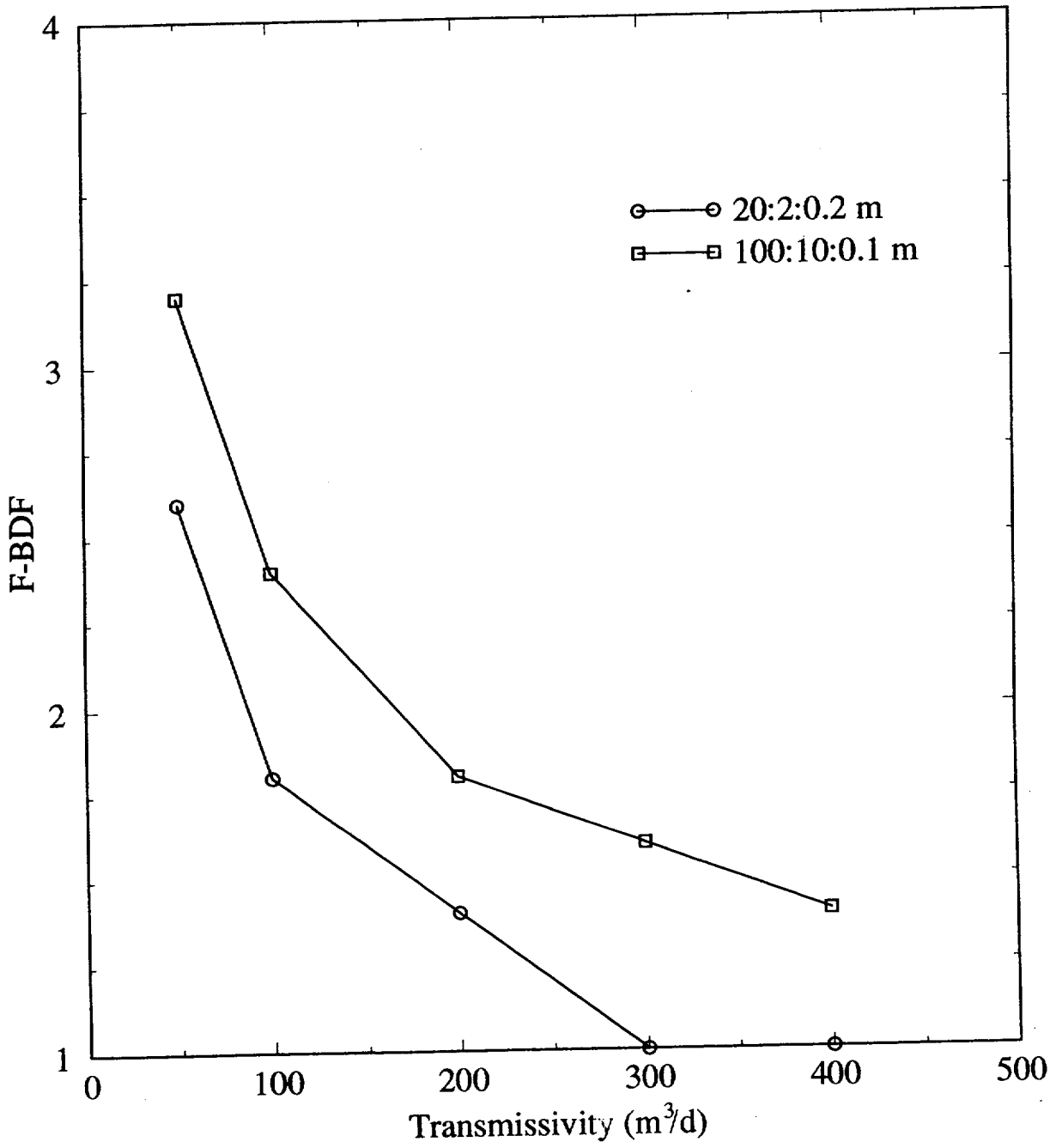

Figure 4-12. Effect of transmissivity (50 to 400 m^2/d) on dilution factors for irrigation sized wells and a plume with 3D dispersion. Curves are plotted for two sets of dispersivity values.

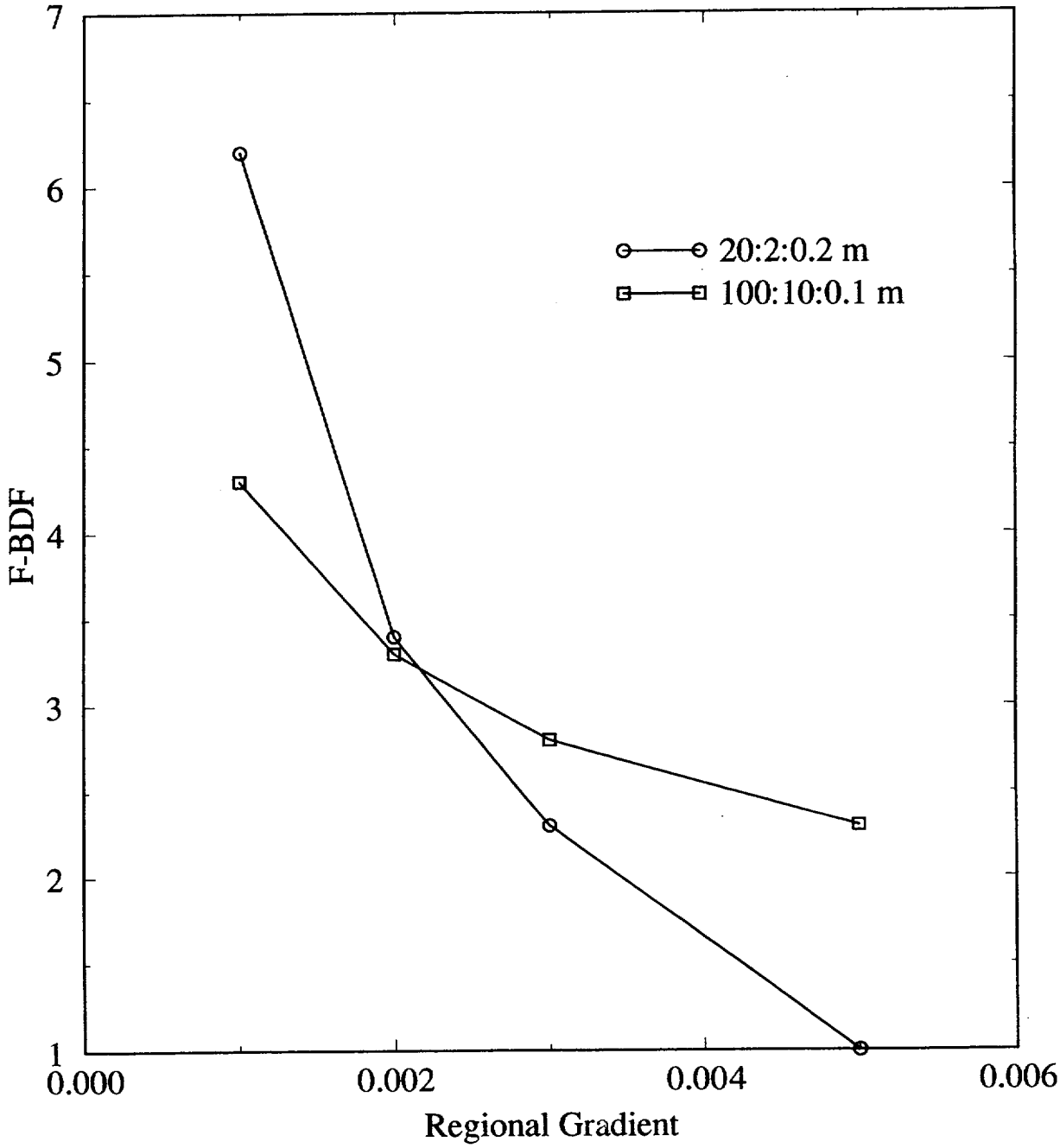

Figure 4-13. Effect of regional hydraulic gradient (0.001 to 0.0005) on dilution factors for irrigation-sized wells and a plume with 3D dispersion. Curves are plotted for two sets of dispersivity values.

dispersivity sets intersect due to the interplay between the thickness of the plume (the 20:2:0.2 plume is thicker) and the point where the entire plume is captured (the 100:10:0.1 plume is larger in area).

In summary, the effect of the plume size has the largest effect on the F-BDF. The values of the dilution factors are tabulated in appendix C. The shapes of plumes described above can be contrasted with the streamtubes used for the TPA (Baca et al., 1997; Manteufel et al., 1997). The plumes increase in size, and volumetric flow rate, with increasing distance from the source. The streamtubes have a fixed thickness and a variable width which depends on the streamlines. The width may increase or decrease for diverging converging, flow fields, respectively, but the volumetric flux does not change.

4.4 BOREHOLE DILUTION FACTORS BASED ON DISPERSIVE TRANSPORT

The F-BDF estimated in the previous section do not account for the concentration distribution of a migrating plume. Kessler and McGuire (1996) accounted for dispersion during plume migration by assuming the dilution factor was the ratio of the source concentration to the centerline concentration. Implicit in their assumption is that the plume has a uniform concentration equal to the centerline value that they justify as a conservative choice in terms of eventual dose to a critical group. This section will address the effect on borehole dilution of a concentration distribution within a plume.

The transport dispersion-based borehole dilution factor (T-BDF) was calculated by integrating the concentration distribution across the area of the portion of the plume which is captured by a pumping well. Portions of the plume not captured by the well do not contribute radionuclide mass to the well. The T-BDF was estimated by numerical integration of the concentration distribution in the area of the plume which was captured. The total borehole dilution factor can be estimated by linear combination of the F-BDF and T-BDF. The effect of domestic and irrigation wells on T-BDF varies significantly due to the thickness of the capture area and will be presented separately.

4.4.1 Domestic Wells

Figures 4-14 and 4-15 illustrate the effect of the concentration distribution within a plume on the T-BDF for two different plume configurations; a thin plume (25-m) with no vertical dispersion and a 3D dispersion plume. The T-BDF for the thin plume is nearly constant and its value is close to that of the P-DF (1.8) for pumping rates in the range of domestic and quasi-municipal wells (figure 4-14). The T-BDF for the plume with 3D dispersion vary from 9 to 18, increasing as the pumping rate increases. The larger values of T-BDF indicate the significance of pumping from less concentrated portions of the plume as compared to the centerline.

T-BDF is inversely proportional to the transmissivity (figure 4-15) with values ranging from 12 to 9 as transmissivity increases. Smaller transmissivity values lead to larger capture areas thus drawing water from portions of the plume with lower concentration. The effect of hydraulic gradient is similar to that of transmissivity.

4.4.2 Irrigation Wells

Figures 4-16 and 4-17 illustrate the effect of the concentration distribution on borehole dilution for irrigation wells. For the plume configuration with 3D dispersion, the T-BDF are as much as five

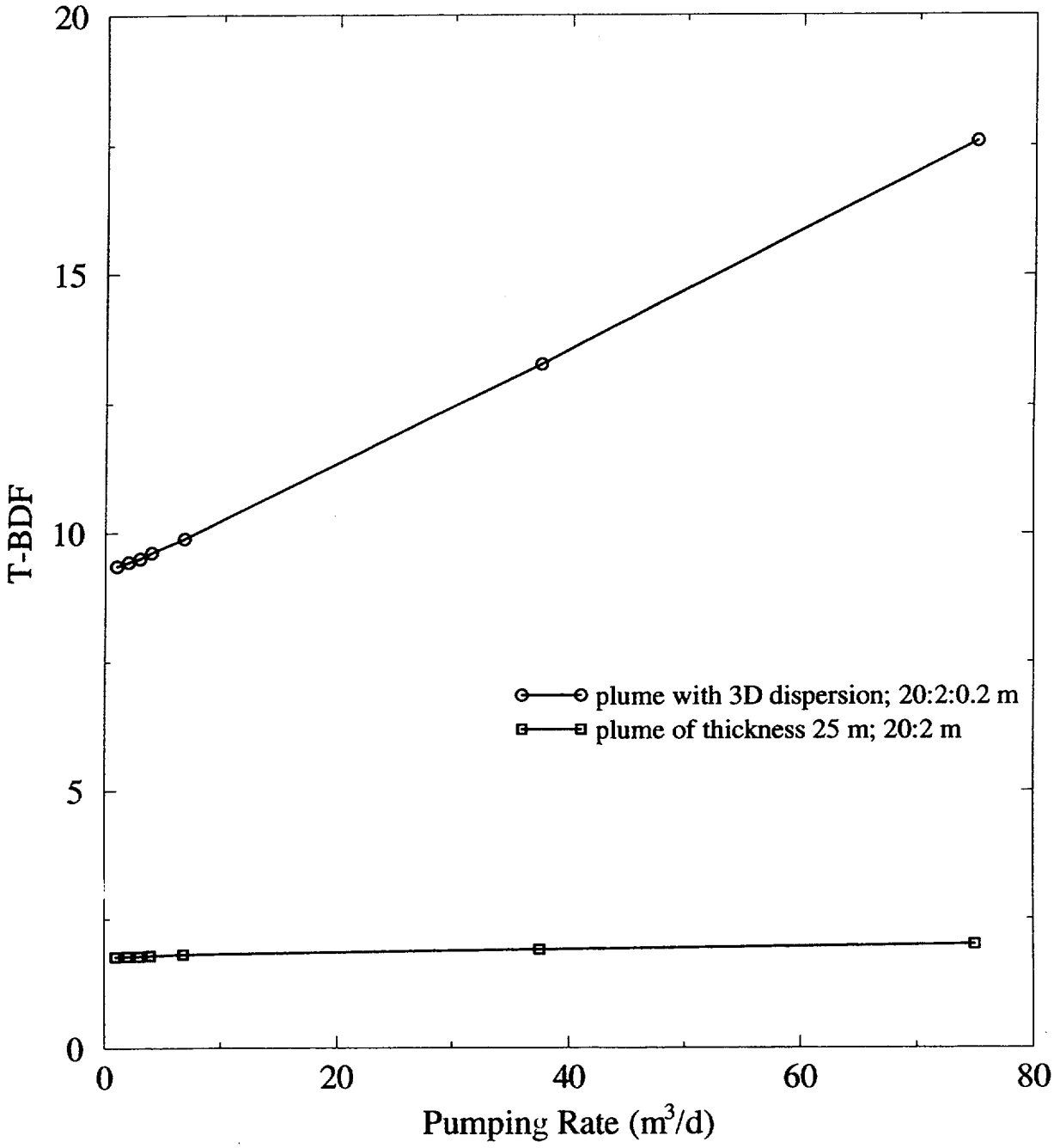

Figure 4-14. Effect of pumping rate (1–75 m^3/d) for domestic wells on transport dispersion-based borehole dilution factor for two different plume configurations: a thin plume with no vertical dispersion and a 3D dispersion plume both with dispersivity ratios as noted in the plot.

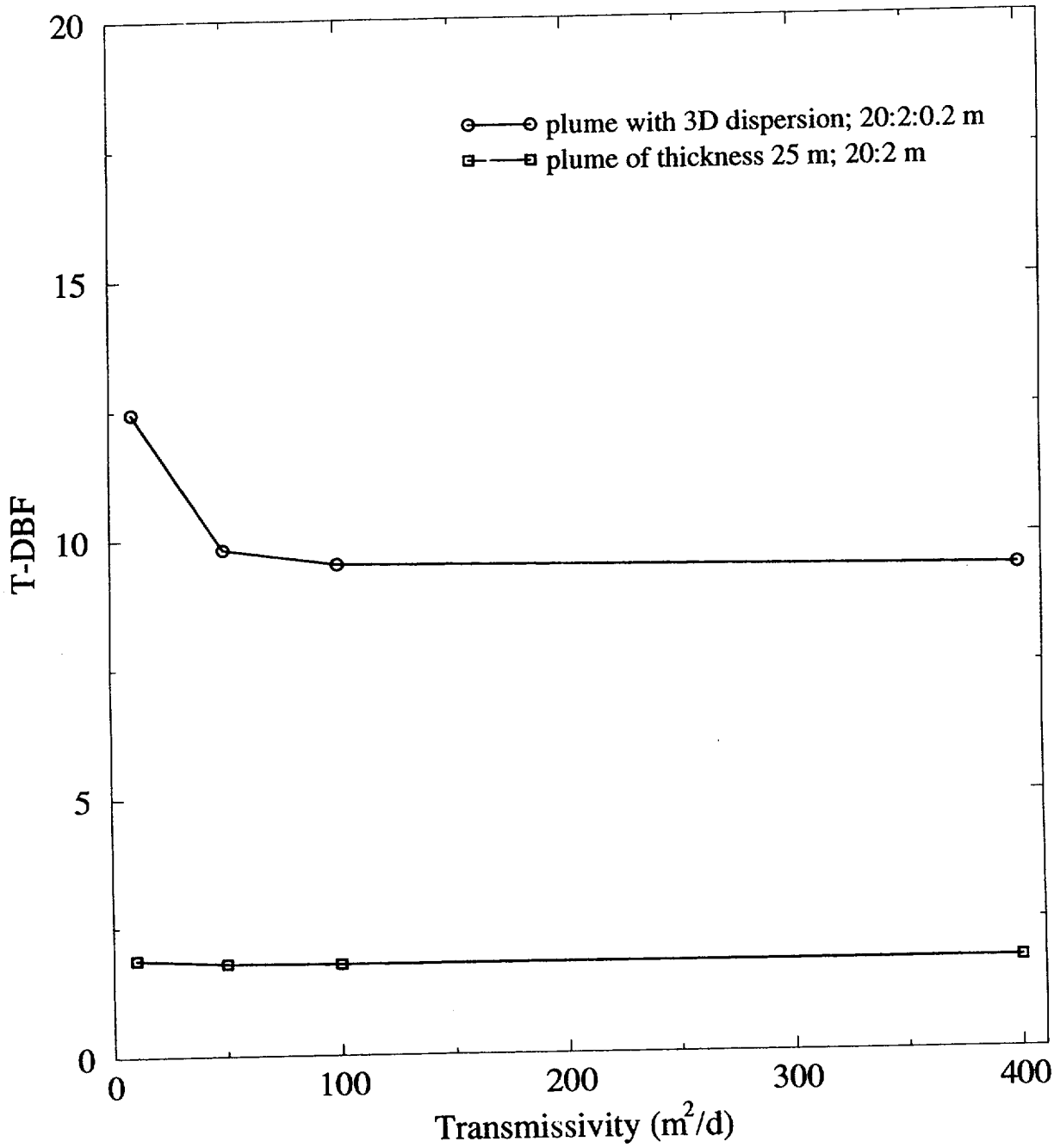

Figure 4-15. Effect of transmissivity (10–400 m^2/d) for domestic wells (Q = 3 m^3/d) on transport dispersion-based borehole dilution factor for two different plume configurations: a thin plume with no vertical dispersion and a 3D dispersion plume, both with dispersivity ratios as noted in the plot.

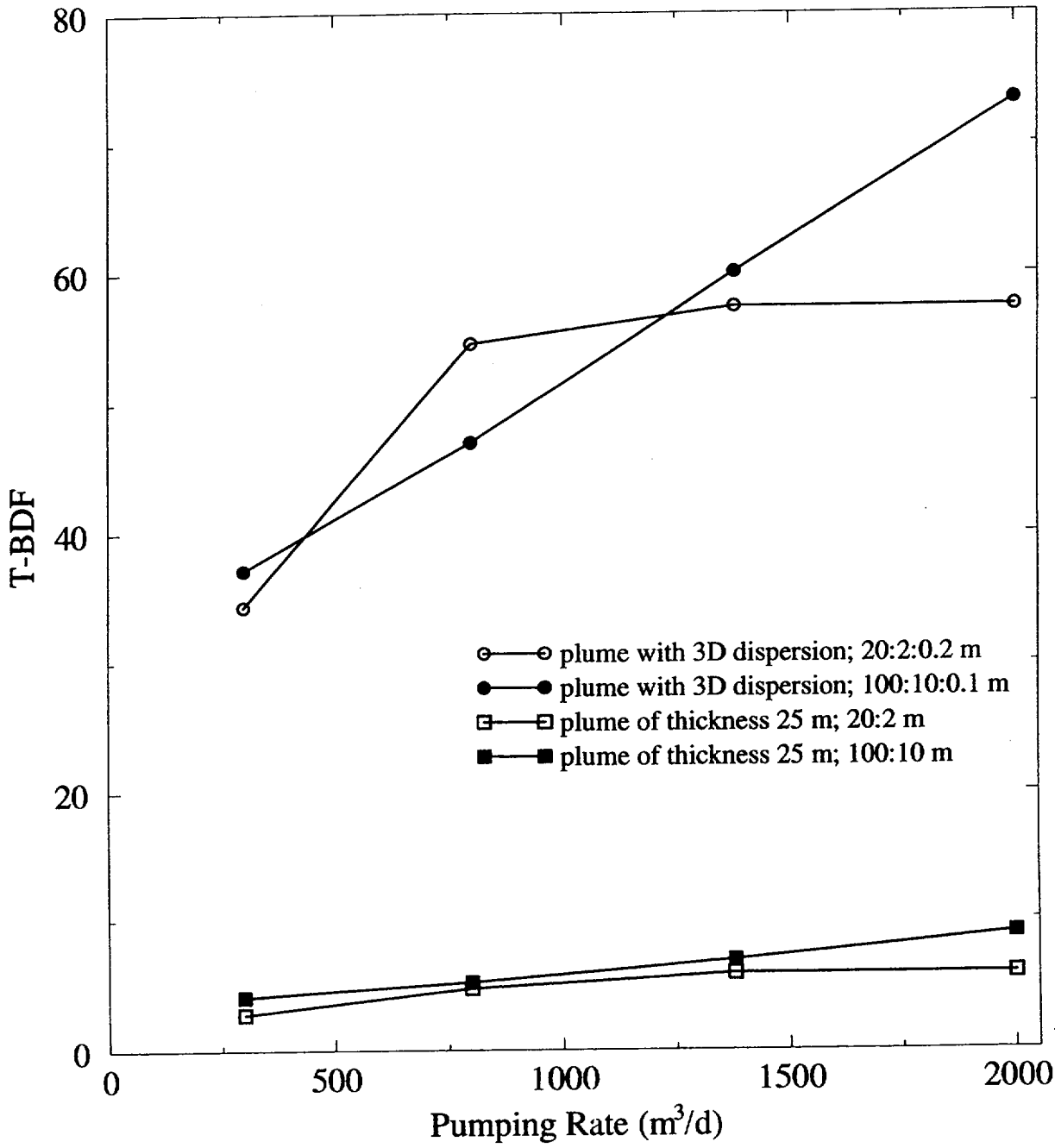

Figure 4-16. Effect of pumping rate (300–2,000 m^3/d) for irrigation wells on transport dispersion-based borehole dilution factor for four different plume configurations: two thin plumes with no vertical dispersion and two 3D dispersion plumes, all with dispersivity ratios as noted in the plot.

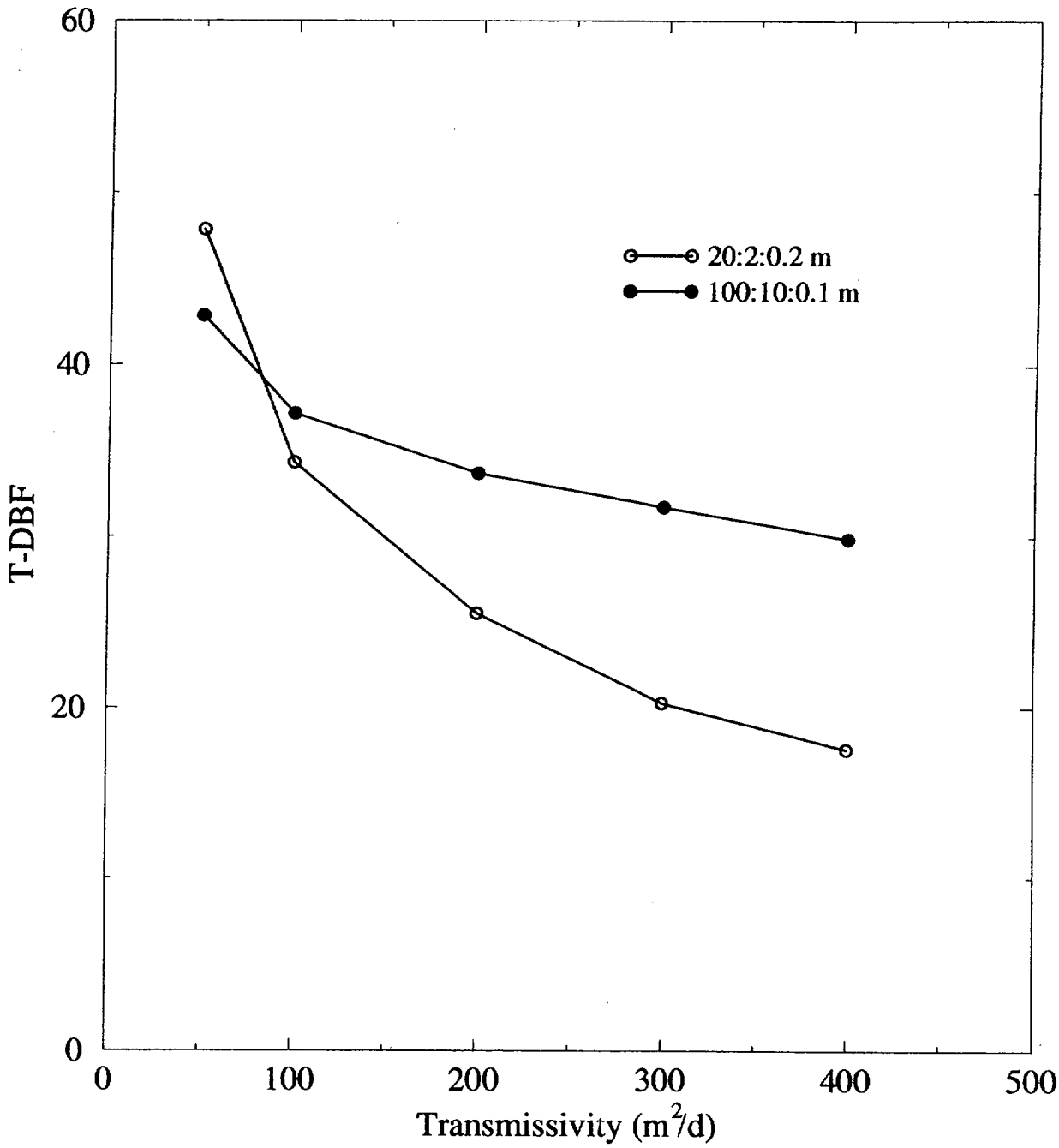

Figure 4-17. Effect of transmissivity (50–400 m^2/d) for large irrigation wells (Q=2116 m^3/d) on transport dispersion-based borehole dilution factor for two different plume configurations: two 3D dispersion plumes with dispersivity ratios as noted in the plot.

times larger (figures 4-14 and 4-16) than those for the domestic wells due to the large thickness of the irrigation capture area drawing in portions of the plume with low concentrations. As with the domestic wells, the T-BDF for thin plumes with no vertical dispersion are near the value of the inverse of the normalized concentration. The straight line increase in T-BDF for the plume with 3D dispersion and dispersivity ratio of 100:10:0.1 m reflects the large size of the plume relative to the capture areas (figure 4-16). The plateau in the curve for the 3D plume with dispersivity ratio of 20:2:0.2 m at the larger pumping rates is due to the entire plume being captured.

For transmissivity increases from 50 to 400 m^2/d, the T-BDF decreases from 48 to 18 for the 3D plume with dispersivity ratio of 20:2:0.2 m and from 43 to 30 for the 3D plume with dispersivity ratio of 100:10:0.1 m. Effects due to hydraulic gradient are similar to those of the transmissivity (appendix C).

5 CONCLUSIONS

The approach used in this report to estimate borehole dilution is to separate it into two components: volumetric flux-based and dispersion transport-based components. The method used to estimate F-BDF in the Amargosa Farms region is to compare the capture area of a pumping well to the cross-sectional area of the portion of the plume which is captured. Borehole dilution factors presented in this report are calculated using the cross-sectional areas normal to the principal direction of regional flow. The method used to estimate the component of borehole dilution due to dispersion during transport is to numerically calculate an areal average for the portion of the plume captured by a pumping well. Since this report is a scoping analysis, the F-BDF and T-BDF have been kept separate in order to better delineate sensitive parameters.

Different configurations for the plume and the capture area were evaluated. For domestic wells, the capture area is generally much smaller than the cross-sectional area of a plume that has undergone horizontal and vertical transverse spreading due to macro-dispersion during transport along a 20- to 30-km pathway as shown in figure 4-1. Thus, as expected, F-BDF was minimal when the domestic well was aligned with the center of the plume. Any borehole dilution that might occur would be solely due to vertical gradients in the plume concentration and would be reflected in the T-BDF. For irrigation wells, or any high-discharge wells, the capture area is generally thicker than the plume, while the capture zone may be wider or narrower than the contaminant plume depending on the particular scenario.

To simulate the case in which stratification of the porous medium minimizes the vertical transverse dispersion and thus confines the plume to a thin layer near the water table, a 2D areal advection-dispersion equation was solved for which a fixed plume thickness was assumed. Based on field observations summarized by Gelhar et al. (1992), this non-vertically dispersing plume closely simulates the behavior of many contaminant plumes characterized in the field, and provides a worst-case scenario in terms of high resident concentrations. The position of the plume relative to the capture area affects the dilution factor.

Several conclusions can be drawn from this study. First, as defined in this study, F-BDF for individual wells are relatively small, ranging from 1 to 5 for an irrigation well extracting contaminant from a 3D plume, from 18 to 40 for an irrigation well extracting contaminant from a thin plume that does not disperse vertically, and from 3 to 18 for a domestic well extracting contaminant from a thin plume that does not disperse vertically. However, one must be careful when comparing F-BDF for different contaminant plume configurations since actual borehole concentrations depend on the mass of radionuclides captured and the volume of water pumped, not the area of the plume that is captured. On the one hand, a high-capacity well may capture the entire mass of radionuclides in a large plume, have an apparent dilution factor of only 1, yet still produce a low borehole concentration because the large plume would have a corresponding low mean resident concentration. On the other hand, a low-capacity domestic well may capture the entire mass of radionuclides in a very small plume, have a dilution factor of 10, yet produce a very high borehole concentration because the plume has a very high mean resident concentration.

The T-BDF account for the low or high mean resident concentrations in the different plume scenarios. T-BDF for domestic wells are generally low and approach the P-DF, whereas T-BDF for irrigation wells are up to two orders of magnitude depending on the plume scenario. The P-DF would be a poor estimate for the effect due to dispersion during transport for irrigation wells.

A second, and perhaps obvious, conclusion can be drawn from this study. Specifically, for a thin wide plume of specified dimensions, a low-capacity well screened over a thick section of the aquifer, may produce a higher dilution factor than a larger capacity well screened over a shorter vertical interval. Indeed, extremes in the individual borehole concentrations within a critical group will be greater if the contaminant plume is thin and borehole construction practices are varied, than if the plume is very thick and borehole construction practices are uniform. These results suggest that attention should be paid to understanding vertical spreading in the saturated zone along the presumed transport pathway. Indirect field evidence (Gelhar et al., 1992; Bedient et al., 1994) suggests minimal vertical spreading in alluvial aquifers; however, vertical spreading may be substantial in the fractured tuff aquifer, especially where flow crosses normal faults across which there is significant offset in the conductive and non-conductive strata.

The dilution factors computed in this study cannot be used to estimate borehole concentrations unless the conceptual model of transport adopted by the user conforms to the following description. The solution to the steady state advection-dispersion equation is used to define a material surface that extends from radionuclide source to radionuclide receptor locations through which all radionuclides are transported. The shape of this material surface is best described as a duct or tube bounded on the top by the water table and having a half-elliptical cross-section that increases in area from source to receptor in proportion to the assigned transverse dispersivities. Although radionuclides do not cross the boundary of this tube, water does; the flow rate of water changes in direct proportion to the cross-sectional area of the tube. Hence, under the assumptions of steady state transport, the mean radionuclide concentration computed over the cross-sectional area of the tube at any point along its length must decrease from source to receptor. For the case where vertical transverse dispersion is neglected, the true shape of the tube is not easily described, but the cross-section may be approximated by a vertical rectangle of fixed height whose width increases in direct proportion to the horizontal transverse dispersivity.

The shapes of plumes described above can be contrasted with the streamtubes used in the study by (Baca et al., 1997). The streamtubes have a fixed thickness and a variable width which depends on the streamlines. The width may increase or decrease for diverging or converging flow fields, respectively, but the volumetric flux remains constant within a streamtube.

Further work on borehole dilution would benefit greatly from both a better delineation of a plume entering the Amargosa Farms region and large-scale modeling of multiple-well systems. This report has shown that the plume configuration is an important component. Modeling multiple-well systems is an extension of this work that would better define the pumping effect on groundwater flow patterns in the Amargosa Farms region. The single-well approach used here should only be compared with approaches where the largest volume used for the pumping input is as small as the pumping from a single well. This also assumes that infiltration through the repository or saturated zone mixing beneath the aquifer would both be smaller than the pumping from a single well.

6 REFERENCES

Akindunni, F.F., W.W. Gillham, B. Conant, Jr., and T. Franz. 1995. Modeling of contaminant movement near pumping wells: Saturated-Unsaturated flow with particle tracking. *Ground Water* 33(2): 264–274.

Baca, R.G. et al. 1997. *NRC High-Level Radioactive Waste Program Annual Progress Report: Fiscal Year 1996. Chapter 9—Activities Related to Development of The U.S. Environmental Protection Agency Yucca Mountain Standard*. NUREG/CR-6513, No. 1. Washington, DC: U.S. Nuclear Regulatory Commission.

Bair, E.S., and T.D. Lahm. 1996. Variations in capture-zone geometry of a partially penetrating pumping well in an unconfined aquifer. *Ground Water* 34(5): 842-852.

Bauer, E.M., and K.D. Cartier. 1995. *Reference Manual for Data Base on Nevada Well Logs*. U.S. Geological Survey Open-File Report 95-460. Washington, DC: U.S. Geological Survey.

Bedient, P.B., H.S. Rifai, and C.J. Newell. 1994. *Ground Water Contamination Transport and Remediation*. Englewood Cliffs, New Jersey: PTR Prentice Hall.

Bedinger, M.S., K.A. Sargent, and W.H. Langer. 1989. *Studies of Geology and Hydrology in the Basin and Range Province, Southwestern United States, for Isolation of High-level Radioactive Waste-characterization of the Death Valley Region, Nevada and California*. U.S. Geological Survey Professional Paper 1370-F. Washington, DC: U.S. Geological Survey.

Buqo, T.S. 1996. *Baseline Water Supply and Demand Evaluation of Southern Nye County, Nevada*. Consultants Report Prepared for the Nye County Nuclear Waste Repository Office, Nye County, Nevada.

Burchfiel, B.C. 1966. *Reconnaissance Geologic Map of the Lathrop Wells 15-Minute Quadrangle, Nye County, Nevada*. USGS Miscellaneous Geological Investigations Map I-474. Washington, DC: U.S. Geological Survey.

Chiang, C., G. Raven, and C. Dawson. 1995. The relationship between monitoring well and aquifer solute concentration. *Ground Water* 33(5): 718–726.

Czarnecki, J.B., and R.K. Waddell. 1984. *Finite-Element Simulations of Groundwater Flow in the Vicinity of Yucca Mountain, Nevada-California*. U.S. Geological Survey Water-Resources Investigations Report 84-4349. Denver, CO: U.S. Geological Survey.

D'Agnese, F.A. 1994. *Using scientific information systems for three-dimensional modeling of regional ground-water flow systems, Death Valley Region, Nevada and California*. Ph.D. Dissertation, Colorado School of Mines.

D'Agnese, F.A., C.C. Faunt, A.K. Turner, and M.C. Hill. 1996. *Hydrogeologic Evaluation and Numerical Simulation of the Death Valley Regional Ground-water Flow System, Nevada and California, Using Geoscientific Information Systems*. Washington, DC: U.S. Geological Survey (Draft).

Denny, C.S., and H. Drewes. 1965. *Geology of the Ash Meadows Quadrangle, Nevada-California*. U.S. Geological Survey Bulletin 1181-L. Washington, DC: U.S. Geological Survey.

Domenico, P.A., and G.A. Robbins. 1985. A new method of contaminant plume analysis. *Ground Water* 23(4): 476-485.

Fabryka-Martin, J.F., P.R. Dixon, S. Levy, B. Liu, H.J. Turin, and A.V. Wolfsberg. 1996. *Summary Report of Chlorine-36 Studies: Systematic Sampling for Chlorine-36 in the Exploratory Studies Facility*. LA-UR-96-1384. Los Alamos, NM: Los Alamos National Laboratory.

Faybishenko, B.A., I. Javandel, and P.A. Witherspoon. 1995. Hydrodynamics of the capture zone of a partially penetrating well in a confined aquifer. *Water Resources Research* 31(4): 859–866.

Fischer, J.M. 1992. *Sediment properties and water movement through shallow unsaturated alluvium at an arid site for disposal of low-level radioactive waste near Beatty, Nye County, Nevada*. U.S. Geological Survey Water-Resources Investigations Report 92-4032. Washington, DC: U.S. Geological Survey.

Flint, A.L., and L.E. Flint. 1994. Spatial distribution of potential near surface moisture flux at Yucca Mountain. *High-Level Radioactive Waste Management: Proceedings of the Fifth International Conference, Las Vegas, Nevada, May 22-26, 1994*. La Grange Park, IL: American Nuclear Society: 2352-2358.

Gelhar, L.W., C. Welty, and K.R. Rehfeldt. 1992. A critical review of data on field-scale dispersion in aquifers. *Water Resources Research* 28(7): 1,955–1,974.

Grubb, S. 1993. Analytical model for estimation of steady-state capture zones of pumping wells in confined and unconfined aquifers. *Ground Water* 31(1): 27–32.

Haitjema, H.M. 1995. *Analytic Element Modeling of Groundwater Flow*. New York: Academic Press.

Hoover, D.L., W.C. Swadley, and A.J. Gordon. 1981. *Correlation Characteristics of Surficial Deposits With a Description of Surficial Stratigraphy in the Nevada Test Site Region*; USGS. Open-File Report 81-512. Washington, DC: U.S. Geological Survey.

Kessler, J., and R. McGuire. 1996. *Yucca Mountain Total System Performance Assessment, Phase 3*. EPRI TR-107191. Palo Alto, CA: Electric Power Research Institute.

Kilroy, K.C. 1991. *Ground-Water Conditions in Amargosa Desert, Nevada-California, 1952-87*. U.S. Geological Survey Water-Resources Investigations Report 89-4101. Washington, DC: U.S. Geological Survey.

Laczniak, R.J., J.C. Cole, D.A. Sawyer, and D.A. Trudeau. 1996. *Summary of Hydrologic Controls on Ground-Water Flow at the Nevada Test Site, Nye County, Nevada.* U.S. Geological Survey Water-Resources Investigations Report 96-4109. Washington, DC: U.S. Geological Survey.

Manteufel, R.D., R.G. Baca, S. Mohanty, M.S. Jarzemba, R.W. Janetzke, S.A. Stothoff, C.B. Connor, G.A. Cragnolino, A.H. Chowdhury, T.J. McCartin, and T.M. Ahn. 1997. *Total-system Performance Assessment (TPA) Version 3.0 Code: Module Descriptions and User's Guide.* San Antonio, TX: Center for Nuclear Waste Regulatory Analyses.

Mohanty, S., G.A. Cragnolino, T. Ahn, D.S. Dunn, P.C. Lichtner, R.D. Manteufel, N. Sridhar. 1997. *Engineered Barrier System Performance Assessment Code: EBSPAC Version 1.1: Technical Description and User's Manual.* San Antonio, TX: Center for Nuclear Waste Regulatory Analyses.

Naff, R.L. 1973. *Hydrogeology of the southern part of the Amargosa Desert in Nevada.* Master's Thesis: University of Nevada at Reno.

Nevada Division of Water Resources. 1997a. *Well Driller's Logs for Amargosa Desert Townships 15,16,17S and Ranges 47,48,49,50E from Nevada Division of Water Resources.* Carson City, NV: Nevada Division of Water Resources.

Nevada Division of Water Resources. 1997b. *Annual Estimates of Water Use for Hydrographic Basin 230, Amargosa Desert.* Carson City, NV: Nevada Division of Water Resources.

Nevada Division of Water Resources. 1997c. *Well Permit Database for Hydrographic Basin 230, Amargosa Desert.* Carson City, NV: Nevada Division of Water Resources.

Nichols, W.D., and J.P. Akers. 1985. *Water-Level Declines in the Amargosa Valley area, Nye County, Nevada, 1962-84.* U.S.G.S. Water-Resources Investigations Report 85-4273. Washington, DC: U.S. Geological Survey.

Nuclear Regulatory Commission. 1995. *NRC Iterative Performance Assessment Phase 2: Development of Capabilities for Review of a Performance Assessment for a High-Level Waste Repository.* NUREG-1464. Washington, DC: Nuclear Regulatory Commission.

Oatfield, W.J., and J.B. Czarnecki. 1991. Hydrogeologic inferences from drillers' logs and from gravity and resistivity surveys in the Amargosa Desert, southern Nevada. *Journal of Hydrology* 124: 131–158.

Osterkamp, W.R., L.J. Lane, and C.S. Savard. 1994. Recharge estimates using a geomorphic/ distributed-parameter simulation approach, Amargosa River Basin. *Water Resources Bulletin* 30(3): 493–507.

Plume, R.W. 1996. *Hydrogeologic Framework of the Great Basin Region of Nevada, Utah, and Adjacent States.* U.S. Geological Survey Professional Paper 1409-B. Washington, DC: U.S. Geological Survey.

Reilly, T.E., O.L. Franke, and G.D. Bennett. 1989. Bias in groundwater samples caused by wellbore flow. *Journal of Hydraulic Engineering* 115(2): 270–276.

Savard, C.S. 1995. *Selected Hydrologic Data from Fortymile Wash in the Yucca Mountain Area, Nevada, Water Year 1992*. U.S. Geological Survey Open-File Report 94-317. Washington, DC: U.S. Geological Survey.

Schafer, D.C. 1996. Determining 3D capture zones in homogeneous, anisotropic aquifers. *Ground Water* 34(4): 628–639.

Stothoff, S.A. 1997. Sensitivity of long-term bare soil infiltration simulations to hydraulic properties in an arid environment. *Water Resources Research* 33(4): 547–558.

Strack, O.D.L. 1989. *Groundwater Mechanics*. Englewood Cliffs, NJ: Prentice-Hall.

Swadley, W.C. 1983. *Map Showing Surficial Geology of the Lathrop Wells Quadrangle, Nye County, Nevada*. USGS Misc. Invest. Series I-1361. Washington, DC: U.S. Geological Survey.

Swadley, W.C., and W.J. Carr. 1980. *Geologic Map of the Quaternary and Tertiary deposits of the Big Dune Quadrangle, Nye County, Nevada, and Inyo County, California*. USGS Misc. Invest. Series I-1361. Washington, DC: U.S. Geological Survey.

TRW Environmental Safety Systems, Inc. 1995. *Total System Performance Assessment-1995: An Evaluation of the Potential Yucca Mountain Repository*. B00000000-01717-2200-00136. Las Vegas, NV: TRW Environmental Safety Systems, Inc.

U.S. Department of Energy. 1988. *Site Characterization Plan: Yucca Mountain Site, Nevada Research and Development Area, Nevada, Volume II, Part A*. Oak Ridge, TN: U.S. Department of Energy, Office of Civilian Radioactive Management.

U.S. Geological Survey. 1989. *National Water Information System User's Manual Volume 2, Chapter 4. Ground-Water Site Inventory System*. U.S. Geological Survey Open-File Report 89-587. Washington, DC: U.S. Geological Survey.

Walker, G.E., and T.E. Eakin. 1963. *Geology and Ground Water of Amargosa Desert, Nevada-California*. Nevada Department of Conservation and Natural Resources, Ground-Water Resources-Reconnaissance Series Report 14. Carson City, NV: Nevada Department of Conservation and Natural Resources.

Wexler, E.J. 1992. Analytical solutions for one-, two-, and three-dimensional solute transport in ground-water systems with uniform flow. *Techniques of Water-Resources Investigations of the U.S. Geological Survey*, Chapter B7, Book 3 of Applications of Hydraulics. Washington, DC: U.S. Geological Survey.

Wilson, M.L., J.H. Gauthier, R.W. Barnard, G.E. Barr, H.A. Dockery, E. Dunn, R.R. Eaton, D.C. Guerin, N. Lu, M.J. Martinez, R. Nilson, C.A. Rautman, T.H. Robey, B. Ross, E.E. Ryder, A.R. Schenker, S.A. Shannon, L.H. Skinner, W.G. Halsey, J.D. Gansemer, L.C. Lewis, A.D. Lamont, I.R. Triay, A. Meijer, and D.E. Morris. 1994. *Total-System Performance Assessment for Yucca Mountain - SNL Second Iteration (TSPA-1993) - Volume 1,* Sandia Report SAND93-2675. Albuquerque, NM: Sandia National Laboratories.

Winograd, I.J., and W. Thordarson. 1975. *Hydrogeologic and Hydrochemical Framework, South-Central Great Basin, Nevada-California, with Special Reference to the Nevada Test Site.* U.S. Geological Survey Professional Paper 712-C. Washington, DC: U.S. Geological Survey.

APPENDIX A

DETAILED WATER USE TABLES FOR 1983, 1985-1996

Table A-1. Annual water use estimates (acre-ft) from NDWR (1997b); qq = quarter-quarter section, qtr = quarter section, sec = section, twn = township, rng = range, xx = not recorded, com = commercial, mm = mining, irr = irrigation, qm = quasi-municipal.

qq qtr sec twn rng	Use	1996	1995	1994	1993	1992	1991	1990	1989	1988	1987	1986	1985	1983
se se 13 15 49	com	0.5	—	—	—	—	—	—	—	—	—	—	—	—
se ne 16 16 48	com	2	—	—	—	—	—	—	—	—	—	—	—	—
ne ne 14 16 49	com	0.1	—	—	—	—	—	—	—	—	—	—	—	—
ne nw 12 17 48	mm	272	349	340	232	347.5	335	383	525	569	298	284	110	255
ne nw 25 18 50	com	—	—	—	—	—	—	—	—	0.5	0.5	0.6	—	—
xx se 35 16 49	com	1.0	—	—	—	—	—	—	—	—	—	—	—	—
xx sw 36 17 49	com	746.5	431	377	512	306	115	503.1	888	427	4	266	840	—
nw ne 10 17 49	com	50	—	—	—	—	—	—	—	—	—	—	—	—
ne nw 10 16 48	irr	—	300	60	—	—	—	—	—	385	385	385	375	400
ne nw 8 16 48	irr	—	—	—	—	—	—	—	—	—	—	—	—	150
ne ne 16 16 48	irr	125	400	280	290	600	400	400	50	700	100	600	400	—
sw nw 7 16 48	irr	92.5	185	185	185	37	37	—	—	—	—	—	—	—
xx xx 36 16 48	irr	799.5	864.5	1,170	1,170	994.5	1170	25	—	—	860	864.5	864.5	625
nw nw 18 16 48	irr	400	400	480	200	—	—	—	—	200	—	600	300	—
ne se 14 16 48	irr	175	175	175	175	—	—	—	—	—	—	—	—	—
ne ne 23 16 48	irr	625	625	625	668.8	625	800	—	—	—	—	—	325	625
ne sw 25 16 48	irr	—	—	—	—	625	—	—	—	—	—	—	625	625
nw ne 17 16 48	irr	—	—	50	—	—	—	—	—	—	—	—	128.9	75
ne nw 15 16 48	irr	5	12.5	15	2	2	—	10	—	—	—	—	—	—
ne nw 15 16 48	irr	7.5	2.5	2.5	1	4	—	—	—	6.3	—	—	—	—
ne ne 8 16 48	irr	5	90	75	90	—	—	—	—	50	—	195	—	—
sw nw 20 16 48	irr	17.5	17.5	10	20	40	20	—	—	—	—	—	—	300

Table A-1. Annual water use estimates (acre-ft) from NDWR (1997b); qq = quarter-quarter section, qtr = quarter section, sec = section, twn = township, rng = range, xx = not recorded, com = commercial, mm = mining, irr = irrigation, qm = quasi-municipal (cont'd).

qq qtr sec twn rng	Use	1996	1995	1994	1993	1992	1991	1990	1989	1988	1987	1986	1985	1983
ne ne 24 16 48	irr	227.5	300	200	175	175	175	150	175	175	175	—	—	—
ne se 24 16 48	irr	625	625	625	—	200	200	—	—	—	—	—	—	—
ne ne 36 16 48	irr	25	50	50	190	16	—	25	25	—	—	—	—	—
se sw 10 16 48	irr	—	400	—	200	—	—	—	—	—	—	—	—	—
se nw 18 16 48	irr	657.5	683	540.8	328.5	—	—	—	—	47.2	—	777.25	656.25	—
se sw 10 16 48	irr	5	5	—	—	—	—	—	—	—	—	—	—	—
nw sw 10 16 48	irr	17.5	17.5	17.5	17.5	17.5	—	5	5	2.5	2.5	2.5	—	—
nw sw 10 16 48	irr	11.25	—	—	—	—	—	—	—	—	—	—	—	—
nw sw 10 16 48	irr	—	—	—	—	1	—	22.5	—	—	—	—	—	—
sw se 8 16	irr	24	99	99	54	—	—	—	—	5	—	—	—	60
nw nw 15 16 48	irr	12.5	10	10	2	6	—	—	—	—	—	—	—	20
se nw 26 16 481	irr	583.5	583.5	223.34	250	—	—	250	—	—	583.5	583.5	583.5	584
se ne 26 16 48	irr	233.4	233.4	—	—	—	—	583.5	—	—	583.5	583.5	583.5	584
sw se 8 16 48	irr	70.7	75	60	30	—	—	—	—	—	—	—	—	—
sw nw 24 16 48	irr	583.5	583.5	583.5	583.4	—	—	583.35	—	—	583.35	538.35	583.35	—
sw nw 15 16 48	irr	10	10	20.65	6	6	—	—	—	34.4	—	—	25	—
nw nw 15 16 48	irr	12.5	—	—	—	—	—	—	—	—	—	—	—	—
ne nw 15 16 48	irr	5	—	—	—	—	—	—	—	—	—	—	—	—
ne nw 15 16 48	irr	1	—	—	—	—	—	—	—	—	—	—	—	—
nw nw 15 16 48	irr	5	—	—	—	—	—	—	—	—	—	—	—	—
ne nw 15 16 48	irr	1	—	—	—	—	—	—	—	—	—	—	—	—

Table A-1. Annual water use estimates (acre-ft) from NDWR (1997b); qq = quarter-quarter section, qtr = quarter section, sec = section, twn = township, rng = range, xx = not recorded, com = commercial, mm = mining, irr = irrigation, qm = quasi-municipal (cont'd).

qq qtr sec twn rng	Use	1996	1995	1994	1993	1992	1991	1990	1989	1988	1987	1986	1985	1983
ne ne 28 16 49	irr	183.4	183.4	183.4	183.4	183.4	—	75	75	183.4	183.4	183.4	109.9	210
ne sw 9 16 49	irr	—	—	—	—	—	—	—	—	—	—	—	—	5
ne se 32 16 49	irr	—	—	—	—	—	—	139.5	—	—	—	—	—	—
ne ne 14 16 49	irr	—	—	—	55	55	—	—	—	—	—	—	—	—
ne nw 30 16 49	irr	665	665	665	665	—	—	677.5	—	—	266	—	—	—
ne nw 35 16 49	irr	—	—	—	2	2	—	—	—	—	—	—	—	—
ne se 19 16 49	irr	625	625	625	625	625	625	400	250	—	—	—	—	—
se sw 9 16 49	irr	105	118.75	50	118.3	118.75	—	118.75	118.8	75	75	75	50	118.8
ne ne 8 16 49	irr	27.5	90	15	10	10	—	25	25	—	—	—	—	98.5
sw se 5 16 49	irr	—	—	1	—	—	—	—	—	—	—	—	—	—
ne se 8 16 49	irr	5	2	—	4	4	—	—	—	—	—	—	—	—
se nw 35 16 49	irr	26.28	26.2	18.2	18.2	18.24	—	—	—	—	—	—	—	—
se sw 9 16 49	irr	25	25	25	25	25	25	25	25	25	25	25	25	25
ne se 23 16 49	irr	625	625	625	625	625	625	—	—	—	—	—	—	625
nw ne 8 16 49	irr	—	—	—	13.7	—	—	—	—	—	—	—	—	—
se sw 9 16 49	irr	25	25	25	25	25	25	25	—	25	25	25	25	25
se se 22 16 49	irr	5	—	35	47.7	—	—	15	15	10	10	—	22.7	—
se ne 12 17 48	irr	—	—	—	—	—	—	—	—	—	—	—	—	25
se nw 12 17 48	irr	65	65	65	65	65	65	65	65	45	45	45	75	—
ne nw 9 17 49	irr	—	—	—	690	540	550	790	400	300	200	—	—	—
ne ne 9 17 49	irr	700	700	700	—	—	—	—	—	—	—	—	—	—

Table A-1. Annual water use estimates (acre-ft) from NDWR (1997b); qq = quarter-quarter section, qtr = quarter section, sec = section, twn = township, rng = range, xx = not recorded, com = commercial, mm = mining, irr = irrigation, qm = quasi-municipal (cont'd).

qq qtr sec twn rng	Use	1996	1995	1994	1993	1992	1991	1990	1989	1988	1987	1986	1985	1983
ne nw 15 17 49	irr	25	25	20	16	16	—	12	12	12	12	—	25	—
se se 8 17 49	irr	—	118.5	—	—	—	—	181.1	—	—	—	—	—	—
ne ne 9 17 49	irr	170	170	—	—	—	—	—	—	—	—	—	—	—
ne ne 9 17 49	irr	628	628	312.5	628	—	—	—	—	—	—	—	—	—
xx sw 4 16 48	irr	—	—	—	—	—	—	—	—	375	—	—	—	—
xx nw 23 16 48	irr	—	—	—	—	—	—	—	—	—	—	—	—	625
xx nw 25 16 48	irr	—	—	—	—	—	—	—	—	—	—	—	—	625
nw nw 15 16 48	irr	7.5	—	—	—	—	—	—	—	—	—	—	—	—
xx nw 25 16 48	irr	625	625	625	—	—	—	—	—	—	—	—	625	—
xx nw 25 16 48	irr	625	625	—	—	—	—	—	—	—	—	—	—	—
ne nw 17 16 48	irr	—	60	60	—	—	—	—	—	—	—	—	240	—
sw se 32 16 49	irr	—	—	100	100	—	175	175	175	—	—	—	—	—
ne ne 28 16 49	irr	—	—	—	—	—	—	—	—	—	—	—	100	—
nw se 1 17 48	irr	—	—	—	—	—	—	—	—	—	—	—	—	625
se nw 12 17 48	irr	—	—	—	—	—	—	—	—	—	—	—	—	300
ne se 12 17 48	irr	50	50	50	50	50	50	125	125	—	—	—	—	—
xx se 1 17 48	irr	40	40	—	—	—	—	—	—	—	375	375	375	—
sw ne 9 17 49	irr	40	40	—	—	—	—	—	—	—	—	—	—	—
se ne 9 17 49	irr	40	40	—	—	—	—	—	—	—	—	—	—	—
xx se 7 17 49	irr	—	—	—	—	—	—	—	—	—	200	—	625	—
xx sw 7 17 49	irr	625	625	—	—	—	—	50	—	312.5	625	625	25	—

Table A-1. Annual water use estimates (acre-ft) from NDWR (1997b); qq = quarter-quarter section, qtr = quarter section, sec = section, twn = township, rng = range, xx = not recorded, com = commercial, mm = mining, irr = irrigation, qm = quasi-municipal (cont'd).

qq qtr sec twn rng	Use	1996	1995	1994	1993	1992	1991	1990	1989	1988	1987	1986	1985	1983
ne sw 9 17 49	irr	200	200	00	—	—	—	—	—	—	—	—	—	—
nw sw 9 17 49	irr	200	200	50	—	—	—	—	—	—	—	—	—	—
nw se 7 17 49	irr	—	—	—	—	—	—	—	—	—	—	—	—	625
nw sw 7 17 49	irr	—	—	—	—	—	—	—	—	—	—	—	—	312.5
nw ne 24 15 49	qm	8	—	—	—	—	—	—	—	—	—	—	—	—
ne nw 27 16 49	qm	3.4	—	—	—	—	—	—	—	—	—	—	—	—
sw se 31 16 49	qm	10.5	—	—	—	—	—	—	—	—	—	—	—	—
se se 26 16 49	qm	0.1	—	—	—	—	—	—	—	—	—	—	—	—
nw ne 16 16 49	qm	20	—	—	—	—	—	—	—	—	—	—	—	—
se sw 1 17 48	qm	7.5	—	—	—	—	—	—	—	—	—	—	—	—
se sw 2 17 49	qm	10	—	—	—	—	—	—	—	—	—	—	—	—
se sw 2 18 49	qm	16	—	—	—	—	—	—	—	—	—	—	—	—
sw sw 2 18 49	qm	50	—	—	—	—	—	—	—	—	—	—	—	—
sw ne 3 18 50	qm	2	—	—	—	—	—	—	—	—	—	—	—	—

APPENDIX B

CAPTURE ZONE DELINEATION TABLE

Table B-1. Calculated capture zone widths and thicknesses. Screen elevation based on 1,000-m-thick aquifer.

ID	Screen Elevation (m)	Pump Rate (m^3/d)	Gradient	Transmissivity (m^2/d)	Width (m)	Thickness (m)	Not Captured on Top (m)
1	940-1,000	1	0.005	100	29	73	—
2	940-1,000	2	0.005	100	54	82	—
3	940-1,000	3	0.005	100	76	88	—
4	940-1,000	4	0.005	100	97	96	—
5	940-1,000	6.815	0.005	100	146	113	—
6	940-1,000	37.5	0.005	100	418	224	—
7	940-1,000	75	0.005	100	607	309	—
8	940-1,000	300	0.005	100	1292	575	—
9	940-1,000	800	0.005	100	2330	825	—
10	940-1,000	1380	0.005	100	3382	941	—
11	940-1,000	2000	0.005	100	4450	985	—
12	940-1,000	3	0.005	10	369	203	—
13	940-1,000	3	0.005	50	133	108	—
14	940-1,000	3	0.005	100	76	88	—
15	940-1,000	3	0.005	400	22	70	—
16	940-1,000	3	0.001	100	248	151	—
17	940-1,000	3	0.0025	100	133	108	—
18	940-1,000	3	0.005	100	76	88	—
19	940-1,000	3	0.05	100	41	78	—
20	940-1,000	3	0.005	100	76	88	—

Table B-1. Table of calculated capture zone widths and thicknesses. Screen elevation based on 1,000-m-thick aquifer (cont'd).

ID	Screen Elevation (m)	Pump Rate (m^3/d)	Gradient	Transmissivity (m^2/d)	Width (m)	Thickness (m)	Not Captured on Top (m)
21	930-990	3	0.005	100	69	98	0.2
22	920-980	3	0.005	100	67	107	5
23	900-960	3	0.005	100	68	127	21
24	980-1,000	3	0.005	100	115	65	—
25	940-1,000	3	0.005	100	76	88	—
26	900-1,000	3	0.005	100	51	122	—
27	0-1,000	300	0.005	100	574	1000	—
28	500-1,000	300	0.005	100	940	752	—
29	810-1,000	300	0.005	100	1238	601	—
30	940-1,000	300	0.005	100	1292	575	—
31	940-1,000	300	0.005	50	1944	751	—
32	940-1,000	300	0.005	100	1292	575	—
33	940-1,000	300	0.005	200	876	424	—
34	940-1,000	300	0.005	300	705	352	—
35	940-1,000	300	0.005	400	607	309	—
36	940-1,000	2116	0.005	200	2810	890	—
37	940-1,000	2116	0.005	300	2146	793	—
38	940-1,000	2116	0.005	400	1798	719	—
39	940-1,000	2116	0.001	100	5596	1000	—
40	940-1,000	2116	0.002	100	3282	934	—

Table B-1. Table of calculated capture zone widths and thicknesses. Screen elevation based on 1,000-m-thick aquifer (cont'd).

ID	Screen Elevation (m)	Pump Rate (m^3/d)	Gradient	Transmissivity (m^2/d)	Width (m)	Thickness (m)	Not Captured on Top (m)
41	940-1,000	2116	0.003	100	2486	850	—
42	940-1,000	2116	0.005	100	1798	719	—

APPENDIX C

TABLE OF BOREHOLE DILUTION FACTORS

Table C-1. Calculated dilution factors for combinations of plume scenarios and capture zones at 25 km. Capture #ID in column No. 2 are in reference to table in appendix B; Q = pumping rate (m^3/d), T = transmissivity (m^2/d), grad = regional gradient. The dilution factors are V-BDF (volumetric flux-based borehole dilution factor), P-DF (point dilution factor based on centerline concentration), and T-BDF (dispersion during transport-based borehole dilution factor). Additional significant figures are reported to illustrate relative differences only.

Plume Description	Capture Description	V-BDF	P-DF	T-BDF
3D plume 1				
20:2:0.2 m	#8, Q = 300	1.4	9.1	34
20:2:0.2 m	#9, Q = 800	2.6	9.1	55
20:2:0.2 m	#10, Q = 1,380	3.5	9.1	57
20:2:0.2 m	#11, Q = 2,000	4.8	9.1	57
Small irrigation well, 3D plume 1				
20:2:0.2 m	#31, T = 50	2.6	9.1	48
20:2:0.2 m	#32, T = 100	1.8	9.1	34
20:2:0.2 m	#33, T = 200	1.4	9.1	26
20:2:0.2 m	#34, T = 300	1.0	9.1	20
20:2:0.2 m	#35, T = 400	1.0	9.1	18
Large irrigation well, 3D plume 1				
20:2:0.2 m	#36, T = 200	2.8	9.1	57
20:2:0.2 m	#37, T = 300	3.0	9.1	52
20:2:0.2 m	#38, T = 400	2.4	9.1	45
20:2:0.2 m	#39, grad = 0.001	6.2	9.1	57.5
20:2:0.2 m	#40, grad = 0.002	3.4	9.1	57.5
20:2:0.2 m	#41, grad = 0.003	2.3	9.1	56.6
20:2:0.2 m	#42, grad = 0.005	1.0	9.1	45
Domestic wells, 3D plume 1				
20:2:0.2m	#21, 940–1,000	9.1	9.5	1
20:2:0.2 m	#22, 930–990	9.1	9.7	1
20:2:0.2 m	#23, 920–980	9.1	9.9	1
20:2:0.2 m	#24, 900–960	9.1	10.4	1
20:2:0.2 m	#1, Q = 1	9.1	9.36	1

Table C-1. Calculated dilution factors for combinations of plume scenarios and capture zones at 25 km. Capture #ID in column No. 2 are in reference to table in appendix B; Q = pumping rate (m^3/d), T = transmissivity (m^2/d), grad = regional gradient. The dilution factors are V-BDF (volumetric flux-based borehole dilution factor), P-DF (point dilution factor based on centerline concentration), and T-BDF (dispersion during transport-based borehole dilution factor). Additional significant figures are reported to illustrate relative differences only (cont'd).

Plume Description	Capture Description	V-BDF	P-DF	T-BDF
20:2:0.2 m	#2, Q = 2	9.1	9.44	1
20:2:0.2 m	#3, Q = 3	9.1	9.5	1
20:2:0.2 m	#4, Q = 4	9.1	9.6	1
20:2:0.2 m	#5, Q = 6.8	9.1	9.9	1
20:2:0.2 m	#6, Q = 37.5	9.1	13	1
20:2:0.2 m	#7, Q = 75	9.1	18	1
20:2:0.2 m	#12, T = 10	9.1	12	1
20:2:0.2 m	#13, T = 50	9.1	9.8	1
20:2:0.2 m	#14, T = 100	9.1	9.5	1
20:2:0.2 m	#15, T = 400	9.1	9.3	1
20:2:0.2 m	#16, grad = 0.001	9.1	11	1
20:2:0.2 m	#17, grad = 0.0025	9.1	9.8	1
20:2:0.2 m	#18, grad = 0.005	9.1	9.5	1
20:2:0.2 m	#19, grad = 0.01	9.1	9.4	1
3D plume 2				
100:10:0.1 m	#8, Q = 300	1.9	14	37
100:10:0.1 m	#9, Q = 800	2.7	14	47
100:10:0.1 m	#10, Q = 1,380	3.3	14	60
100:10:0.1 m	#11, Q = 2,000	4.1	14	73
Small irrigation well, 3D plume 2				
100:10:0.1 m	#31, T = 50	3.2	14	43
100:10:0.1 m	#32, T = 100	2.4	14	37
100:10:0.1 m	#33, T = 200	1.8	14	34
100:10:0.1 m	#34, T = 300	1.6	14	32
100:10:0.1 m	#35, T = 400	1.5	14	30

Table C-1. Calculated dilution factors for combinations of plume scenarios and capture zones at 25 km. Capture #ID in column No. 2 are in reference to table in appendix B; Q = pumping rate (m^3/d), T = transmissivity (m^2/d), grad = regional gradient. The dilution factors are V-BDF (volumetric flux-based borehole dilution factor), P-DF (point dilution factor based on centerline concentration), and T-BDF (dispersion during transport-based borehole dilution factor). Additional significant figures are reported to illustrate relative differences only (cont'd).

Plume Description	Capture Description	V-BDF	P-DF	T-BDF
Large irrigation well, plume 2				
100:10:0.1 m	#36, T = 200	3.0	14	53
100:10:0.1 m	#37, T = 300	2.6	14	45
100:10:0.1 m	#38, T = 400	2.3	14	41
100:10:0.1 m	#39, grad = 0.001	4.3	14	—
100:10:0.1 m	#40, grad = 0.002	3.3	14	59
100:10:0.1 m	#41, grad = 0.003	2.8	14	49
100:10:0.1 m	#42, grad = 0.005	2.3	14	41
Thin plumes, Domestic wells at 25 km, 20:2 m dispersivity ratio				
25 m thick; 20:2 m	#21, 940-1,000	3.3	1.8	1.78
25 m thick; 20:2 m	#22, 930-990	4.3	1.8	1.77
25 m thick; 20:2 m	#23, 920-980	5.4	1.8	1.77
25 m thick; 20:2 m	#24, 900-960	43	1.8	1.76
10 m thick; 20:2 m	#21, S = 940-1,000	8.2	1.8	1.78
10 m thick; 20:2 m	#22, S = 930-990	10.3	1.8	1.77
10 m thick; 20:2 m	#23, S = 920-980	26	1.8	1.70
10 m thick; 20:2 m	#24, S = 900-960	N/A	1.8	N/A
25 m thick; 20:2 m	#1, Q = 1	2.8	1.8	1.76
25 m thick; 20:2 m	#2, Q = 2	3.1	1.8	1.77
25 m thick; 20:2 m	#3, Q = 3	3.3	1.8	1.78
25 m thick; 20:2 m	#4, Q = 4	3.5	1.8	1.78
25 m thick; 20:2 m	#5, Q = 6.8	4.0	1.8	1.80
25 m thick; 20:2 m	#6, Q = 37.5	7.6	1.8	1.90
25 m thick; 20:2 m	#7, Q = 75	10.2	1.8	2.01
10 m thick; 20:2 m	#1, Q = 1	7.0	1.8	1.76

Table C-1. Calculated dilution factors for combinations of plume scenarios and capture zones at 25 km. Capture #ID in column No. 2 are in reference to table in appendix B; Q = pumping rate (m^3/d), T = transmissivity (m^2/d), grad = regional gradient. The dilution factors are V-BDF (volumetric flux-based borehole dilution factor), P-DF (point dilution factor based on centerline concentration), and T-BDF (dispersion during transport-based borehole dilution factor). Additional significant figures are reported to illustrate relative differences only (cont'd).

Plume Description	Capture Description	V-BDF	P-DF	T-BDF
10 m thick; 20:2 m	#2, Q = 2	7.7	1.8	1.77
10 m thick; 20:2 m	#3, Q = 3	8.2	1.8	1.78
10 m thick; 20:2 m	#4, Q = 4	8.8	1.8	1.78
10 m thick; 20:2 m	#5, Q = 6.8	10.1	1.8	1.80
10 m thick; 20:2 m	#6, Q = 37.5	19	1.8	1.90
10 m thick; 20:2 m	#7, Q = 75	26	1.8	2.01
25 m thick; 20:2 m	#12, T = 10	6.9	1.8	1.88
25 m thick; 20:2 m	#13, T = 50	3.9	1.8	1.80
25 m thick; 20:2 m	#14, T = 100	3.3	1.8	1.78
25 m thick; 20:2 m	#15, T = 400	2.7	1.8	1.76
25 m thick; 20:2 m	#16, grad = 0.001	5.3	1.8	1.84
25 m thick; 20:2 m	#17, grad = 0.0025	3.9	1.8	1.80
25 m thick; 20:2 m	#18, grad = 0.005	3.3	1.8	1.78
25 m thick; 20:2 m	#19, grad = 0.01	2.9	1.8	1.77
10 m thick; 20:2 m	#12, T = 10	17	1.8	1.88
10 m thick; 20:2 m	#13, T = 50	9.8	1.8	1.80
10 m thick; 20:2 m	#14, T = 100	8.2	1.8	1.78
10 m thick; 20:2 m	#15, T = 400	6.8	1.8	1.76
10 m thick; 20:2 m	#16, grad = 0.001	13.2	1.8	1.84
10 m thick; 20:2 m	#17, grad = 0.0025	9.8	1.8	1.80
10 m thick; 20:2 m	#18, grad = 0.005	8.2	1.8	1.78
10 m thick; 20:2 m	#19, grad = 0.01	7.4	1.8	1.77
Thin plumes irrigation wells @ 25 km				
25m thick; 20:2 m	#8, Q = 300	19	1.8	2.8
25m thick; 20:2 m	#9, Q = 800	26	1.8	4.8

Table C-1. Calculated dilution factors for combinations of plume scenarios and capture zones at 25 km. Capture #ID in column No. 2 are in reference to table in appendix B; Q = pumping rate (m^3/d), T = transmissivity (m^2/d), grad = regional gradient. The dilution factors are V-BDF (volumetric flux-based borehole dilution factor), P-DF (point dilution factor based on centerline concentration), and T-BDF (dispersion during transport-based borehole dilution factor). Additional significant figures are reported to illustrate relative differences only (cont'd).

Plume Description	Capture Description	V-BDF	P-DF	T-BDF
25m thick; 20:2 m	#10, Q = 1,380	36	1.8	5.9
25m thick; 20:2 m	#11, Q = 2,000	49	1.8	5.9
25m thick; 50:5 m	#8, Q = 300	19	2.6	3.3
25m thick; 50:5 m	#9, Q = 800	26	2.6	4.8
25m thick; 50:5 m	#10, Q = 1,380	30	2.6	6.8
25m thick; 50:5 m	#11, Q = 2,000	33	2.6	8.8
25m thick; 100:10 m	#8, Q = 300	19	3.6	4.1
25m thick; 100:10 m	#9, Q = 800	26	3.6	5.2
25m thick; 100:10 m	#10, Q = 1,380	30	3.6	6.9
25m thick; 100:10 m	#11, Q = 2,000	32	3.6	8.9

ATTACHMENT C
MATRIX DIFFUSION SUMMARY REPORT